Parameters estimation with coprime samplers and arrays

Zhe Fu

UNIVERSITE BRETAGNE LOIRE MATHSTIC

UNIVERSITÉ DE NANTES

THESE DE DOCTORAT DE

L'UNIVERSITE DE NANTES

COMUE UNIVERSITE BRETAGNE LOIRE

ECOLE DOCTORALE N° 601
Mathématiques et Sciences et Technologies de l'Information et de la Communication
Spécialité : Traitement du Signal

Par
Zhe FU

Parameters estimation with coprime samplers and arrays

Thèse présentée et soutenue à Nantes, le 24 septembre 2020
Unité de recherche : IETR UMR CNRS 6164

Rapporteurs avant soutenance :

Salah BOURENNANE Professeur, Ecole Centrale Marseille
Pascal CHEVALIER Professeur, CNAM Paris

Composition du Jury :

Président :	Jean-Pierre CANCES	Professeur, Université de Limoges
Examinateurs :	Salah BOURENNANE	Professeur, Ecole Centrale Marseille
	Pascal CHEVALIER	Professeur, CNAM Paris
Dir. de thèse :	Pascal CHARGÉ	Professeur, Université de Nantes
Co-Dir thèse :	Yide WANG	Professeur, Université de Nantes

Acknowledgement

Time just flows, it turns to the end of my PhD period even the memory of my fresh-PhD days just feels like yesterday. I really value my life in Nantes, a very beautiful city and the people here are so kind.

I would like to thank my families who have supported me unconditionally. Helping me through the darkness and difficulty. And especially, I would like to thank my love, Simei Yang. All the time and our memory in Nantes will definitely be a life-time memory to us.

I would also like to thank my supervisor, Professor Pascal Chargé, for providing me this chance to pursue my PhD. And also I am grateful to my co-supervisor, Professor Yide Wang, for offering the chance to work with him. I really appreciate their kindly suggestions, patience to my work and insightful discussions which help me to improve my skills during my PhD. It is my great pleasure to work with them.

I also wish to express my appreciation to my committee members. It is my honor to have them joining my defense. They provide me so many insightful remarks and helpful suggestions, which help me to further improve my work.

Finally, I would like to thank my colleagues, Ali Mohydeen, David Roszczyypala, Gatien Septembre, HaiDang Vu, Irfan Ali Tunio, Julien Weckbrodt, Taoufi Bouguera, Tien Thanh Nguyen, Safouane Noubir, Yunniel Arencibia Noa, Xiao Yang and the others. They bring so much happiness to my life and inspiring ideas to my mind. And special thanks to Xiao Yang for all the traveling, cooking, party time from 2015 to 2020. Also, I would also thank Mrs. Sandrine Charlier, Mr. Marc Brunet for their supports to my work and daily life.

In the end, I would like to quote a sentence which always reminds me about the past and future:

The more you go through, the more you can realize what true life is.

RÉSUMÉ

Résumé(Français)

Les techniques de traitement d'antenne sont largement utilisées dans de nombreux scénarios d'application, tels que le radar, le sonar, le satellite, la navigation, la communication sans fil. Dans un scénario classique, plusieurs capteurs ou plusieurs échantillonneurs sont régulièrement répartis pour recueillir des mesures du milieu environnant. Généralement, l'information recherchée est enfouie dans les données mesurées contaminées par le bruit. Il est alors nécessaire de développer des techniques appropriées pour extraire les paramètres souhaités des échantillons collectés afin d'obtenir l'information.

Dans cette thèse, nous nous concentrons principalement sur l'estimation des paramètres dans deux scénarios, qui sont l'estimation de la direction des arrivées (DOA) dans le domaine spatial et l'estimation de la fréquence dans le domaine temporel. La DOA et la fréquence sont deux paramètres importants dans de nombreuses applications. Dans le scénario spatial, le réseau linéaire uniforme (ULA), dont l'espacement entre les éléments voisins est fixé à la moitié de la longueur d'onde, est l'une des géométries de réseau couramment utilisées pour l'estimation de la DOA. Mais le nombre maximum de sources détectables est limité par le nombre de capteurs dans le ULA. Lorsque le nombre de sources devient important, le coût du matériel nécessaire pour un ULA est élevé car il faut plus de capteurs.

Dans le scénario temps ou fréquence, les approches classiques exigent de collecter des échantillons à un taux d'échantillonnage qui correspond à deux fois la fréquence maximale du signal. Cependant, dans l'industrie du sans-fil de nos jours, la fréquence des signaux pourrait être distribuée dans une très large gamme et elle pourrait inclure des signaux de très haute fréquence. Cela constitue un défi sur le plan matériel.

Pour réduire le coût du matériel, une stratégie prometteuse est la configuration basée sur un échantillonnage non uniforme, dans l'espace ou dans le temps. Si la configuration d'échantillonnage non uniform ou sparse est correctement conçue, il est possible d'obtenir un ensemble de données virtuelles équivalant aux cas classiques, tels que l'échantillonnage à la fréquence de Nyquist dans le domaine temporel ou le ULA dans le domaine spatial. De cette manière, le coût du matériel peut être limité à un faible niveau par rapport au scénario conventionnel.

Après avoir construit un ensemble de données virtuelles, de nombreuses techniques peuvent être appliquées pour estimer les paramètres comme par exemple les techniques de sous-espace MUSIC ou ESPRIT, de formation voies, ou encore des techniques de compressive sensing. En fait, ces techniques ne sont pas directement applicables aux échantillons directs de données. Un prétraitement doit être opéré pour obtenir un ensemble de données virtuelles afin de pouvoir appliquer les techniques d'estimation des paramètres. Dans cette thèse, notre but principal est d'étudier l'échantillonnage "sub-nyquist" afin de mettre en œuvre l'estimation de paramètres avec un coût moindre en termes de capteurs ou d'échantillons. La méthode MUSIC sera privilégiée dans notre étude.

Les techniques basé sur le principe de sparse sensing permettent de réduire le coût du matériel. Parmi ces techniques récemment proposées, la détection coprime et la configuration de détection nested attirent de plus en plus l'attention en raison de leurs avantages, notamment un faible taux d'échantillonnage, la possibilité d'une expression analytique et une mise en œuvre matérielle facile. De nombreux travaux appliquant l'échantillonnage coprime pour l'estimation des paramètres ont été proposés ces dernières années, dans le domaine temporel et spatial.

La théorie de la détection exploite principalement les intercorrélations entre différents échantillons pour estimer les paramètres souhaités. Pour analyser les intercorrélations, on considère généralement la matrice de covariance utilisant des statistiques de second ordre ou la matrice des cumulants utilisant des statistiques d'ordre supérieur. Il est bien établi que la matrice de covariance ou la matrice des cumulants contiennent des éléments qui correspondent à différents retards. Si ces éléments sont correctement sélectionnés et

ordonnés, il est possible de construire une configuration virtuelle similaire au scénario classique. Par exemple, en utilisant l'échantillonnage coprime dans le domaine temporel, on peut obtenir un ensemble de données d'échantillonnage virtuelles du taux de Nyquist avec beaucoup plus d'échantillons que les échantillons coprime mesurés physiquement. Cet ensemble de données virtuelles est appelé "coarray". En fonction de la manière dont les intercorrélation est calculée, le coarray peut être classé en difference coarray et sum coarray.

Dans cette thèse, nous nous concentrons sur la technique d'échantillonnage coprime pour l'estimation de la fréquence, tandis que le réseau coprime et réseau nested array sont considérés pour l'estimation de la DOA. Grâce à ces stratégies de détection et d'échantillonnage non uniformes, le coût du matériel peut être réduit. En d'autres termes, avec peu de mesures, nous pouvons obtenir un degré de liberté élevé (DOF) et détecter plus de sources que le nombre d'échantillons ou le nombre de capteurs. Les principaux travaux de cette thèse sont résumés ci-dessous.

(1) Nous étudions d'abord le schéma d'échantillonnage coprime pour l'estimation de la fréquence. Nous avons constaté que l'échantillonnage coprime pouvait échouer dans des conditions spécifiques en pratique, qui correspondent aux paramètres du signal et aux paramètres du système d'échantillonnage. La matrice de covariance souffre d'une perte de propriété diagonale dans ces conditions et le sous-espace du signal et le sous-espace du bruit sont contaminés. Pour résoudre ce problème, nous proposons un nouveau schéma d'échantillonnage basé sur le principe coprime en introduisant des retards aléatoires avant chaque bloc d'échantillonnage.

(2) Nous proposons une technique d'interpolation pour combler les éléments manquants dans le schéma de difference coprime. La propriété des éléments manquants est d'abord modélisée. Ensuite, nous concevons une technique à taux multiples pour obtenir plusieurs ensembles de données différents, où les éléments manquants du difference-coarray original sont inclus dans les difference-coarrays qui correspondent à différents ensembles de données à taux multiples. L'interpolation est réalisée en sélectionnant ces éléments et le difference-coarray résultant devient alors un ULA virtuel sans trous. En outre,

nous prouvons que si les paramètres à taux multiples sont correctement conçus, aucun processus d'échantillonnage supplémentaire n'est nécessaire, de sorte que notre proposition n'entraîne aucune charge d'échantillonnage supplémentaire pour les échantillonneurs physiques.

(3) Une autre méthode permettant de combler les éléments manquants dans le difference-coarray est conçue pour l'estimation de la DOA à l'aide de reseaux coprime. Nous analysons la propriété des éléments manquants et caractérisons avec une structure triangulaire. De plus, certains capteurs du coprime array se révèlent redondants, ce qui implique que la suppression de ces capteurs ne changera pas la structure du différence-coarray. Nous réorganisons ces capteurs redondants afin de combler au maximum éléments manquants dans la matrice de différences. Les DOFs peuvent être augmentés avec notre proposition. De plus, l'effet de couplage mutuel est limité avec le réarrangement puisque les capteurs réarrangés sont situés à des positions plus espacées.

(4) Nous considérons également l'estimation de la DOA dans un scénario de détection active avec une configuration de réseau éparse. Alors que la plupart des méthodes existantes considèrent les statistiques du deuxième ordre dans le système de détection active à entrées et sorties multiples (MIMO), nous introduisons des statistiques du quatrième ordre pour le coprime array de détection active afin de construire un réseau virtuel de différences du quatrième ordre de la somme (4-DCSC). Nous prouvons que le 4-DCSC est équivalent à appliquer deux fois le réseau de différences d'ordre 2 et une fois le réseau de sommes. Cela permet d'étendre encore l'ouverture de l'ULA virtuel et d'obtenir des DOFs élevés. La propriété du 4-DCSC est également étudiée.

(5) Étant donné que le coprime array est conçu pour générer des matrices de différence de second ordre, ses DOFs dans le 4-DCSC sont limités et des améliorations supplémentaires sont possibles. Nous proposons une nouvelle géométrie de réseau pour le 4-DCSC. Nous reformulons le problème du 4-DCSC en deux problèmes distincts : un problème de sum-coaaray du quatrième ordre (4-SC) et un problème de différence-coarray du deuxième ordre. Nous optimisons le problème 4-SC en le modélisant comme un problème de type postage stamp problem. Ensuite, le problème de différence-coarray d'ordre deux est

formulé comme un problème de nested array. La géométrie que nous proposons permet d'obtenir des DOFs extrêmement importants par rapport aux réseaux coprime et autres configurations.

Nos travaux fournissent une illustration détaillée de l'estimation des paramètres souhaités avec des configurations éparses bien conçues. Nous optimisons l'estimation du point de vue de l'algorithme et évitons d'introduire une charge importante dans le matériel. Si nous pouvons résumer nos travaux en une phrase, ce sera «Difference makes difference, less is more.»

Abstract(English version)

Array signal processing techniques are widely utilized in many application scenarios, such as radar, sonar, satellite, navigation, wireless communications. Considering one conventional scenario, multiple sensors or multiple samplers are properly distributed to collect measurements of the surrounding environment. Generally, the desired information is buried in the measured data contaminated by noise. It is then necessary to develop some appropriate techniques to extract the desired parameters from the collected samples in order to obtain the information.

In this dissertation, we mainly focus on parameter estimation in two scenarios, which are direction of arrival (DOA) estimation in the spatial domain and frequency estimation in the temporal domain. DOA and frequency are two important parameters in many applications. In the spatial scenario, uniform linear array (ULA), whose inter-element spacing is set to be no more than half of the wavelength to avoid angle ambiguity, is one of the commonly used array geometries for DOA estimation. But the maximum number of detectable sources is limited by the number of sensors in ULA. When the number of sources becomes large, high hardware cost will be required in ULA because more sensors are required.

In time or frequency scenario, the conventional approaches require to collect samples under sampling rate which corresponds to two times the maximum frequency of signal.

This is to avoid frequency aliasing according to the well known Nyquist rate sampling theory. However, in the wireless industry nowadays, the frequency of signals could be distributed in a very wide range and it may include signals of very high frequency. This will bring challenge to the hardware.

To reduce the hardware cost, a promising strategy is the sparse sensing configuration, including sparse array in spatial domain and sparse sampling in time domain. If the sparse configuration is properly designed, it is possible to obtain a virtual data set equivalent to the conventional cases, such as Nyquist rate sampling in time domain or half-wavelength ULA in spatial domain. By doing so, the hardware cost can be maintained at a low level compared with the conventional scenarios.

After constructing the virtual data set, many techniques can be applied to estimate the desired parameters, such as, subspace techniques including MUSIC and ESPRIT, or beamforming methods, compressive sensing technique. Since these techniques are not directly applied to the physical measurements, they need to be reformulated to adjust the virtual data set. In this dissertation, our main goal is to properly design the sparse configuration and to estimate the parameters with less hardware cost, we only consider the MUSIC technique in our work.

The sparse sensing based techniques allow reducing the hardware cost. Among these recently proposed theories, coprime sensing and nested sensing configuration attract increasing attention due to their benefits, including low sampling rate, closed-form expression, and easy for hardware implementation. Many works applying coprime and nested sensing theory for parameter estimation have been proposed in the past few years, especially in the time domain and the spatial domain.

Sparse sensing theory mainly exploits the cross correlations between different samples to estimate the desired parameters. To analyze the cross correlations, the covariance matrix utilizing second order statistics or the cumulant matrix utilizing high order statistics are commonly considered. It is well established that the covariance matrix or the cumulant matrix contains elements corresponding to different lags. If these elements are properly selected and arranged, it is possible to construct a virtual configuration similar

to the conventional scenario. For instance, using coprime sampling in time domain, one can obtain a virtual Nyquist rate sampling data set with much more samples than the physically measured coprime samples. This virtual data set is named as coarray. Based on the way that the cross correlation is calculated, coarray can be categorized into difference coarray and sum coarray.

In this dissertation, we focus on the coprime sampling technique for frequency estimation, and on the coprime array and nested array for DOA estimation. With these sparse sensing and sparse array strategies, the hardware cost can be reduced. In other words, with few sparse measurements, we can still obtain high degrees of freedom (DOFs) and detect more sources than the number of samples or the number of sensors. The main contributions of this dissertation are summarized below.

(1) We first investigate the coprime sampling scheme for frequency estimation. We have found that the coprime sampling could fail under some specific conditions in practice, which are related to the signal parameters and the sampling system parameters. The covariance matrix suffers from diagonal property loss under these conditions and the signal subspace and noise subspace are contaminated. To address this problem, we propose a novel coprime based sampling scheme by introducing random delays before each sampling block.

(2) We propose an interpolation technique to fill the missing elements in the difference coarray of coprime sampling. The property of missing elements is first analyzed. Then we design a multi-rate countermeasure for coprime sampling such that several different sets of data can be obtained, where the missing elements of the original coprime difference coarray are included in the difference coarrays corresponding to different sets of multi-rate data. The interpolation is accomplished by selecting these elements and the coprime difference coarray becomes a hole free virtual ULA. Furthermore, we prove that if the multi-rate parameters are properly designed, no extra sampling process is required such that our proposition brings no extra sampling burden to hardware samplers.

(3) Another method to fill the missing elements in coprime difference coarray is designed for DOA estimation with coprime array. We analyze the property of the missing

elements and describe them with a triangle-like structure. Furthermore, some sensors in coprime array are shown to be redundant, which implies that the removal of these sensors will not change the structure of the difference coarray. We rearrange these redundant sensors to new position to fill the missing elements in the original difference coarray. The DOFs can be increased with our rearrangement. Moreover, the mutual coupling effect is limited with the rearrangement since the rearranged sensors are located at sparser positions.

(4) We also consider the DOA in active sensing scenarios with sparse array configuration. While most of the existing methods consider second order statistics in the active sensing multi input multi output (MIMO) system, we introduce fourth order statistics for active sensing coprime array to construct fourth order difference coarray of sum coarray (4-DCSC). We prove that the 4-DCSC is equivalent to apply the second order difference coarray twice and the sum coarray once. This results in further extension of the virtual ULA aperture and high DOFs can be obtained. The property of 4-DCSC is also investigated.

(5) Since coprime array is designed for generating second order difference coarray, its DOFs in 4-DCSC are limited and further improvement is possible. We propose a novel sparse array geometry for 4-DCSC. We reformulate the 4-DCSC problem into two separate problems: a fourth order sum coarray (4-SC) problem and a second order difference coarray problem. We optimize the 4-SC problem by modeling it as a postage stamp problem. Then the second order difference coarray problem is formulated as a nested array problem. Our proposed geometry can achieve extremely large DOFs compared with coprime array and other sparse array configurations.

Our works provide detailed illustration about estimating the desired parameters with properly designed sparse configurations. We optimize the estimation from the algorithm aspect and avoid introducing much burden to the hardware. If we can summarize our works in one sentence, it will be «Difference makes difference, less is more.»

Table of Contents

List of Figures

List of Tables

Publication list

Published papers:

[1] Fu Z, Chargé P, Wang Y. Coprime sampling with embedded random delays[J]. Signal Processing, 2019, 158: 150-155.

[2] Fu Z, Chargé P, Wang Y. Multi-rate coprime sampling for frequency estimation with increased degrees of freedom[J]. Signal Processing, 2020, 166: 107258.

[3] Fu Z, Chargé P, Wang Y. Fourth Order Cumulant Based Active Direction of Arrival Estimation Using Coprime Arrays[C] ICASSP 2020-2020 IEEE International Conference on Acoustics, Speech and Signal Processing (ICASSP). IEEE, 2020: 4547-4551.

[4] Fu Z, Chargé P, Wang Y. A virtual nested MIMO array exploiting fourth order difference coarray[J]. IEEE Signal Processing Letters, 2020: Paper SPL-28305-2020.

Submitted paper:

Zhe, Fu, Pascal Chargé, and Yide Wang. "Rearranged Coprime Array to Increase Degrees of Freedom and Reduce Mutual Coupling" Submitted to Elsevier Signal Processing

INTRODUCTION

Array processing background

Along with the development of communication technology and wireless application, array signal processing plays an important role in many applications, such as radar, sonar, navigation, wireless communication (fifth generation communication, massive MIMO systems, mmWave communication), etc.. Data measured from sensor arrays allows to collect information of surrounding environment, including spatial and temporal information. By exploiting proper array signal processing techniques, one is able to extract information buried in the measured data and obtain the estimation of desired parameters.

Among these applications, the conventional estimation algorithms are mostly considered under the Nyquist rate sampling assumption for the temporal scenario, or the uniform linear array (ULA) assumption for the spatial cases (with inter-element spacing no more than half of the wavelength) to avoid estimation ambiguity. However, with the rapid technology innovation, higher sampling rate or more sensors are required in some applications. This could cause challenge to the limited physical hardware resources, including power, bandwidth, synchronization between sensors, number of sensors, etc.. On the other hand, the amount of measured data is also increased when more sensors are utilized or higher sampling rate is implemented, which introduces high complexity for the estimation techniques. It naturally comes the following questions: Can we reduce the cost? Is it possible to limit the amount of data? Can we breakthrough the Nyquist rate limitation in temporal scenario, or the ULA limitation in spatial case?

Fortunately, sparse sensing and sparse arrays provide promising solution to these problems. They allow to recover desired information with some representative sparse samples. With properly designed sparse configurations, it is possible to equivalently construct vir-

tual samples with Nyquist rate or a virtual half wavelength spacing ULA by using few sparse samples or sparse array sensors. In this dissertation, our general focus is to investigate the sparse temporal sensing for frequencies estimation in spectrum sensing domain and the sparse array for direction of arrival (DOA) estimation in spatial domain. More specifically, we consider the coprime sensing for frequencies estimation and seek for further improvement. In spatial domain, we focus on the increase of degrees of freedom (DOFs) by utilizing the coprime array and nested array. In this introductory chapter, we mainly revisit the history of spectrum sensing and DOA estimation. More techniques which are closely related to our work are reviewed in the state-of-arts chapter.

Spectrum sensing

Motivation

Radio spectrum is one of the key resources of the wireless communication industry. The conventional static mechanism for spectrum management is to allocate a license to one device in a specific frequency band for a given period. By doing so, different devices will not conflict with each other in the same frequency band at the same period. Accompanied with the strong development of communication techniques and the exponential increase of wireless devices, the demand for radio spectrum increases rapidly while the spectrum resource remains limited. A histogram of number of cellular subscriptions is provided in Figure 1. It becomes more and more obvious that the static management scheme cannot accommodate the requirement of increasing number of wireless devices. The spectrum shortage problem has become a bottleneck which constraints the development of the wireless communication industry.

While it becomes hard to allocate free spectrum to new devices, it should be noticed that the licensed spectrum allocated to specified users is not always efficiently utilized. As shown in Figure 2, in a wide frequency spectrum band, only a few sub-bands are utilized at a specific period while other sub-bands remain unoccupied. In other words, the licensed spectrum is rarely continuously used across the whole temporal and spatial domain. This

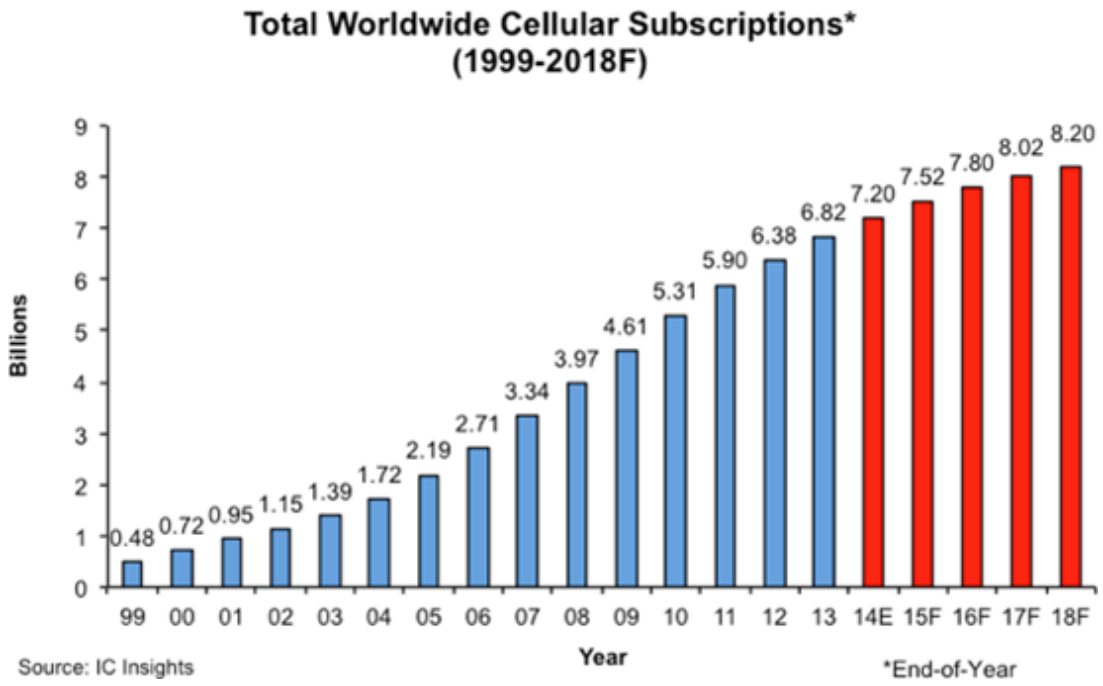

Figure 1 – Increasing number of worldwide cellular subscriptions from 1999 to 2018

is mainly because one specific frequency band is allocated to one device and the device will not occupy the frequency band when it is deactivated. To optimally utilize the spectrum opportunities, a promising solution is using cognitive radio [1–3], which allows secondary users to access to the licensed spectrum band when the primary user is absent.

To be more specific, we consider the cognitive radio concept defined by the Federal Communication Commission in this dissertation: *A radio or system that senses its operational electromagnetic environment and can dynamically and autonomously adjust its radio operating parameters to modify system operation, such as maximize throughput, mitigate interference, facilitate interoperability, access secondary markets [4, 5].* Cognitive radio mainly includes the following parts: spectrum sensing, where the available frequency spectrum bands are detected; decision, where the system determines the spectrum sharing strategy for secondary users; mobilization, where the available spectrum bands are allocated to the secondary users; sharing, where the secondary users access to the allocated spectrum bands. Among these parts, spectrum sensing plays a fundamental role since other parts are based on the assumption that the frequency spectrum bands are correctly

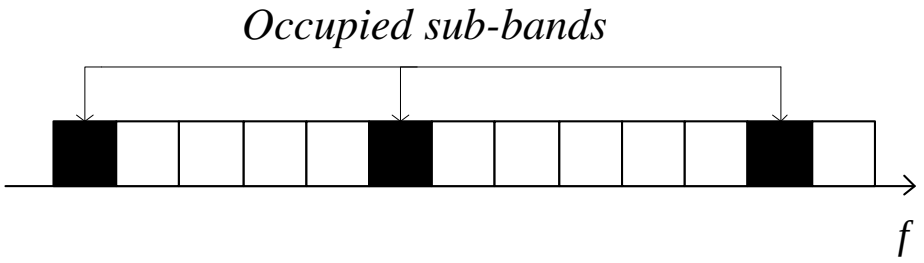

Figure 2 – Sparse occupancy of sub-band in wide frequency range.

detected.

Traditionally, spectrum sensing is achieved by detecting the spectrum usage over time, measuring the energy over the spectrum band, discovering the frequency availability over space, investigating the existence of primary users. While secondary users seeking for spectrum opportunity, it may cause interference to the primary users. In the case of very week primary user signal, the interference resulted by the secondary users should be kept at a minimal level.

Spectrum sensing techniques

Many techniques have been developed to dynamically detect narrow frequency spectrum bands. In [6–11], estimators based on energy detectors are proposed. The signals are captured and measured by comparing with a given energy threshold. Energy based estimators have low complexity and they don't require prior knowledge of the signals [12]. These algorithms are mainly evaluated by two criteria:

Probability of detection, which indicates the probability of detecting a correct signal when it occurs;

Probability of false alarm, the probability that the estimators consider the frequency spectrum being utilized while actually it is unoccupied.

However, energy based estimators strongly rely on the energy threshold and the noise level. The performance could be degraded in the low signal to noise ratio (SNR) scenarios

[13].

Another research direction is to exploit the cyclostationarity features of signals to determine the existence of primary users. Most artificial signals hold some cyclic features corresponding to channel coding, symbol rate, etc. [14, 15]. Given some prior information of the cyclic properties of signals, estimator is able to detect frequency opportunities by capturing the cyclostationarity or signal statistics (including time domain and frequency domain) [16–22]. Different from the power spectral density, cyclic properties can help to distinguish the noise from the signals since the noise is normally wide sense stationary while the modulated signals are cyclostationary.

If the prior knowledge of the primary users is perfectly known, including the spectral properties such as the central frequency, bandwidth, and the modulation property, frame format property, etc., the optimal estimator for spectrum sensing is the matched filter based estimators [23–26]. These estimators can maximize the SNR and require short period to achieve a good probability of detection for a given probability of false alarm. But on the other hand, the prior knowledge of primary users required for the matched filter may not be satisfied in practical scenarios [8]. And the implementation complexity could be remarkably increased due to several implementation modules, for instance, the demodulate part, synchronization between filters, etc. [27].

Multi-taper estimators are another type of estimators similar with the matched filter estimators. Its complexity is lower than the matched filter while it is nearly optimal [26, 28]. The Slepian sequences, which are orthonormal and have maximal energy in the main lobe, are utilized as filter coefficients [14]. Other spectrum sensing techniques could be found in the literatures, including Random Hough transform estimator [29], eigenvalue based blind estimator [30].

The above techniques are well adopted in narrowband scenario. In practice, one needs to deal with a wide spectrum band in many scenarios. The narrowband techniques can not be directly exploited in the wideband case since they consider the whole spectrum band as one and make binary decision. This will degrade the spectrum sharing efficiency because the whole spectrum band will be considered occupied even only one sub-band

within the whole spectrum band is occupied. Other available sub-bands can not be sensed and shared. Another important aspect for wideband spectrum sensing is that the sampling rate is very high considering the Nyquist sampling theory [31].

A direct approach for wideband spectrum sensing is to exploit high performance analog-to-digital converter (ADC) to detect the wide spectrum band. By dividing the wide band into several sub-bands [32], one can apply Fast Fourier transform to categorize the sampled data into multiple frequency domains to detect the information about the presence of the primary user [33]. Wavelets based methods can also be utilized to locate the discontinuities of power spectral density between neighboring occupied sub-bands and available sub-bands [34]. As a result, high performance ADC is required, which could be hardware expensive and with high energy consumption.

Direction of arrival estimation

Motivation

DOA estimation is referred to as estimating the arriving angle of the impinging electromagnetic signals or locating the direction of source targets as shown in Figure 3. It has a wide range of applications in sonar, radar, navigation, surveillance, wireless communications. Data measured by sensor arrays are exploited to extract spatial direction information of the received signals.

DOA sensor array traditionally can be categorized into two major types: passive sensing array and active sensing array. A passive sensing array consists of only receive sensors which are used for receiving the impinging electromagnetic signals. Active sensing array consists of transmit array and receive array. Transmit array emits multiple narrowband sequentials from different sensors. These transmissions are reflected from the targets and received by the receive array.

There are several kinds of array geometries that are well designed for DOA estimation, such as linear array, circular array [35], planar array [36]. The linear array is one of the most commonly adopted array since it is one dimension and easy to implement. In this

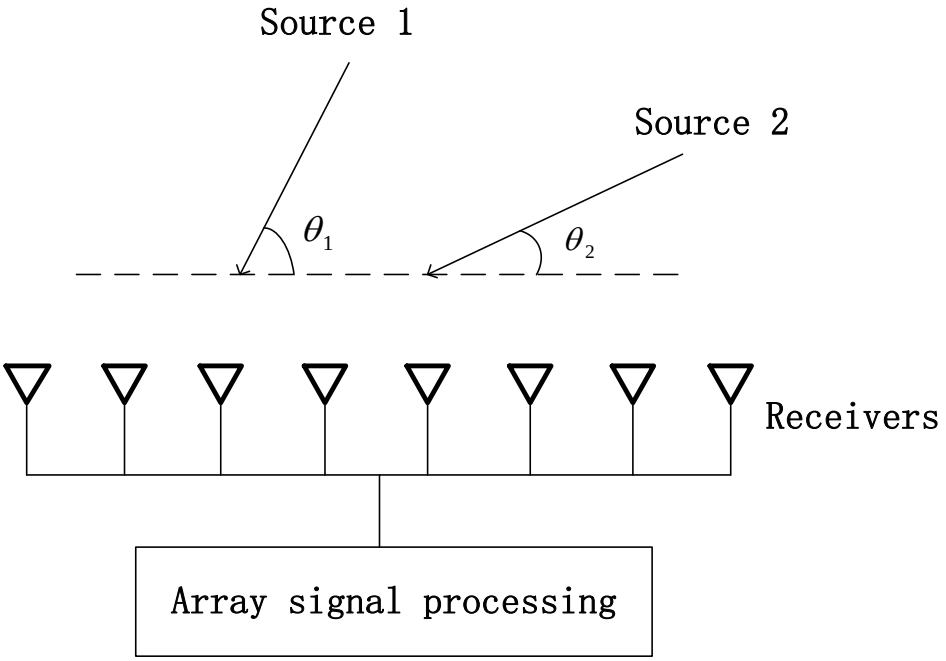

Figure 3 – DOA estimation with receiver array.

dissertation, we focus on the linear array for both passive sensing and active sensing cases. One most well known linear array is the uniform linear array (ULA) with spacing between neighboring sensors is no greater than half the wavelength of impinging signals to avoid the spatial spectrum ambiguity.

Subspace based DOA estimation techniques

DOA estimation has received significant amount of attentions for decades. Plenty of techniques have been proposed for different applications. Beamforming methods for DOA estimation can be considered as spatial filters. They include classical beamforming [37], Capon beamforming [38], linear prediction [39]. Classical beamforming technique is equivalent to a Fourier transform of outputs, which means calculation time is short. However, the sidelobes can degrade the estimation performance if several signals coexist. The sidelobes effect in the coexistence of several signals is taken into account in the Capon beamforming [40] to increase the performance.

In 1960s, linear prediction method which minimizes the mean square prediction error of observations is introduced in DOA estimation. Other linear prediction based methods are then developed, including backward linear prediction, forward-backward linear prediction, autoregressive estimator [41–43]. However, linear prediction methods have long calculation time and the resolution is limited by interference and noise.

In 1980s, another type of technique is proposed to promote the DOA estimation, which is the subspace based technique. The subspace is obtained with the eigenvalue decomposition of the covariance matrix of received signals. It can be categorized into signal subspace and noise subspace where the two subspaces are orthogonal to each other. A method named estimation of signal parameters via rational invariance technique (ESPRIT) [44] is proposed to exploit the signal subspace for estimating DOA. ESPRIT divides the array into two sub-arrays such that the steering vectors of the two sub-arrays can be related by a diagonal matrix. The DOA is evaluated under the assumption that two sub-arrays share the same signal subspace.

The multiple signal classification (MUSIC) method [45] chooses to exploit noise subspace for DOA estimation. It is based on the assumption that the source directional vectors are orthogonal to the noise subspace. However, MUSIC method needs to implement exhaustive search through the parameter space to achieve DOA estimation, which leads to high computation burden. The root-MUSIC method [46] is proposed to avoid the exhaustive search and fasten the calculation.

Main contributions

In this dissertation, we investigate on the frequency estimation for spectrum sensing problem and the DOA estimation problem in the context of sparse reconstruction theory. More specifically, we aim to promote the sparse sensing for frequency estimation utilizing coprime sensing technique to ease the hardware sampling burden. For DOA, the sparse linear array including coprime array and nested array are considered such that the number of sensors in sparse array can be decreased. It will be illustrated in the following chapters

that with sparse sampling or sparse array, the degrees of freedom (DOFs) can be increased by exploiting the concept of coarray, including difference coarray and sum coarray which can be equivalently considered as a virtual linear array with larger aperture. The main contributions are summarized as follows.

(1) We first investigate the coprime sampling scheme for frequency estimation. We have found that the coprime sampling could fail under some specific conditions in practice, which are related to the signal parameters and the sampling system parameters. Under these conditions, the covariance matrix has no more diagonal structure and the signal and noise subspaces are contaminated. To address this problem, we propose a novel coprime based sampling scheme by introducing random delays before each sampling block.

(2) We propose an interpolation technique to fill the missing elements in the difference coarray of coprime scheme. The property of missing elements is first summarized. Then we design a multi-rate countermeasure for coprime sampling to obtain several different sets of data such that the missing elements of coprime difference coarray are included in the difference coarrays corresponding to different sets of multi-rate data. The interpolation is accomplished by selecting these elements and the coprime difference coarray becomes a hole free virtual ULA. Furthermore, we prove that if the multi-rate parameters are properly designed, no extra sampling process is required and our proposition brings no extra sampling burden to the hardware samplers.

(3) Another method to fill the missing elements in coprime difference coarray is designed for DOA estimation with coprime array. We analyze the property of the missing elements and describe them into a triangle-like structure. Furthermore, some sensors in coprime array are shown to be redundant, implying that the removal of these sensors will not modify the structure of difference coarray. We rearrange these redundant sensors to new positions to fill the missing elements in the difference coarray such that the DOFs can be greatly increased. Moreover, the mutual coupling effect is reduced with the rearrangement since the rearranged sensors are located at sparser positions.

(4) We also consider the DOA estimation in active sensing scenario with sparse array configuration. While most of the existing methods consider second order statistics in

the active sensing multi input multi output (MIMO) system, we introduce fourth order statistics for active sensing coprime array to construct fourth order difference coarray of sum coarray (4-DCSC). We prove that the 4-DCSC is equivalent to apply the second order difference coarray twice and the sum coarray once. This results in further extension of the virtual ULA aperture and high DOFs can be obtained.

(5) Since coprime array is designed for generating second order difference coarray, its DOFs in 4-DCSC are limited and further improvement is possible. We propose a novel sparse array geometry for 4-DCSC. We reformulate the 4-DCSC problem into two separate problems: a fourth order sum coarray (4-SC) problem and a second order difference coarray problem. We optimize the 4-SC problem by modeling it as a postage stamp problem. Then the second order difference coarray problem is formulated as a nested array problem. Our proposed geometry can achieve extremely large DOFs compared with coprime array and other sparse array configurations.

Thesis organization

The remainder of this dissertation is organized as follows. In Chapter 1, we first review the state of the art for frequency estimation in spectrum sensing using sparse sensing techniques, as well as DOA estimation using sparse array. Then we introduce the coarray based signal model and the coarray based MUSIC estimator. Chapter 2 provides our propositions using coprime sampling. The diagonal property loss phenomenon is first illustrated before the random delay proposition. And the multi-rate sampling scheme is elaborated under the assumption that the diagonal property loss phenomenon will not happen.

Then we explain the holes filling proposition for DOA estimation with coprime array by rearranging physical sensors in Chapter 3. The property of holes are discussed and the holes-triangle structure is proposed to expound our proposition. In Chapter 4, we switch our focus to active DOA detection. The fourth order cumulants are introduced to coprime array and the property of 4-DCSC is investigated. Then we consider the optimization

problem of sparse array in the 4-DCSC scenario and propose a nested array based solution to enhance the number of DOFs.

Chapter 1

State of the art

1.1 Introduction

In this chapter, we review the sparse sensing techniques for frequency estimation in spectrum sensing, including the coprime sampling, nested sampling, etc. These sparse configurations are also adopted in DOA estimation. Possible algorithms for reconstructing sparse samples and estimating the parameters could be compressive sensing, MUSIC, ESPRIT, etc. Since our main concern is the sparse configuration, we consider MUSIC for both frequency and DOA estimations without loss of generality. The coarray based signal model will also be introduced in this chapter. Since the coarray is a virtual array, the MUSIC method is reformulated to a coarray based MUSIC.

1.2 Spectrum sensing using sub-Nyquist sampling

1.2.1 Sub-Nyquist sampling techniques

As discussed above, the Nyquist sampling rate could be extremely high and the number of collected samples could be huge if the sampling frequency is very high, especially in the wideband frequency scenario. An example of Nyquist rate sampling data is shown in Figure 1.1. To address the high sampling rate burden corresponding to the highest frequency, sampling at a lower rate is of importance. Frequency mixing technique can be adopted to transform the desired wide spectrum band to a lower frequency domain such that the conventional narrowband techniques can be directly exploited [47]. Filter band method exploits a prototype filter to estimate the baseband of signal. Other bands of

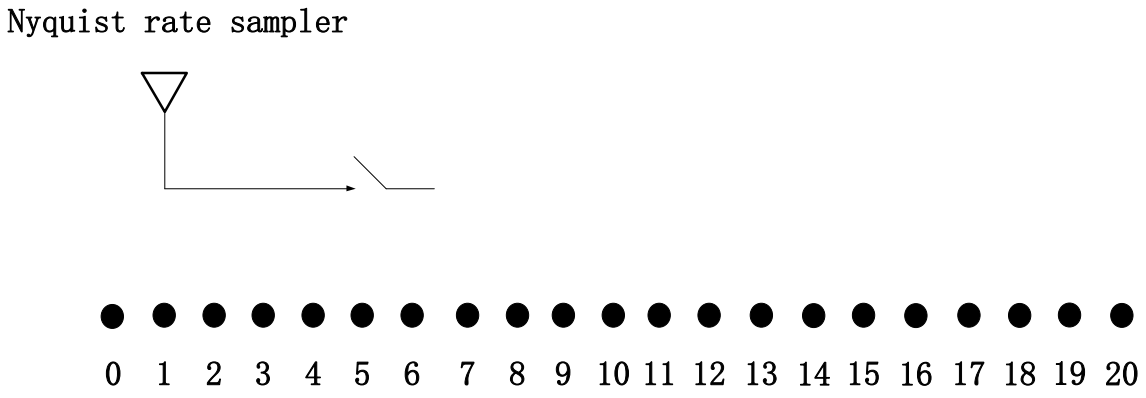

Figure 1.1 – Data obtained with Nyquist sampler.

signal are separately transformed to lower frequency by modulating the prototype filter and then low-pass filtered [24].

Another solution for sub-Nyquist rate sampling is multichannel based estimator. Modulated wideband converter (MWC) [48, 49] multiplies the analog signal from multiple channels with a periodic waveform. The acquired data is processed by low pass filters and then sampled at a rate significantly lower than the Nyquist rate. Multicoset sampling strategy obtains samples from multiple channels by properly tuning the sampling parameters in different channels. It can be equivalently considered as selecting part of sparse samples obtained by Nyquist rate or even higher rate [50, 51].

Notice that the aim of spectrum sensing is to detect the empty frequency bands, which indicates that there could exist sparseness in the whole frequency band of interest considering the low spectrum utilization. Compressive sensing techniques can be introduced as a promising solution for wideband spectrum sensing [52, 53]. Inspiring by the compressive sensing theory, only few sub-Nyquist samples are required to extract the second order statistics of signals and the wideband signal can be reconstructed [54–56]. Compressive sensing techniques can also be combined with other spectrum sensing techniques to ease the sampling burden for hardware [57–59].

More recently, sparse sampling theory provides a promising strategy to decrease the sampling rate while achieving a high number of DOFs. This can be accomplished by using

the difference coarray to generate a virtual sampling data set. In the following, we will provide a detail review of sparse sampling configurations and the concept of difference coarray.

1.2.2 Subspace based MUSIC technique

We first introduce the general signal model under Nyquist rate sampling and the subspace based technique, named MUSIC, is employed for frequency estimation. Consider the following signal composed of D sinusoidal components buried in an additive noise

$$x(t) = \sum_{i=1}^{D} A_i e^{j(2\pi f_i t + \phi_i)} + \omega(t) \tag{1.1}$$

where A_i is the amplitude, f_i is the frequency of the i-th sinusoidal component, ϕ_i is the corresponding phase assumed to be uniformly distributed in range $[0, 2\pi]$ and independent from each other, and $\omega(t)$ is a zero mean additive white Gaussian noise, independent from the D sinusoidal components.

A Nyquist rate samplers operating at sampling interval T is utilized to sample the noise contaminated signal, with $\frac{1}{T} = 2f_{max}$ the Nyquist rate ($f_i < f_{max}$). Assume that K samples ($K > D$) are collected, the collected samples are organized in the following vector form

$$\mathbf{y}(t) = \sum_{i=1}^{D} \mathbf{a}_0(q_i) A_i e^{j\phi_i} + \mathbf{w} \tag{1.2}$$

where $\mathbf{a}_0(q_i) = [1, e^{jq_i\pi}, ...e^{jq_i\pi(K-1)}]^T$ and $q_i = 2f_iT = \frac{f_i}{f_{max}}$ is the normalized frequency with $q_i \in (-1, 1)$, $\mathbf{w}$ is the corresponding noise vector. The covariance matrix of the observed data vector is given by

$$\mathbf{R} = E[\mathbf{y}\mathbf{y}^H] = \sum_{i=1}^{D} A_i^2 \mathbf{a}_0(q_i)\mathbf{a}_0^H(q_i) + \sigma_n^2\mathbf{I} = \mathbf{A}_0\mathbf{R}_\mathbf{s}\mathbf{A}_0^H + \sigma_n^2\mathbf{I} \tag{1.3}$$

where $\mathbf{A}_0 = [\mathbf{a}_0(q_1) \quad \mathbf{a}_0(q_2) \quad ... \quad \mathbf{a}_0(q_D)]$ and $\mathbf{R}_\mathbf{s} = diag(A_1^2, A_2^2, ..., A_D^2)$, σ_n^2 is the noise power and $\mathbf{I}$ is the $K \times K$ identity matrix.

The eigenvalue decomposition of the covariance matrix $\mathbf{R}$ leads to

$$\mathbf{R} = \mathbf{U}\mathbf{\Sigma}\mathbf{U}^H = \mathbf{U}_s\mathbf{\Lambda}_s\mathbf{U}_s^H + \mathbf{U}_n\mathbf{\Lambda}_n\mathbf{U}_n^H \tag{1.4}$$

Here, $\mathbf{U}$ is composed of the signal subspace $\mathbf{U}_s$ and the noise subspace $\mathbf{U}_n$ matrices. And $\mathbf{\Sigma} = diag[\lambda_1, \lambda_2, ..., \lambda_K]$ is the diagonal eigenvalue matrix with its eigenvalue elements in descending order $\lambda_1 \geq \lambda_2 \geq ... \geq \lambda_K$. $\mathbf{\Lambda}_s$ is a diagonal matrix corresponding to the D largest eigenvalues and $\mathbf{\Lambda}_s$ corresponds to the remaining $K - D$ eigenvalues. Considering the orthogonality between the signal subspace (spanned by the steering vector) and the noise subspace, one can estimate the frequencies by searching the peaks of the MUSIC spectrum, given by

$$P_{MUSIC}(q) = \frac{1}{\mathbf{a}_0^H(q)\mathbf{U}_n\mathbf{U}_n^H\mathbf{a}_0(q)} \tag{1.5}$$

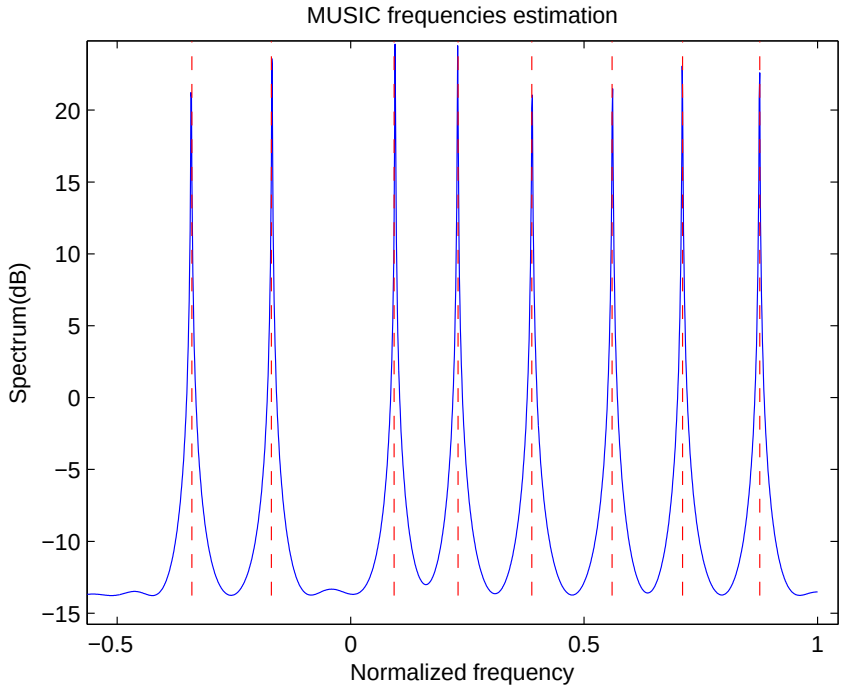

Figure 1.2 – MUSIC spectrum for frequency estimation with 8 different sinusoidal components, SNR=0dB.

After searching the whole parameter range, there will be some peaks near the frequencies of the signal and one can determine the estimated frequencies according to the peaks. An example of MUSIC spectrum is provided in Figure 1.2. The red discontinuous lines are the positions of the true frequencies of the signals. It can be seen that the peaks of MUSIC spectrum locate very close to the true frequencies.

1.2.3 Coprime sensing and other sparse sensing techniques

Recent advances in sparse theory inspire researchers to explore the possibility of reducing the sampling rate. Nested sampling mechanism employs two standard samplers for down sampling the data [60]. One sampler is required to collect few dense measure data at the Nyquist sampling rate and the other sampler is designed to acquire data at a rate much lower than the Nyquist rate. It will be illustrated in the following part that by exploiting the difference coarray, elements in the covariance matrix of sampled data can be equivalently selected to represent a set of Nyquist rate sampled data. For instance, with N_1 physical measurements from the dense sampler and $N_2 = N_1 + 1$ sparse physical measurements from the sparse sampler, nested sampling scheme is able to equivalently represent N_1N_2 virtual measurements obtained with the Nyquist rate. Minimum redundancy sampling [61] aims to search for optimal physical sampling strategy such that it can obtain a larger number of virtual measurements than nested sampling. This is achieved by increasing the number of consecutive elements in the difference coarray.

However, the nested sampling scheme collects some data at the Nyquist rate which still causes hardware complexity. In minimum redundancy sampling, the Nyquist rate sampling could be avoided but the samplers do not have closed-form expression for the physical measurement. When the number of measurements is high, searching for the optimal solution requires high computational cost since combinatorial search is required. Another sparse sampling mechanism named coprime sampling becomes attractive for frequency estimation due to its closed-form expression for sampling configuration and down converting sampling rate.

Coprime sampling scheme acquires measurement data using two standard samplers

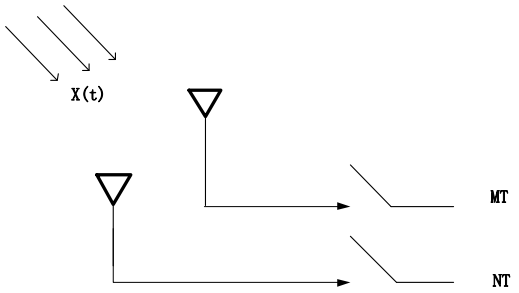

Figure 1.3 – Coprime samplers

[62], where one sampler is implemented with sampling interval MT and another with NT as shown in Figure 1.3. Here M, N are two coprime integers. It is obvious that if M, N are big, the sampling interval can be much larger than the Nyquist rate interval T. The collected data of two samplers can be arranged as shown in Figure 1.4. We denote samples within the period $[(k-1)MN, kMN)$ as a sampling unit, where k is a positive integer. In [63], multiple units from two samplers are combined as a sampling block to calculate the covariance matrix and the DOFs can be increased. In this dissertation, one of the most commonly used scenario, where one sampling unit from sampler 1 and two units from sampler 2, are considered as a sampling block. The data subsets from two samplers associated to the l-th ($l \geq 0$) block can be expressed as

$$x_M[Nl+n] = \sum_{i=1}^{D} A_i e^{j\left(\pi q_i M(Nl+n)+\phi_i\right)} + \omega(M(Nl+n)T) \tag{1.6}$$

$$x_N[Ml+m] = \sum_{i=1}^{D} A_i e^{j\left(\pi q_i N(Ml+m)+\phi_i\right)} + \omega(N(Ml+m)T) \tag{1.7}$$

where $1 \leq m \leq 2M-1, 0 \leq n \leq N-1$ are the indices of data.

The sampling signal vectors of the l-th block can be constructed with the above data

$$\mathbf{y}_M[l] = [x_M[Nl], x_M[Nl+1], ..., x_M[Nl+N-1]]^T \tag{1.8}$$

$$\mathbf{y}_N[l] = [x_N[Ml+1], ..., x_N[Ml+2M-1]]^T \tag{1.9}$$

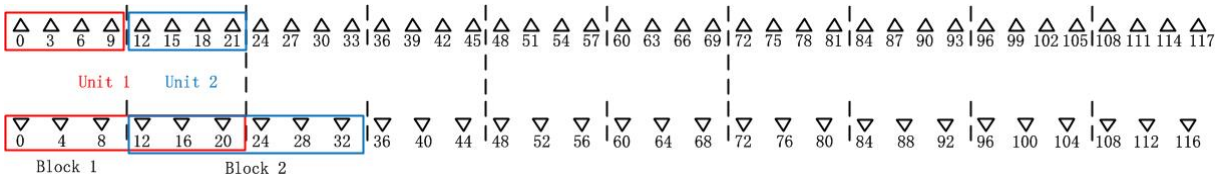

Figure 1.4 – Collected samples of two samplers with $M = 3, N = 4$.

Concatenating $\mathbf{y}_M[l]$ and $\mathbf{y}_N[l]$ leads to the following observed data vector

$$\mathbf{y}[l] = [\mathbf{y}_M^T[l], \mathbf{y}_N^T[l]]^T = \sum_{i=1}^{D} \mathbf{a}(q_i) A_i e^{j\phi_i} e^{j\pi q_i MNl} + \mathbf{w}[l] \tag{1.10}$$

with $\mathbf{a}(q_i) = [[1 ... e^{jq_i\pi M(N-1)}][e^{jq_i\pi N} ... \quad e^{jq_i\pi N(2M-1)}]]^T$. Calculating the covariance matrix

$$\mathbf{R}_\mathbf{y} = E[\mathbf{y}[l]\mathbf{y}[l]^H] = \mathbf{A}\mathbf{R}_\mathbf{s}\mathbf{A}^H + \sigma_n^2\mathbf{I} \tag{1.11}$$

We can categorize the elements of the covariance matrix into self correlations and cross correlations. Furthermore, we can derive that the self correlations of elements from the two samplers hold the following forms

$$\sum_{i=1}^{D} A_i^2 e^{jq_i M(n_j - n_k)} \tag{1.12}$$

$$\sum_{i=1}^{D} A_i^2 e^{jq_i N(m_j - m_k)} \tag{1.13}$$

where m, n are the indices of data. Similarly, the cross correlations of elements between the two samplers can be written as

$$\sum_{i=1}^{D} A_i^2 e^{jq_i[\pm(Mn - Nm)]} \tag{1.14}$$

It has been proved that the self correlation terms are all included in the cross correlation terms [64]. In the following, we only consider the cross correlation for simplification.

1.3 Second order difference coarray based MUSIC method

Before further discussion, we first define the second order difference coarray (2-DC).

Definition 1: For a given geometry specified by position set $\mathbb{S} = \{n_1, n_2, ..., n_K\}$, its 2-DC can be expressed as

$$\mathbb{D} = \{n_i - n_j \mid n_i, n_j \in \mathbb{S}\} \tag{1.15}$$

Observing the form of elements in the covariance matrix, we can find that they are similar with (1.1). The main differences are the magnitude A_i^2 instead of A_i and the sampling timing term $(Mn - Nm)$ instead of t. Vectoring the covariance matrix, we can obtain a vector

$$\mathbf{r} = vec(\mathbf{R_y}) = \sum_{i=1}^{D} p_i \mathbf{a}^*(q_i) \otimes \mathbf{a}(q_i) + \sigma_n^2 \mathbf{i} = \mathbf{A}_d \mathbf{p} + \sigma_n^2 \mathbf{i} \tag{1.16}$$

where $\mathbf{A}_d = \mathbf{A}^* \odot \mathbf{A}$, $\mathbf{p} = [p_1, p_2, ..., p_D]^T$ with p_i the power of i-th signal, $\odot$ denotes the Khatri-Rao product, $\otimes$ denotes the Kronecker product and $\mathbf{i} = vec(\mathbf{I})$. Notice that the term $(Mn - Nm)$ can include many integers from $-(2M-1)N$ to $(2M-1)N$ with $1 \leq m \leq 2M-1, 0 \leq n \leq N-1$. If we properly select the distinct elements and rearrange them, which can be expressed as

$$\mathbf{z} = \mathbf{F}\mathbf{r} = \mathbf{A}_c \mathbf{p} + \sigma_n^2 \mathbf{F}\mathbf{i} \tag{1.17}$$

Here, $\mathbf{F}$ is the selecting matrix [65], $\mathbf{z}$ is the virtual signal vector after rearrangement, which is commonly recognized as the difference coarray based virtual signal and $\mathbf{A}_c$ is the manifold matrix corresponding to the coarray. A graphic illustration of 2-DC with $M = 3, N = 4$ is provided in Figure 1.5. It can be observed that using $2M + N - 1$ data in block 1 as shown in Figure 1.4, we can equivalently obtain a set of data which ranges in $[-(2M-1)N, (2M-1)N]$. Most elements represented with solid circle in 2-DC can be selected from the covariance matrix while there are some missing elements represented

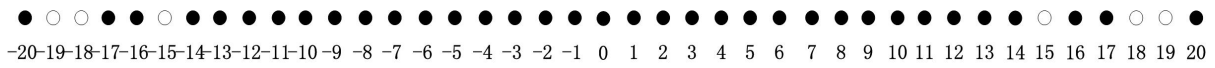

Figure 1.5 – Difference coarray of data from two samplers with $M = 3, N = 4$. • : elements selected from covariance matrix; ∘ : holes in 2-DC

with hollow circle. These missing elements are conventionally named "*hole*".

Then we can consider this 2-DC based virtual signal samples as Nyquist rate sampls with a few holes and the MUSIC method can be exploited. Notice that MUSIC method can only be used for a set of consecutive data, we only consider the longest central consecutive part and discard the inconsecutive part. When calculating the covariance matrix of the virtual signal, one will obtain a low rank matrix since the virtual signal vector is equivalent to a one snapshot sampling process. To recover the rank, we can use the well established spatial smoothing technique [66], which can be written as

$$\mathbf{R}_{ss} = \frac{1}{MN+M} \sum_{i=0}^{MN+M-1} \mathbf{z}_i \mathbf{z}_i^H \tag{1.18}$$

with $\mathbf{z}_i$ denotes the data in vector $\mathbf{z}$ from $-(MN+M-1)+i$ to i. Then the MUSIC method can be applied to $\mathbf{R}_{ss}$ to estimate the frequencies.

1.4 Direction of arrival estimation with sparse array

1.4.1 Passive sensing sparse array configurations

Similar with the Nyquist sampling in time and frequency domain, subspace based techniques are introduced to DOA estimation in spatial spectrum domain using ULA. A traditional ULA structure for DOA estimation is provided in Figure 1.6. Consider K sensors with position integer set $\mathbb{S} = \{n_1, n_2, ..., n_K\}$ with unit inter-element spacing $d_0 = \frac{\lambda}{2}$ the half wavelength of impinging signals, the received signal at the k-th sensor corresponding to direction θ_i can be given by

$$s_i(t) e^{j\frac{2\pi}{\lambda} n_k sin(\theta_i)} \tag{1.19}$$

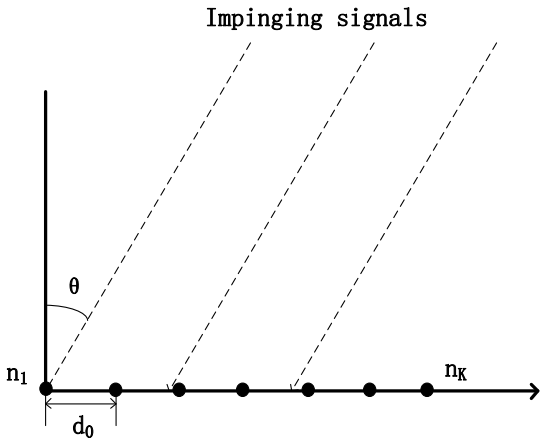

Figure 1.6 – Passive receiving ULA for DOA estimation.

where $s_i(t)$ is the i-th source signal. As derived above in the sparse sampling part, one can formulate the received signal into vector form and calculate the covariance matrix before applying the MUSIC method.

One key character of the ULA scheme is that its DOFs are limited by the number of sensors. The number of maximum resolvable sources is $K-1$ with K sensors. Sparse array configurations can break through this limitation by enlarging the inter-element spacing to a value which is multiple of d_0. For simplification, d_0 will be omitted in the following and the inter-elements spacing in sparse arrays is represented by a multiple integer.

Several sparse arrays have been proposed to estimate more sources than physical sensors, including the minimum redundancy array (MRA), minimum hole array (MHA), nested array, coprime array. The MRA, nested and coprime arrays follow the same spirit as sparse sampling in frequency domain. The MHA aims to find a strategy with minimum number of holes in the 2-DC, which requires similar combinatorial search as MRA in sparse sampling. In [67], Cantor array is designed to be hole-free and maximally economic, which means every sensor is essential to build the 2-DC. Composite singer array provides an iterative way to generate a robust sparse array [68]. Another sparse configuration considers maximum inter-element spacing constraint (MISC) [69] to maximize the length of consecutive part in the 2-DC. Under this criterion, the designed prototype can achieve

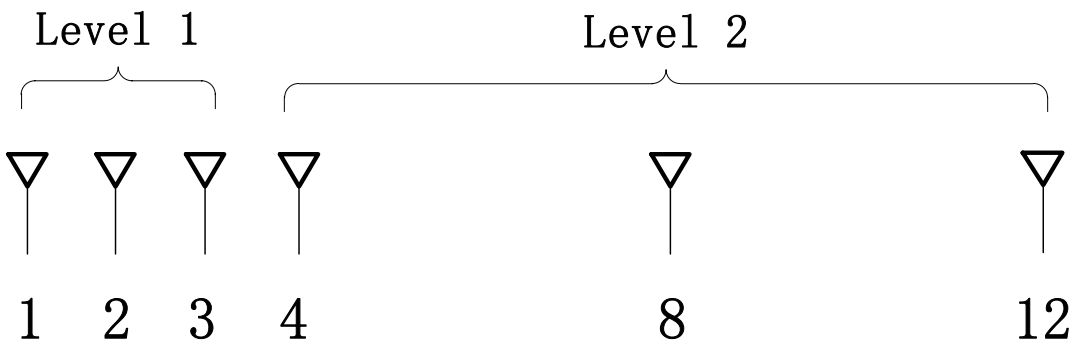

Figure 1.7 – Nested array with 6 sensors.

larger DOFs in the 2-DC. With less than 20 sensors, this MISC based geometry can achieve the same DOFs as MRA.

Nested array and coprime array attract increasing research interest in recent years due to their closed-form expression. The conventional coprime array is generalized to two types, which are coprime array with compressed inter-element spacing (CACIS) and coprime array with displaced subarrays (CADiS) [64]. The nested array and coprime array can be unified within the CACIS configuration since the nested array can be considered as a special case of coprime array with inter-element spacing of one subarray equals to d_0. An example of nested array is given in Figure 1.7. In general, for a given number of sensors, nested array could obtain a higher number of DOFs than coprime array with inter-element spacing larger than d_0. An attempt to improve the DOFs of nested array is illustrated in [70]. Augmented nested array (ANA) with four different geometries is proposed in [71] to further increase the DOFs.

However, as discussed above, the 2-DC of coprime array has some holes and the information in the inconsecutive part can not be directly utilized by the MUSIC method. An instinct solution is to adopt some interpolation methods to fill the holes and enlarge the consecutive part in the 2-DC. A multi frequency based mechanism is proposed in [72] to fill the holes. Multiple frequencies are properly chosen to generate several scaled versions of the original 2-DC and the holes can be selected from these coarrays to fill the original

2-DC. The matrix completion and Toeplitz matrix interpolation techniques are adopted in [73, 74]. In [75], nuclear norm minimization is proved to be a good convex solution for the coprime 2-DC interpolation problem. Zhou et al. [76] first divide the virtual coarray signals into multiple virtual measurements, which are considered as atoms, then the atomic norm minimization technique is applied to reconstruct the Toeplitz covariance matrix.

Another direction for filling the holes is to interpolate the holes from the physical array aspect. A k times extended coprime array is proposed to further increase the consecutive part in the difference coarray by increasing the M-elements sub-array to a (kM)-elements sub-array [77]. A complementary coprime array (CCA) mechanism is then added in the k times coprime array. Another approach expands the two sub-arrays of classical coprime array from one period subarray to multi-period subarray [78] to enlarge the consecutive coarray part. In [79], the inter-element spacing of classical coprime array is designed with two integers larger than M, N such that the redundancy of coarray elements is minimized and the consecutive coarray is extended. In [80, 81], by moving the physical array at a certain velocity, the cross correlation between the received signals before and after the array motions is used to fill the holes in the difference coarray.

1.4.2 DOA estimation considering mutual coupling in sparse arrays

In DOA estimation, it is well established that two closely located sensors could suffer from strong mutual coupling effect [82–84]. This effect becomes more significant as the inter-element spacing of two sensors gets smaller. Considering the mutual coupling in the received signal, we can write the signal vector as

$$\mathbf{x}_\theta(t) = \mathbf{C}\mathbf{A}_\theta\mathbf{s}(t) + \mathbf{n}(t) \tag{1.20}$$

where $\mathbf{C}$ is the mutual coupling matrix, $\mathbf{A}_\theta$ is the manifold matrix of sparse array and $\mathbf{s}(t)$ is the source signal vector. The entries of $\mathbf{C}$ can be very complicated in practice. In this dissertation, the considered array has a linear configuration. $\mathbf{C}$ can be approximately

represented by a B-band symmetric Toeplitz matrix [85, 86] whose entries are given by

$$\langle \mathbf{C} \rangle_{i,j} = \begin{cases} c_{|n_i - n_j|}, & \text{if } |n_i - n_j| \leq B \\ 0, & \text{otherwise.} \end{cases} \tag{1.21}$$

where $n_i, n_j \in \mathbb{S}$ and the magnitudes of coupling coefficients $c_0, c_1, ..., c_B$ meet the relations $|c_0| = 1 > |c_1| > ... > |c_B|$. The magnitudes of the coupling coefficients are assumed to be inversely proportional to their sensor separations, which can be written as

$$\frac{|c_k|}{|c_l|} = \frac{l}{k} \tag{1.22}$$

where l, k are positive integers indicating the position separation between the corresponding sensors. Many techniques have been developed to address the mutual coupling problem in ULA geometry [87–89]. In this dissertation, the sparse array geometry is considered and the mutual coupling in the 2-DC is mainly due to few closely distributed sensors in the physical array. For the sparsely distributed sensors, mutual coupling effect is at a low level and it may not be necessary to apply decoupling techniques to all sensors. Therefore, we consider the mutual coupling mitigating problem from another aspect in our work, which is to rebuilt the array configuration and enlarge the inter-element spacing between the closely distributed sensors.

1.4.3 DOA in active sensing

Apart from the passive sensing, many applications need to perform DOA estimation in an active sensing scenario, including military, satellite, aircraft detection and location. The multiple-input multiple-output (MIMO) radar with sparse array has been considered as a promising configuration for active array due to their equivalent sum coarray property to achieve high DOFs [90, 91]. Considering a MIMO radar with co-located transmit and receive arrays, we assume that the transmit and receive arrays are identical in this dissertation without loss of generality. An example of coprime MIMO is given in Figure 1.8 It should be noticed that our work can be easily extended to the case of distinct transmit

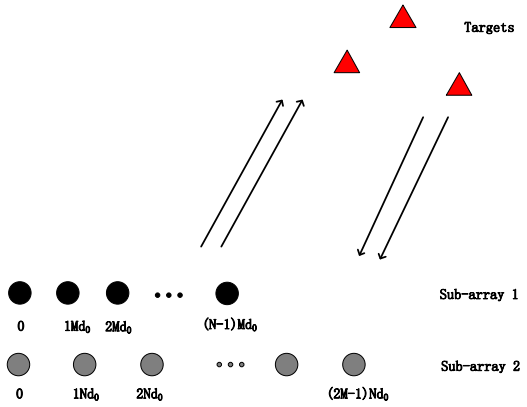

Figure 1.8 – Coprime MIMO structure.

and receive arrays.

Assuming D uncorrelated targets, multiple narrowband sequential transmissions from the transmit array impinge the targets and the reflected signals are captured by the receive array. The position of the K sensors of the MIMO radar is given by $\{n_1, n_2, ..., n_K\}$. To simplify the problem, the mutual coupling effect is not considered for the active radar in our work. The received signal vector is given by

$$\mathbf{x}_s(t) = \sum_{i=1}^{D} \mathbf{a}_t(\theta_i) \otimes \mathbf{a}_r(\theta_i) s_i(t) + \mathbf{n}(t) = \mathbf{A}_s \mathbf{s}(t) + \mathbf{n}(t) \tag{1.23}$$

where $\mathbf{a}_t(\theta_i), \mathbf{a}_r(\theta_i)$ are the steering vector of the transmit and receive arrays corresponding to the i-th target, $\mathbf{s}(t)$=$[s_1(t), s_2(t), ..., s_D(t)]^T$ is the source signal vector and $\mathbf{n}(t)$ is the noise vector. The manifold matrix $\mathbf{A}_s$ is denoted as

$$\mathbf{A}_s = [\mathbf{a}_s(\theta_1), ..., \mathbf{a}_s(\theta_D)] \tag{1.24}$$

where $\mathbf{a}_s(\theta_i)$=$\mathbf{a}_t(\theta_i) \otimes \mathbf{a}_r(\theta_i)$, whose elements are given by

$$e^{j\pi(n_i+n_j)\sin(\theta_i)} \tag{1.25}$$

with $n_i, n_j \in \mathbb{S}$. Then $\mathbf{x}_s(t)$ can be equivalent to the received signal in the receiver only

passive sensing case and one can follow the same process as discussed in the passive sensing part to estimate the DOA. Similar with 2-DC, for any two elements in $\mathbb{S}$, we can define their summation as the second order sum coarray (2-SC).

Definition 2: The 2-SC of $\mathbb{S}$ is the summation of two elements in $\mathbb{S}$, given by

$$\mathbb{S}_s = \{v = n_i + n_j \mid n_i, n_j \in \mathbb{S}\} \tag{1.26}$$

The coprime array configuration is adopted for the sparse MIMO radar to simultaneously detect coherent and uncorrelated targets in [92], where the transmit and receive arrays can be identical or distinct in different scenarios. To increase the DOFs, the second order difference coarray of sum coarray (2-DCSC) [93] is considered, where the 2-DC is applied to 2-SC to obtain further enhancement of DOFs. More recently, given distinct transmit and receive arrays, the array geometry optimization to achieve larger 2-DCSC is addressed for nested MIMO by designing a proper larger inter-element spacing of the receive array [94]. The inter-element spacing of the receive array in [94] is set as a scaled version of the 2-DC aperture of the transmit array, where the transmit array is no more identical as the receive array.

1.5 Second order statistics and high order statistics

The techniques discussed above mainly exploit the second order statistics property of signal. Apart from the second order statistics, higher order statistics cumulants can also be used for parameter estimation. The property of high order cumulants, saying $2q$ order, is analyzed in [95] and it is proved that the high order cumulants of a ULA can be considered as a virtual array with larger aperture. However, the virtual array concept proposed in [95] is different from the virtual array corresponding to difference coarray. Given a same ULA geometry, its virtual array configuration generated with the method of [95] could have different structures due to different choices of parameters, while the difference coarray has only one structure regardless of the choice of parameters.

To use the subspace based methods, the MUSIC method is modified to adjust the

virtual array of high order cumulants and the $2q$-MUSIC is present in [96]. It can detect a maximum of $q(N-1)+1$ statistically independent sources with a ULA having N sensors. Specifically, the fourth order cumulants attract increasing attention due to its immunity to Gaussian noise. Many works have introduced fourth order cumulants in ULA to improve the performance of DOA estimation [97–99].

Recently, the fourth order cumulants are investigated from another aspect. Similar to the utilization of 2-DC in parameter estimation, the high order difference coarray concept is introduced to achieve higher DOFs than the 2-DC [100] by adopting the high order cumulants. In [101], the coprime array is modified to achieve larger 4-DC by adding a third subarray with larger inter-element spacing. Similar operation is applied to the nested array as proposed in [100, 102]. The nested array is extended to include multiple level subarray, saying $2q$ level for $2q$ order difference coarray, with q a positive integer here. To further increase the consecutive DOFs in the coarray, a newly subarray is added and the inter-element spacing of the subarray is expanded according to the number of virtual sensors in the 2-DC [103, 104] of the original array.

1.6 Conclusion

In this chapter, we review the sub-Nyquist rate spectrum sensing methods and the sparse arrays for DOA estimation. The sub-Nyquist rate sampling can greatly ease the hardware sampling burden while the sparse arrays can reduce the cost for hardware sensors and also the mutual coupling effect. The idea of difference coarray is introduced to sub-Nyquist sampling and sparse arrays to increase the DOFs. By properly selecting the elements in the difference coarray, one is able to construct a virtual signal model having plenty of virtual samples or virtual sensors compared to physical measurements.

Many techniques can be adopted to the difference coarray based virtual signal model to extract the desired parameters. In this dissertation, we introduce the subspace based MUSIC method for further discussion. The coprime sampling scheme is adopted for frequency estimation due to its sparse sampling interval and easy implementation. Since the

MUSIC method performance is limited by the holes in coprime sampling scheme, several interpolation techniques for coprime scheme are reviewed from different aspects.

Apart from the coprime configuration, other sparse configurations including nested array, MRA, MHA are also reviewed in this chapter. We also introduce the application of sparse array in active sensing MIMO radar scenario. The sum coarray signal model is first formulated to increase the DOFs before applying the difference coarray model. Different from the sparse configurations designed for the passive sensing difference coarray, the sparse MIMO configurations considering both the sum coarray and difference coarray to achieve higher DOFs are also introduced. Then we present the high order statistics for the sparse configurations. Some sparse geometries designed for the fourth order cumulants based estimators are also reviewed.

In the following chapters, we will further present our works related to the above discussed parts.

Chapter 2

Spectrum sensing with coprime sampling using second order difference coarray

2.1 Introduction

In this chapter, we focus on the frequency estimation using coprime sampling scheme. Coprime sampling has been recognized as an attractive mechanism because it allows to significantly reduce the sampling rate. With two samplers sampling data at rate MT and NT, respectively, one can acquire two data sets as the example shown in Figure 1.4. However, the coprime sampling mechanism is based on the hypothesis of uncorrelated sinusoidal components, which is not always satisfied for a finite number of data samples, even if the different signals are statistically independent. For some specific conditions, the coprime sampling based technique completely fails. We will investigate this phenomenon in the first section of this chapter.

Our second work on coprime sampling focuses on the holes problem in 2-DC. We aim to fill the holes with an appropriately designed processing technique and without extra hardware requirement. We first show that the 2-DC can be easily scaled since it is related to the sampling rate. If one properly selects the sampling rate, it is possible to obtain a scaled version of the 2-DC which could contain some hole elements in the original 2-DC obtained by sampling rate MT and NT. We then propose a multi-rate coprime sampling method to fill all the holes. Furthermore, thanks to the fact that the sampling process

consists of several sampling blocks of data, we show that it is possible to avoid extra sampling hardware implementation if the multi-rate method is cleverly designed.

2.2 Signal model of coprime sampling

As discussed in previous chapter, data measured by two coprime samplers are arranged in vector form, given by

$$\mathbf{y}[l] = [\mathbf{y}_M^T[l], \mathbf{y}_N^T[l]]^T = \sum_{i=1}^{D} \mathbf{a}(q_i) A_i e^{j\phi_i} e^{j\pi q_i MNl} + \mathbf{w}[l] \tag{2.1}$$

In practice, we can only obtain a finite number of samples of a particular realization of $\mathbf{y}[l]$, for which the sinusoidal component parameters q_i, A_i and ϕ_i $(i = 1, 2, \dots D)$ are constant. For convenience and without loss of generality, we consider the noise-free situation to illustrate the signal model. The covariance matrix is then estimated, over L blocks of samples, by

$$\begin{aligned} \hat{\mathbf{R}}_{\mathbf{y}} &= \frac{1}{L} \sum_{l=0}^{L-1} \mathbf{y}[l] \mathbf{y}^H[l] \\ &= \mathbf{A} \hat{\mathbf{R}}_{\mathbf{s}} \mathbf{A}^H \end{aligned} \tag{2.2}$$

Notice that the coprime sampling scheme is generalized in [63], data of several sampling units from two samplers is utilized to construct a sampling block. Covariance matrices of different blocks are averaged to reduce the variance. Since a block includes several units, the sampling units in one block may also be included in other blocks. This leads to the categorization of different averaging mechanisms, including overlapping and non-overlapping. In non-overlapping averaging, a sampling unit can not be included in different blocks. In contrast, the overlapping mechanism indicates that a unit can be included in different blocks simultaneously. As the example provided in Figure 2.1, five units from each sampler are used for constructing a block. The third unit data ranging from $[3MN, 4MN)$ is included in block 1, block 2 and block 3. It is obvious that the data of a unit is reused in several blocks. In other words, the number of blocks is increased with a given set of

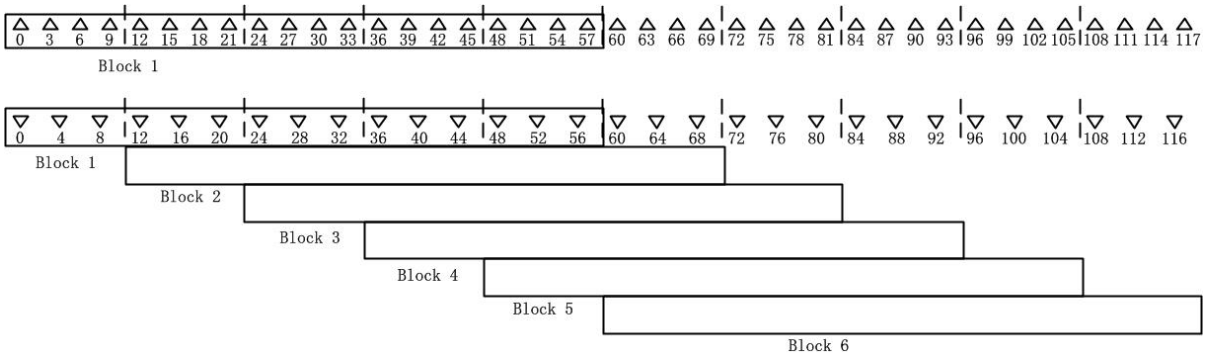

Figure 2.1 – Overlap coprime sampling with $M = 3, N = 4$.

data. The data is utilized several times for averaging such that the bias of the estimated covariance matrix can be limited.

To evaluate the performance of estimators, the Cramér Rao Bound (CRB) offers a theoretical lower bound of estimation variance of any unbiased estimator. The CRB has been widely studied for traditional ULA [105, 106] and coprime coarray [65, 107, 108]. In this section, we give the CRB of the classical coprime sampling in frequency estimation. For signal model present above, the parameter vector is defined as

$$\boldsymbol{\eta} = [q_1, ..., q_D, p_1, ...p_D, \sigma_n^2]^T \tag{2.3}$$

The (i, j)-th element of the Fisher information matrix (FIM) can be given as

$$FIM_{i,j} = L\ trace[\frac{\partial \mathbf{R_y}}{\partial \eta_i}\mathbf{R_y}^{-1}\frac{\partial \mathbf{R_y}}{\partial \eta_j}\mathbf{R_y}^{-1}] \tag{2.4}$$

Following the similar derivations in [65], FIM can be given as

$$\mathbf{FIM} = L \begin{bmatrix} \mathbf{M}_f^H\mathbf{M}_f & \mathbf{M}_f^H\mathbf{M}_s \\ \mathbf{M}_s^H\mathbf{M}_f & \mathbf{M}_s^H\mathbf{M}_s \end{bmatrix} \tag{2.5}$$

where

$$\mathbf{M}_f = (\mathbf{R}_\mathbf{y}^T \otimes \mathbf{R}_\mathbf{y})^{-1/2}\mathbf{A}_d\mathbf{R}_s \tag{2.6}$$

$$\mathbf{M}_s = (\mathbf{R}_\mathbf{y}^T \otimes \mathbf{R}_\mathbf{y})^{-1/2}[\mathbf{A}_c, \mathbf{i}] \tag{2.7}$$

with $\mathbf{A}_d = \mathbf{A}_{der}^* \odot \mathbf{A}_s + \mathbf{A}_s^* \odot \mathbf{A}_{der}$ and

$$\mathbf{A}_{der} = \left[\frac{\partial \mathbf{a}(q_1)}{\partial q_1}, \frac{\partial \mathbf{a}(q_2)}{\partial q_2}, ..., \frac{\partial \mathbf{a}(q_D)}{\partial q_D}\right] \tag{2.8}$$

The CRB of the estimated frequencies can be obtained as

$$\mathbf{CRB}_f = \frac{1}{L}(\mathbf{M}_f^H(\mathbf{I} - \mathbf{M}_s(\mathbf{M}_s^H\mathbf{M}_s)^{-1}\mathbf{M}_s^H)\mathbf{M}_f)^{-1} \tag{2.9}$$

2.3 Diagonal property loss phenomenon

2.3.1 Problem statement

For a given realization in practise, the estimated covariance matrix $\hat{\mathbf{R}}_\mathbf{y} = \mathbf{A}\hat{\mathbf{R}}_\mathbf{s}\mathbf{A}^H$ is used, where $\hat{\mathbf{R}}_\mathbf{s}$ is no longer a diagonal matrix, but it is a matrix whose $\{i,k\}$-th element can be expressed as

$$\hat{\mathbf{R}}_\mathbf{s}(i,k) = \frac{A_i A_k e^{j(\phi_i - \phi_k)}}{L}\sum_{l=0}^{L-1} e^{j\pi(q_i - q_k)MNl} \tag{2.10}$$

where, A_i, A_k, ϕ_i, ϕ_k, with $i,k = 1,2,...,D$, are constant for a given realization.

In the conventional coprime sampling scheme [66], $\hat{\mathbf{R}}_\mathbf{s}$ can be equivalently considered to be diagonal in most cases since (2.10) could be a small value when L is large enough. However it can be observed that if there exists a pair of normalized frequencies verifying

$$\Delta = q_i - q_k = \frac{2b}{MN} \tag{2.11}$$

where b is an integer, then the term in equation (2.10) turns to be equal to $A_i A_k e^{j(\phi_i - \phi_k)}$,

which is independent of L. It is obvious that matrix $\hat{\mathbf{R}}_\mathbf{s}$ will not be diagonal even for a big value of L. In fact, in this situation, this matrix becomes rank deficient. For any pair of distinct frequencies q_i and q_k satisfying this condition, the diagonal property of $\hat{\mathbf{R}}_\mathbf{s}$ can no more be hold. This phenomenon has never been reported in the framework of practical coprime sampling. In this situation which seems to happen quite frequently, the estimated covariance matrix (2.2) obtained from finite samples does not exhibit the same properties as the theoretical matrix.

For co-array MUSIC method, matrix $\hat{\mathbf{R}}_\mathbf{y}$ is vectorized and spatial smoothing is applied to construct a new covariance matrix of the virtual signal. The vectorization of $\hat{\mathbf{R}}_\mathbf{y}$ can be given as

$$vec(\hat{\mathbf{R}}_\mathbf{y}) = \sum_{i=1}^{D} A_i^2 \mathbf{a}^*(q_i) \otimes \mathbf{a}(q_i) + \sum_{h=1}^{D} \sum_{k=1, h\neq k}^{D} \xi_{hk} A_h A_k e^{j\pi\phi_{hk}} \mathbf{a}^*(q_k) \otimes \mathbf{a}(q_h) \tag{2.12}$$

where $\phi_{hk} = \phi_h - \phi_k$, $\xi_{hk} = 1$ only when condition (2.11) is met. Then the virtual signal vector can be written as

$$\mathbf{x}_v = \mathbf{F} vec(\hat{\mathbf{R}}_\mathbf{y}) = \mathbf{FBp} + \mathbf{FB'p'} \tag{2.13}$$

where $\mathbf{F}$ is the selection matrix [65], $\mathbf{B} = [\mathbf{a}^*(q_1) \otimes \mathbf{a}(q_1), ..., \mathbf{a}^*(q_D) \otimes \mathbf{a}(q_D)]$, $\mathbf{p} = [p_1, ..., p_D]^T$ and $\mathbf{B'} = [\mathbf{a}^*(q_1) \otimes \mathbf{a}(q_2), ..., \mathbf{a}^*(q_1) \otimes \mathbf{a}(q_D), ..., \mathbf{a}^*(q_D) \otimes \mathbf{a}(q_1), ..., \mathbf{a}^*(q_D) \otimes \mathbf{a}(q_{D-1})]$, $\mathbf{p'} = [\xi_{21} A_2 A_1 e^{j\phi_{21}}, ..., \xi_{D1} A_D A_1 e^{j\phi_{D1}}, ..., \xi_{1D} A_1 A_D e^{j\phi_{1D}}, ..., \xi_{(D-1)D} A_{D-1} A_D e^{j\phi_{(D-1)D}}]^T$. Here, $h \neq k$ for each $\mathbf{a}^*(q_k) \otimes \mathbf{a}(q_h)$ in $\mathbf{B'}$ and $\xi_{hk} A_h A_k e^{j\phi_{hk}}$ in $\mathbf{p'}$. We can write $\mathbf{FBp}$ as

$$\mathbf{FBp} = \left[\sum_{i=1}^{D} A_i^2 e^{j\pi q_i (1-(M+N))}, \sum_{i=1}^{D} A_i^2 e^{j\pi q_i (2-(M+N))}, ..., \sum_{i=1}^{D} A_i^2 e^{j\pi q_i (M+N-1)} \right]^T = \mathbf{A}_v \mathbf{p} \tag{2.14}$$

where $\mathbf{A}_v = [\mathbf{d}(q_1), ..., \mathbf{d}(q_D)]$ with $\mathbf{d}(q_i) = [e^{j\pi q_i (1-(M+N))}, e^{j\pi q_i (2-(M+N))}, ..., e^{j\pi q_i (M+N-1)}]^T$. Before applying the co-array MUSIC, the spatial smoothing is applied to $\mathbf{x}_v$. It can be seen that if the diagonal property of $\hat{\mathbf{R}}_\mathbf{s}$ holds, the virtual signal vector $\mathbf{x}_v$ can be written as $\mathbf{A}_v \mathbf{p}$. If the diagonal property loss condition is met, vector $\mathbf{FB'p'}$ consisting of some cross terms between different frequencies will cause some problems to the co-array MU-

SIC. Due to the cross terms of different frequencies, the virtual signal vector $\mathbf{x}_v$ can no longer be written in the form $\mathbf{A}_v\mathbf{p}$, which is the basis of all spatial smoothing based high resolution techniques. As a consequence, the co-array MUSIC fails in this case.

2.3.2 Embedded delay mechanism

In this section, we propose a technique to overcome the above mentioned diagonal property loss phenomenon. The main idea is to introduce randomness in the sampling process to artificially keep the uncorrelation between the sampled sinusoidal components. This is achieved by introducing random delays such that the phase of different sinusoidal components becomes random because of the different frequencies. This proposition only considers non-overlappling averaging.

After acquiring the first block of data, a discrete random delay is introduced before starting each new block at both samplers as illustrated in Figure 2.2. It should be noticed that the DOFs are $M+N-1$ in this case because we embed the random delays after each block. The proposed scheme can be easily generalized to increase the DOFs by embedding the random delays after every k blocks. For instance, if the random delays are embedded after the 2-nd, 4-th, 6-th,...blocks, data from two blocks can be jointly used to construct the covariance matrix and the DOFs can be increased to $MN+M+N-1$. Indeed, the DOFs can be further increased to $(k-1)MN+M+N-1$ [63] if the random delays are embedded after the k-th, $2k$-th, $3k$-th,...blocks. In this work, our main concern is to show the diagonal property loss problem and give a way to fix it. Without loss of generality, we have embedded the random delays after each block in this dissertation.

In this work, discrete random delay is considered but continuous random delay could have been chosen too. For practical convenience of implementation, we consider the introduced random delays to be multiple of the Nyquist sampling period T with a discrete uniform distribution. The delay embedded at the front of the p-th block is denoted as t_pT, where t_p is a random integer ruled by the discrete uniform distribution $U[0,\alpha-1]$ ($\alpha \geq 2$). It means that t_p randomly takes one integer value in set $[0,\alpha-1]$ with probability $\frac{1}{\alpha}$. At the l-th block, the total accumulated delay is

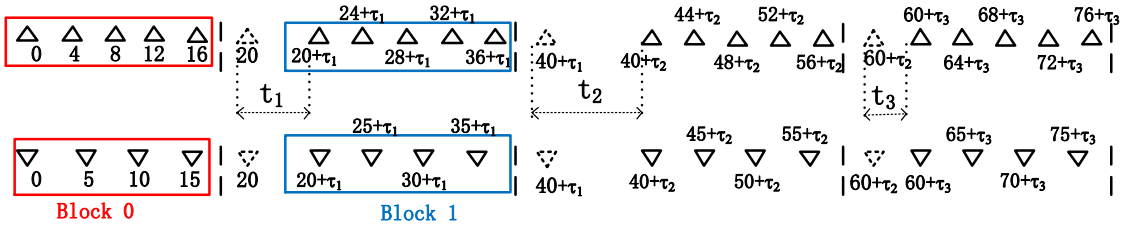

Figure 2.2 – Random delay between coprime sampling blocks, M=4, N=5

$$\tau_l T = \sum_{p=1}^{l} t_p T \tag{2.15}$$

Then the new concatenated samples block vector can be modified as

$$\tilde{\mathbf{y}}[l] = \sum_{i=1}^{D} \mathbf{a}(q_i) A_i e^{j\phi_i} e^{j\pi q_i (MNl+\tau_l)} + \tilde{\mathbf{w}}[l] \tag{2.16}$$

Its covariance matrix can then be estimated over the L obtained blocks. Similarly to (2.10), the $\{i,k\}$-th element in $\tilde{\mathbf{R}}_{\mathbf{s}}$ can be written as

$$\tilde{\mathbf{R}}_{\mathbf{s}}(i,k) = \frac{A_i A_k e^{j(\phi_i-\phi_k)}}{L} \sum_{l=0}^{L-1} e^{j\pi(q_i-q_k)(MNl+\tau_l)} \tag{2.17}$$

Since A_i, A_k, ϕ_i, ϕ_k are constant for a particular realization, we consider only the summation item in $\tilde{\mathbf{R}}_{\mathbf{s}}(i,k)$. It should be noticed that even for a set of received samples, only one realization of the random delays is drawn. It is impossible to derive a closed-form expression of the summation term in equation (2.17). However it makes sense to observe the statistical mean of this term, which is given by

$$E\left[\frac{1}{L}\sum_{l=0}^{L-1} e^{j\pi(q_i-q_k)(MNl+\tau_l)}\right] = \frac{1}{L}\sum_{l=0}^{L-1}\left(\frac{e^{j\pi(q_i-q_k)(MN+\frac{\alpha-1}{2})}}{\alpha}\frac{sin(\frac{\pi(q_i-q_k)\alpha}{2})}{sin(\frac{\pi(q_i-q_k)}{2})}\right)^l \tag{2.18}$$

To better understand how the embedded delays affect the non-diagonal terms and fix the diagonal property loss problem, we use equation (2.18) to approximately show

the impact of the introduced delays. When L increases, the summation term in equation (2.17) tends to take a value close to its statistical mean. Observing equation (2.18), it comes that the value of the summation item is given as the sum of the first L terms of a geometric series for which the modulus of the common ratio is less than or equal to one (equal to one only when $|q_i - q_k|$ is even). Since $\alpha \geq 2$ and $q_i \neq q_k$ with $|q_i - q_k| < 2$ by definition, the modulus of the common ratio will be always less than one. Hence, as L is chosen large enough, the non diagonal elements of the estimated signal covariance matrix $\tilde{\mathbf{R}}_{\mathbf{s}}$ will be small for any α and normalized frequencies. In fact, the non diagonal elements tend to zero as L goes to infinity. Therefore, even in the diagonal property loss condition defined in (2.11), two distinct signal components ($q_i \neq q_k$) will never be linearly correlated, which means that no diagonal property loss will occur in the proposed scheme. The coprime subspace based methods can then be applied for frequencies estimation even under the diagonal property loss condition.

It seems that parameter α could be chosen to optimize the performance of frequencies estimation, because the smaller the amplitude of (2.18) is, the better is the performance of the subspace based techniques. However, for a given number of blocks L, it is not possible to optimally choose α to obtain a lowest value of (2.18) because the normalized frequencies are not known initially.

To better understand the effect due to α, we provide the statistical mean of (2.18) in Figure 2.3 and Figure 2.4 considering only two frequencies with $M = 4, N = 5$. The x-axis denotes the value of the difference between two frequencies and the y-axis denotes the mean value of (2.18). Based on the above discussions, if no random delays are introduced ($\tau_l = 0$), the mean value of (2.18) will have a peak value which equals to one when the condition (2.11) is met, i.e. $\Delta = 0.1, 0.2, 0.3, ...$ Otherwise it will be small for other values of Δ.

After adding the random delays, it can be observed from Figure 2.3 and Figure 2.4 that there exist some peaks where the peak values are smaller than 1. Furthermore, if the distribution of delays is distributed in a wider range, the corresponding peak values can further decrease to a smaller value. Apart from a few peak values in Figure 2.3 and

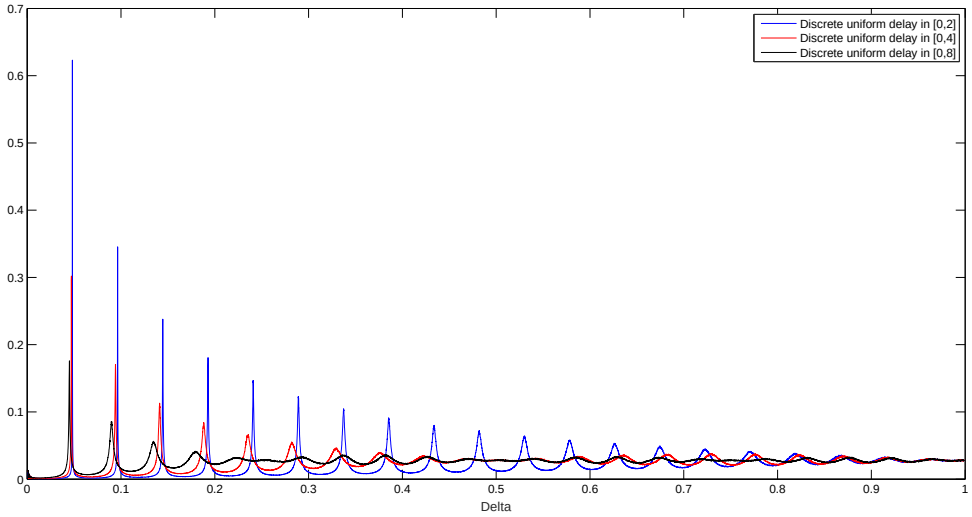

Figure 2.3 – Statistical mean of (2.18) versus different values of Δ, α satisfies discrete uniform distribution, distributed in range [0,2],[0,4],[0,8]. $M = 4, N = 5$.

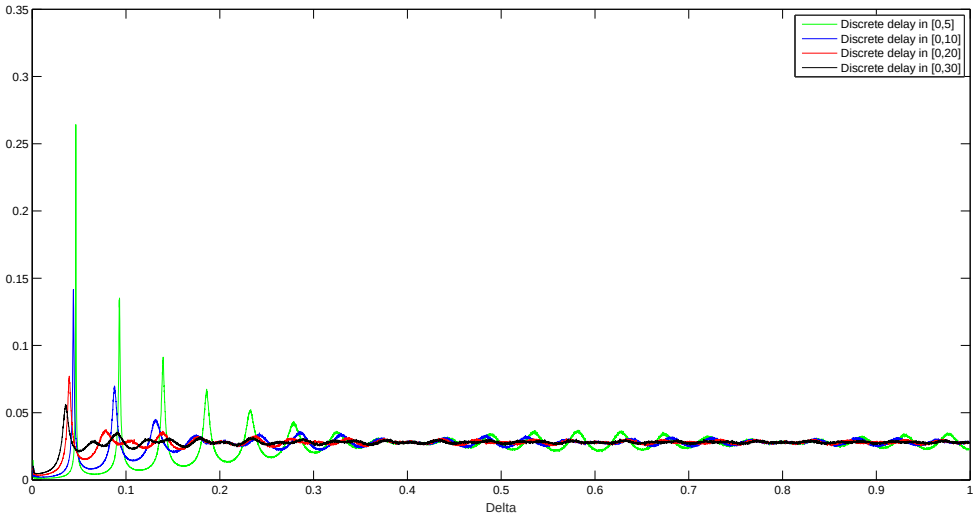

Figure 2.4 – Statistical mean of (2.18) versus different values of Δ, α satisfies discrete uniform distribution, distributed in range [0,5],[0,10],[0,20],[0,30]. $M = 4, N = 5$.

Figure 2.4, we can notice that most values of (2.18) are quiet small for most cases of Δ. For example smaller than 0.1. This indicates that by introducing the random delay, the non-diagonal terms in covariance matrix can be limited to a small value for most of the cases to ensure the success of coarray based MUSIC method.

2.3.3 Results and discussion

In order to illustrate the above highlighted problem, firstly we provide the MUSIC spectrum under the diagonal property loss condition with the classical coprime sampling. Then, the MUSIC spectrum obtained from the proposed embedded random delay sampling is displayed to show the benefit brought by the new proposed coprime sampling scheme. Finally, RMSE performance is given to show that the proposed sampling scheme does not affect the estimation performance when there is no diagonal property loss.

In order to illustrate the diagonal property loss phenomenon, we consider the coprime integers $M = 4$ and $N = 5$, and $D = 7$ sinusoidal components with unit amplitude. The signal-to-noise ratio (SNR) is set to $20dB$. Consider $L = 1000$ blocks of samples. The 7 normalized frequencies in this example are selected such that there exist exactly two pairs among them verifying the diagonal property loss condition (2.11). The normalized frequencies are $q_1 = -0.40, q_2 = -0.34, q_3 = -0.17, q_4 = 0.23, q_5 = 0.39, q_6 = 0.56, q_7 = 0.88$, and the condition is met with $q_4 - q_3$ and $q_6 - q_2$.

The coprime sampling MUSIC algorithm [66] is then applied in two scenarios:
1) the number of components $D = 7$ is known and the dimension of the signal subspace dimension is set to 7 when performing MUSIC algorithm;
2) no prior knowledge of the number of components is assumed, and the minimum description length criteria (MDL) [109] is used to determine the signal subspace dimension.

In this situation, the subspace signal dimension is found to be equal to 5. Fig. 2.5 shows the estimated MUSIC spectrum under diagonal property loss phenomenon. The vertical discontinuous lines refer to the true positions of frequencies. It can be observed that the frequencies are not correctly estimated in both scenarios. Phantom peaks appear at wrong frequency position and some true frequencies can not be detected.

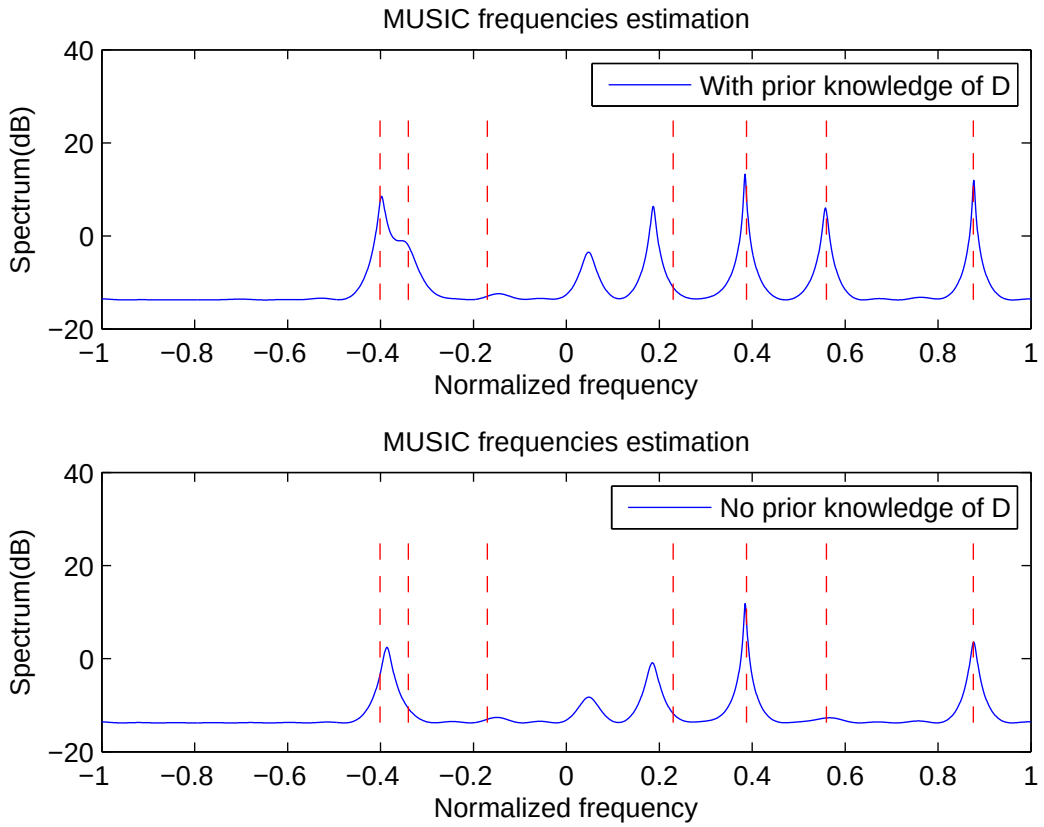

Figure 2.5 – MUSIC spectrum with coprime sampling in the diagonal property loss condition, 7 sinusoidal components, $M = 4$ and $N = 5$.

Fig. 2.6 depicts the estimated MUSIC spectrum with the proposed embedded random delays sampling method. The same frequencies setting as before is considered and α is set to 6. It can be observed that the frequencies are correctly estimated even with two pairs of frequencies verifying contidion (2.11).

In the following, the proposed embedded random delays scheme and the classical coprime scheme are compared. The performance is assessed in terms of RMSE, defined as

$$RMSE = \sqrt{\frac{1}{DU}\sum_{i=1}^{D}\sum_{u=1}^{U}(\hat{q}_i(u) - q_i)^2} \tag{2.19}$$

where $\hat{q}_i(u)$ is the estimate of the normalized frequency q_i in the u-th estimation trial, $u = 1, 2, ..., U$. In the following simulations, the following parameters are chosen, $U =$

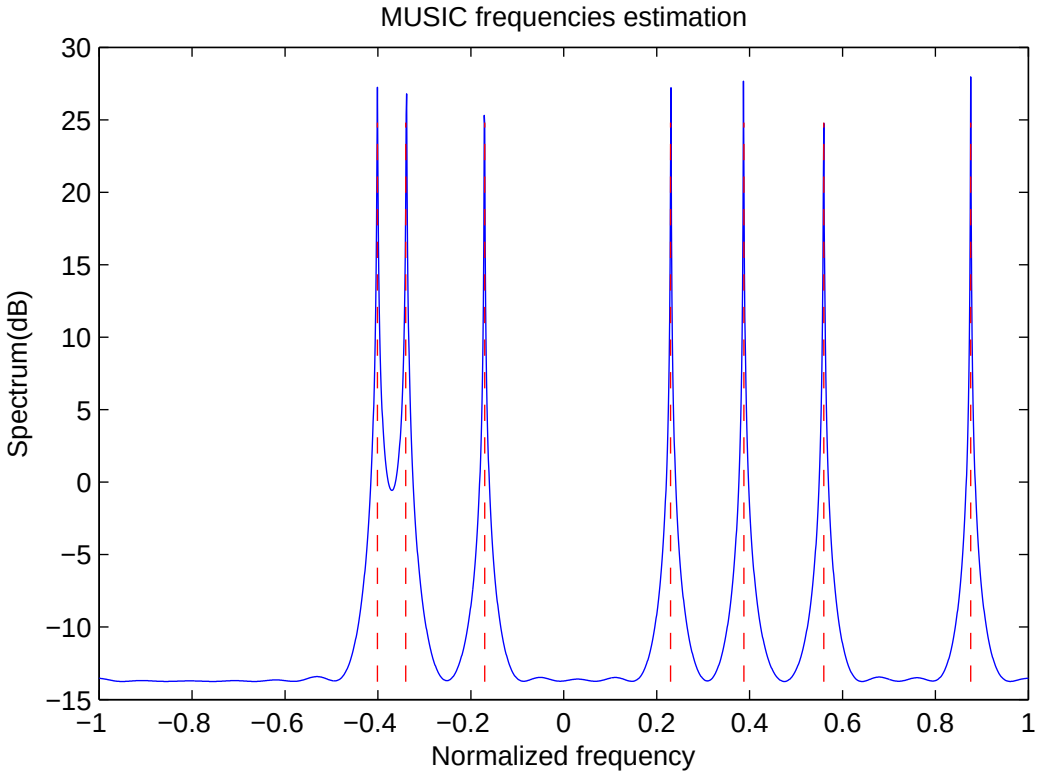

Figure 2.6 – MUSIC spectrum using embedded random delays coprime sampling, 7 sinusoidal components, $M = 4$ and $N = 5$.

1000, $M = 4, N = 5$

As explained above, the classical co-array MUSIC fails when condition (2.11) is met. We first show the performance of the classical co-array MUSIC algorithm when the difference between some frequencies is close to $2b/(MN)$. In Figure 2.7, we consider 2 frequencies, which are $q_1' = -0.17$ and $q_2' = 0.23 + \delta$ such that $q_2' - q_1' = 0.4 + \delta$, where δ is a small offset and $b = 4$. We set δ to several values for comparison and no prior knowledge of D is assumed in this case. It can be observed from Figure 2.7 that when δ varies from 0.01 to 0.0001, the classical co-array MUSIC achieves similar performance. When δ continues to decrease, RMSE increases dramatically. This indicates that when the difference between some frequencies tends to be close to $2b/(MN)$, the non-diagonal terms in $\hat{\mathbf{R}}_{\mathbf{s}}$ become non-negligible. The diagonal property loss problem becomes significant.

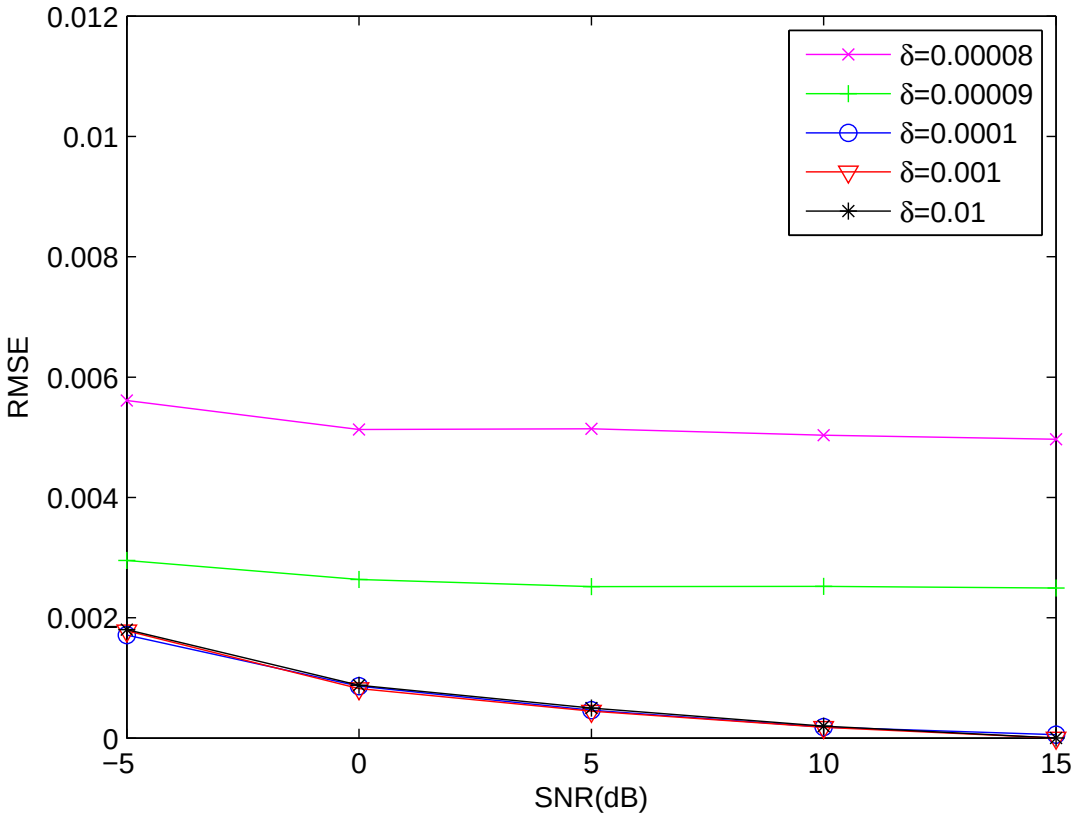

Figure 2.7 – RMSE performance when the difference between some frequencies is close to $2b/(MN)$, $b = 4, M = 4, N = 5$.

The classical coprime scheme and the proposed scheme are compared in Figure 2.8. For simplicity, signal with only two sinusoidal components (q_1, q_2) is considered. Because the classical coprime mechanism fails under the diagonal property loss condition while our proposed method can still robustly perform, we arbitrarily choose frequencies which do not satisfy the diagonal property loss condition for comparison. Without loss of generality, q_1 is chosen to be -0.84 and q_2 is randomly chosen in each estimation trial. Also, we consider different values of α to compare how the embedded delay distributions affect the performance, namely $\alpha = 6, 16, 31$.

It can be observed from Fig. 2.8 that the proposed scheme can obtain similar RMSE performance as that of the classical coprime scheme. Moreover, with different values of α,

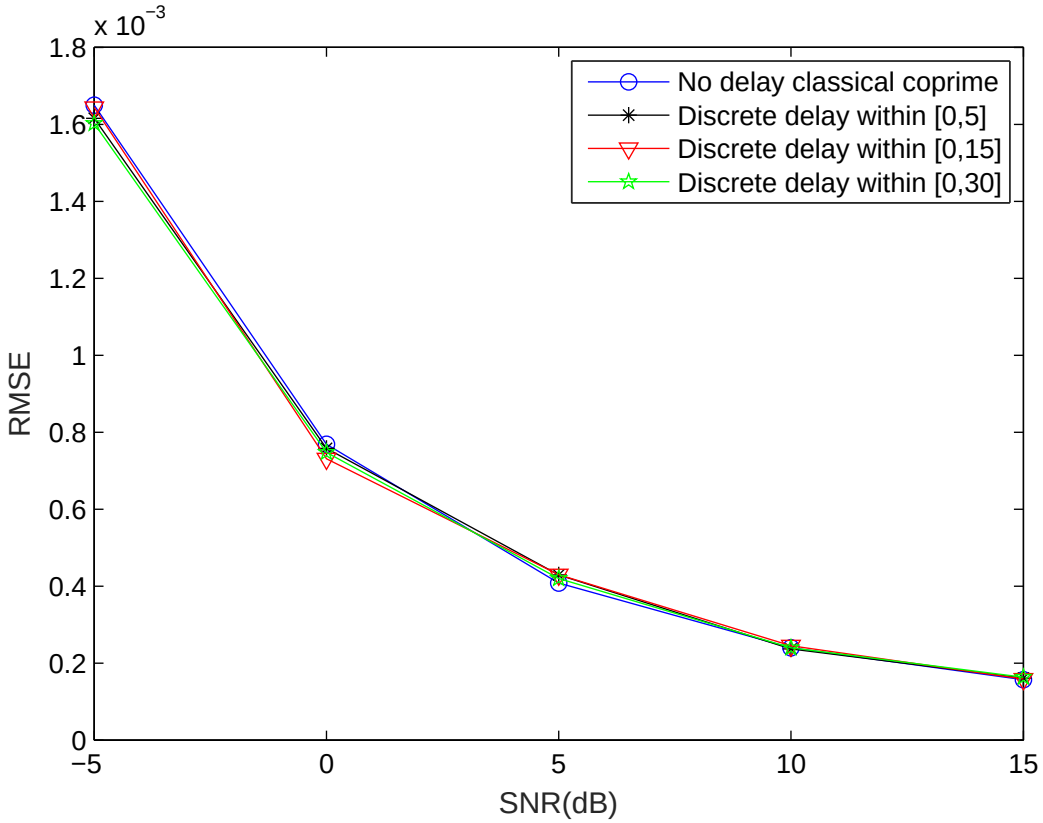

Figure 2.8 – RMSE performance with classical coprime sampling and embedded random delay coprime sampling, $M = 4, N = 5$.

the performance does not significantly change, which means that the embedded delays do not significantly affect the performance of coprime sampling process while being able to fix the problem of the diagonal property loss.

2.4 Multi-rate coprime sampling to fill the holes in second order difference coarray

2.4.1 Problem statement

In coprime sampling configuration, the 2-DC generated by coprime configuration is a linear virtual array structure with some missing elements. This leads to information

loss if only the contiguous part of the virtual coarray is used. It is interesting to apply interpolation techniques to fill the holes. Many techniques have been developed in the DOA scenario with coprime array, including multi-frequency method [72], interpolation with moving array [80, 81], multi-period subarray [78], etc. However, these techniques are not applicable in frequency estimation domain. The nuclear norm minimization method and the atomic norm optimization method can be utilized in the frequency estimation. However, the performance of nuclear norm minimization and atomic norm optimization strongly relies on the parameter tuning and the noise level. It could lead to high complexity if high performance is required.

2.4.2 Multi-rate coprime sampling model

The conventional coprime sampling requires two samplers acquiring data with sampling rate MT and NT, respectively. To address the holes problem, we propose a multi-rate coprime sampling scheme to interpolate the holes in the 2-DC. The signal model of conventional coprime sampling has been discussed in the previous part. Correspondingly, we denote the 2-DC integers set related to the conventional coprime sampling as

$$\mathbb{L} = \{\pm(Mn - Nm)\} \tag{2.20}$$

The maximum value in $\mathbb{L}$ is $(2M-1)N$, which is much larger than $2M+N-1$ for two coprime integers. Coprime sampling scheme uses the concept of difference coarray to construct a virtual coarray and increase the DOF. Elements in $\mathbb{L}$ can be equivalently considered as the indices of a virtual Nyquist rate sampler, whose samples are the corresponding elements in $\mathbf{R_y}$.

It can be noticed that the vectorized vector $\mathbf{r}$ contains all the self-lags and cross-lags correlation. By selecting the appropriate elements corresponding to the self-lags and cross-lags in $\mathbb{L}$, we can construct a virtual coarray integer set ranging from $-(2M-1)N$ to $(2M-1)N$ [65], in which some missing elements exist. An illustration of the virtual coarray is given in Figure 2.9a with $M = 4, N = 5$. It is clear that there are some

holes in the virtual coarray and the nonuniform coarray can not be directly employed for efficient frequency estimation. In this section, we elaborate how the holes can be filled by exploiting multi-rate coprime sampling without additional samples, such that all the information included in the virtual coarray can be fully exploited.

It is worth noting that we consider the conventional coprime sampling [66] to elaborate the proposed method in this dissertation. The proposed multi-rate method can be easily extended to the generalized coprime sampling scheme [63] by choosing the appropriate sampling rates in accordance with the positions of the holes. By doing so, the DOF can be further increased.

Consider two samplers similar to the conventional coprime samplers, whose sampling intervals are a_rMT and a_rNT with a_r the multi-rate coefficient ($a_r > 0$), respectively, the two collected sample subsets associated with the l-th block are given by

$$\begin{aligned} x_{M,a_r}[Nl+n] &= \sum_{i=1}^{D} A_i e^{j\left(\pi q_i a_r M(Nl+n)+\phi_i\right)} + \omega(a_r M(Nl+n)T) \\ x_{N,a_r}[Ml+m] &= \sum_{i=1}^{D} A_i e^{j\left(\pi q_i a_r N(Ml+m)+\phi_i\right)} + \omega(a_r N(Ml+m)T) \end{aligned} \tag{2.21}$$

where $x_{M,a_r}[Nl+n] = x(M(Nl+n)a_rT)$, $x_{N,a_r}[Ml+m] = x(N(Ml+m)a_rT)$, with $1 \le m \le 2M-1$, $0 \le n \le N-1$. It can be observed that the number of elements in each block remains the same as in the original classical coprime sampling, while the sampling interval is scaled up by a factor a_r. The corresponding sampling signal vector of the l-th block can be written as

$$\mathbf{y}_{a_r}[l] = \sum_{i=1}^{D} \mathbf{a}(a_r q_i) A_i e^{j\phi_i} e^{j\pi q_i a_r MNl} + \mathbf{n}_{a_r}[l] \tag{2.22}$$

Its covariance matrix can be expressed as

$$\mathbf{R}_{\mathbf{y}}(a_r) = E[\mathbf{y}_{a_r}[l]\mathbf{y}_{a_r}^H[l]] = \sum_{i=1}^{D} A_i^2 \mathbf{a}(a_r q_i)\mathbf{a}^H(a_r q_i) + \sigma_n^2 \mathbf{I} \tag{2.23}$$

Similarly to the 2-DC of conventional coprime sampling, the self-lags and cross-lags under

sampling rates a_rMT and a_rNT can be described by the following set

$$\mathbb{L}(a_r) = \{\pm a_r(Mn - Nm)\} \tag{2.24}$$

It is obvious that $\mathbb{L}(a_r)$ is a scaled version of $\mathbb{L}$ with multi-rate coefficient a_r. With an appropriate value of a_r, $\mathbb{L}(a_r)$ can include some missing elements in $\mathbb{L}$ (2.20). After vectorizing and rearranging the elements, the virtual coarray obtained with sampling rates a_rMT and a_rNT contains some hole elements in the original virtual coarray with sampling rates MT and NT. The idea of multi-rate coprime scheme is to find all the hole elements from the resultant virtual coarrays generated by multi-rate coprime sampling. These elements can be employed to fill the holes in the classical coprime coarray. This is achieved by choosing some appropriate values of a_r in accordance with the positions of the holes.

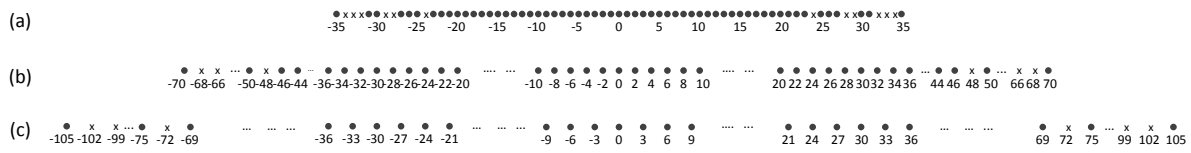

Figure 2.9 – Sampling indices of virtual coarrays with different sampling rates. (a) Sampling rates MT, NT (b) Sampling rates $2MT, 2NT$ (c) Sampling rates $3MT, 3NT$, with $M = 4$ and $N = 5$, $\bullet$: existed elements, $\times$: holes.

2.4.3 Holes filling in 2-DC with different sampling rate

The maximum value in $\mathbb{L}$ is $K = (2M - 1)N$. We consider a covariance matrix $\mathbf{R}_v$ that can utilize all the DOFs. Therefore, we can define a set of values corresponding to the full DOFs as

$$\mathbb{L}_{DOF} = \{\pm i | 0 \leq i \leq K\} \tag{2.25}$$

Then we can construct the following Toeplitz covariance matrix

$$\mathbf{R}_v = \begin{pmatrix} r[0] & r[-1] & ... & r[-K] \\ r[1] & r[0] & ... & r[-K+1] \\ ... & ... & ... & ... \\ r[K] & r[K-1] & ... & r[0] \end{pmatrix} \tag{2.26}$$

where $r[i] = E[x(t)x^*(t-iT)]$ only depends on the lag $i = 0, 1, ..., (2M-1)N$. In other words, $r[i]$ corresponds to the data of the i-th position in the virtual coarray. An example of virtual coarray with $M = 4, N = 5$ is shown in Figure 2.9a. For a given realization, $\mathbf{R}_v$ and $r[i]$ are represented by $\hat{\mathbf{R}}_v$ and $\hat{r}[i]$, respectively.

To estimate $r[i]$, the covariance matrix is estimated by averaging the available sample blocks

$$\hat{\mathbf{R}}_{\mathbf{y}} = \frac{1}{L}\sum_{l=0}^{L-1} \mathbf{y}[l]\mathbf{y}^H[l] \tag{2.27}$$

where L is the number of blocks. For the i-th position in the virtual coarray, there may be several elements in $\hat{\mathbf{R}}_{\mathbf{y}}$ that correspond to the same position. The i-th position $r[i]$ is estimated by averaging all the corresponding elements in $\hat{\mathbf{R}}_{\mathbf{y}}$ to get $\hat{r}[i]$ [110].

Notice that there are some missing integers in $\mathbb{L}$ which are related to the missing elements in $\hat{\mathbf{R}}_v$. These elements correspond to the holes that can not be directly obtained from $\hat{\mathbf{R}}_{\mathbf{y}}$. We define the missing elements set as

$$\mathbb{L}_{holes} = \{i | i \in (\mathbb{L}_{DOF} - \mathbb{L})\} \tag{2.28}$$

Alternatively, a new covariance matrix can be estimated under multi-rate coprime sampling with coefficient a_r, which is represented by $\hat{\mathbf{R}}_{\mathbf{y}}(a_r)$. By choosing some appropriate values of a_r, the set of lags associated with $\hat{\mathbf{R}}_{\mathbf{y}}(a_r)$ can be equivalently represented as (2.24). All the missing elements $\hat{r}[i]$ can be obtained from the intersection between $\mathbb{L}_{holes}$ and the selected sets $\mathbb{L}(a_r)$ to reconstruct matrix $\hat{\mathbf{R}}_v$. In other words, we can define $\mathbb{I}_{rates}$

as a set of selected multi-rate coefficients allowing to fill all the holes such that

$$\mathbb{L}_{holes} = \bigcup_{a_r \in \mathbb{I}_{rates}} \{\mathbb{L}_{holes} \cap \mathbb{L}(a_r)\} \tag{2.29}$$

For illustration, we consider the holes ± 24 as shown in Figure 2.9a. Many values of a_r can be used to fill these two holes. A condensed coarray can be obtained with value $a_r = \frac{24}{25}$, which requires to implement another two samplers at new sampling rates $\frac{24}{25}MT$ and $\frac{24}{25}NT$. If we choose $a_r > 1$, the coarray will be extended, as shown in Figure 2.9b for $a_r = 2$.

Meanwhile, an interesting fact is that if the multi-rate coefficient a_r is set to be an integer greater than 1, the required samples are included in the initial samples obtained with the classical sampling rates MT and NT. These samples can be equivalently considered as the samples of the multi-rate sampling. In other words, these samples can be directly obtained by decimating the original classical coprime samples. A graphic illustration is given in Figure 2.10 with $M = 4, N = 5$ and $a_r = 2$. This is of great importance to the sampling process because the multi-rate samples can be obtained by choosing the appropriate samples from the original classical coprime sampling sample stream. In this case, the resultant multi-rate covariance matrix can be expressed as follows

$$\hat{\mathbf{R}}_{\mathbf{y}}(a_r) = \frac{1}{\lfloor \frac{L}{a_r} \rfloor} \sum_{l=0}^{\lfloor \frac{L}{a_r} \rfloor} \mathbf{y}_{a_r}[l] \mathbf{y}_{a_r}^H[l] \tag{2.30}$$

Here, only $\frac{1}{a_r}$ samples from the x_M and x_N samplers are chosen for the multi-rate scheme, which indicates that the multi-rate scheme has totally $\lfloor \frac{L}{a_r} \rfloor$ blocks ($\lfloor \cdot \rfloor$ is the floor operator). No additional sampling operation is required and this will not cause extra sampling burden to the samplers. In the following sections, we only consider the case where a_r is an integer greater than 1.

Filling holes without data reusing

As shown in Figure 2.9, we consider $M = 4, N = 5$ to illustrate the mechanism without reusing data. The holes occur at positions $\{\pm 24, \pm 28, \pm 29, \pm 32, \pm 33, \pm 34\}$. As shown in

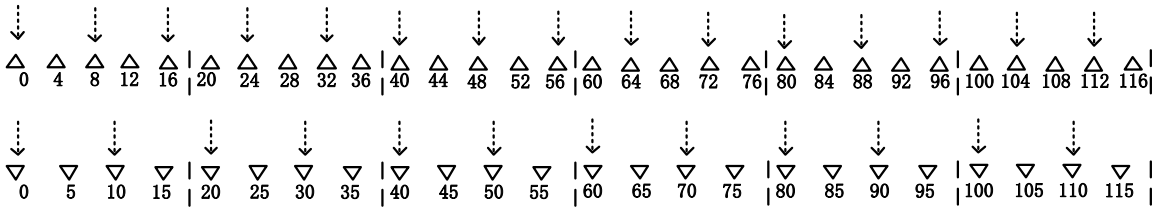

Figure 2.10 – Multi-rate coprime sampling indices selected from the classical coprime sampling, $M = 4, N = 5, a_r = 2$. $\downarrow$: sampling indices selected for multi-rate coprime sampling.

Figure 2.9b, a new virtual coarray can be constructed by setting $a_r = 2$. It can be easily observed that the lags $\{\pm 24, \pm 28, \pm 32, \pm 34\}$ can be obtained via this new coarray and we can directly select these elements from Figure 2.9b to fill the holes in Figure 2.9a. In addition, the holes $\{\pm 33\}$ and $\{\pm 29\}$ can also be filled by setting $a_r = 3$ (Figure 2.9c) and $a_r = 29$ respectively. The resultant integer sets can be expressed as

$$\mathbb{L}(a_r = 2) = \{\pm 2(Mn - Nm)\} \tag{2.31}$$

$$\mathbb{L}(a_r = 3) = \{\pm 3(Mn - Nm)\} \tag{2.32}$$

$$\mathbb{L}(a_r = 29) = \{\pm 29(Mn - Nm)\} \tag{2.33}$$

Here, m, n are the indices of samples in one block. By selecting the appropriate elements from $\hat{\mathbf{R}}_{\mathbf{y}}(a_r = 2), \hat{\mathbf{R}}_{\mathbf{y}}(a_r = 3), \hat{\mathbf{R}}_{\mathbf{y}}(a_r = 29)$, the holes in Figure 2.9a can all be filled correspondingly. It comes that

$$\{\pm 24, \pm 28, \pm 32, \pm 34\} \subseteq \{\mathbb{L}_{holes} \cap \mathbb{L}(a_r = 2)\} \tag{2.34}$$

$$\{\pm 33\} \subseteq \{\mathbb{L}_{holes} \cap \mathbb{L}(a_r = 3)\} \tag{2.35}$$

$$\{\pm 29\} \subseteq \{\mathbb{L}_{holes} \cap \mathbb{L}(a_r = 29)\} \tag{2.36}$$

Notice that each value of a_r can only fill one or several specific holes. In other words, we use only the corresponding elements in each $\hat{\mathbf{R}}_{\mathbf{y}}(a_r)$ to fill the holes and discard the remaining elements. We define this mechanism as data no-reusing mechanism. In the

following sections, we will explain the data reusing mechanism.

Filling holes with data reusing

The estimation variance can generally be reduced if higher number of data can be used for calculating the average value. Comparing Figure 2.9a, Figure 2.9b and Figure 2.9c, it can be found that there are some overlapped positions, i.e., $\{0, \pm 2, \pm 4, \pm 6...\}$ in Figure 2.9a and Figure 2.9b, $\{\pm 6, \pm 12, \pm 18...\}$ in Figure 2.9a, Figure 2.9b and Figure 2.9c. It means that $\mathbb{L} \cap \mathbb{L}(a_r)$ is not an empty set. The data in the initial coarray (Figure 2.9a) are constructed by averaging the respective data from the sampling covariance matrix. In Figure 2.9b and Figure 2.9c, though the data from the selected matrices $\hat{\mathbf{R}}_{\mathbf{y}}(a_r)$ are intended to fill the holes, they simultaneously generate some data which can be reused for calculating the overlapped positions in Figure 2.9a. In this case, we can jointly use all the useful data in $\hat{\mathbf{R}}_{\mathbf{y}}(a_r)$ with the data in $\hat{\mathbf{R}}_{\mathbf{y}}$ to construct the complete virtual coarray.

For illustration, we consider the position $\{\pm 6\}$, which can be found in Figure 2.9a, Figure 2.9b and Figure 2.9c. The respective elements in $\hat{\mathbf{R}}_{\mathbf{y}}$, $\hat{\mathbf{R}}_{\mathbf{y}}(a_r = 2)$, $\hat{\mathbf{R}}_{\mathbf{y}}(a_r = 3)$ can be selected to calculate the average and be used to fill the position $\{\pm 6\}$. This data reusing mechanism can be applied to all the overlapped positions including the holes. The information in the virtual coarrays generated by multi-rates can then be maximally exploited.

Let us denote the set of multi-rate integer coefficients $\mathbb{I}_{rates}$ as in (2.29), and define the union set of overlapped positions between the original classical coprime coarray and multiple rate coarrays as

$$\mathbb{L}_{rates} = \bigcup_{a_r \in \mathbb{I}_{rates}} \{\mathbb{L} \cap \mathbb{L}(a_r)\} \tag{2.37}$$

Furthermore, assume that there are N_i entries in $\hat{\mathbf{R}}_{\mathbf{y}}$ and N_{i,a_r} entries in $\hat{\mathbf{R}}_{\mathbf{y}}(a_r)$, which are denoted by $\hat{\mathbf{R}}_{\mathbf{y}}^{(i,k)}, k = 1, 2, ..., N_i$ and $\hat{\mathbf{R}}_{\mathbf{y}}^{(i,k)}(a_r), k = 1, 2, ..., N_{i,a_r}$, which correspond to the same i-th position in the coarray, then the data reusing mechanism can be summarized as follows:

1) If $i \in \{\mathbb{L} - \mathbb{L}_{rates}\}$, we select all the corresponding entries from $\hat{\mathbf{R}}_{\mathbf{y}}$ to calculate $\hat{r}[i]$:

$$\hat{r}[i] = \frac{1}{N_i} \sum_{k=1}^{N_i} \hat{\mathbf{R}}_{\mathbf{y}}^{(i,k)} \tag{2.38}$$

2) If $i \in \mathbb{L}_{holes}$, we first choose several different values of $a_r \in \mathbb{I}_{rates}$ to generate different versions of $\hat{\mathbf{R}}_{\mathbf{y}}(a_r)$, then select all the corresponding entries from different $\hat{\mathbf{R}}_{\mathbf{y}}(a_r)$ to calculate $\hat{r}[i]$:

$$\hat{r}[i] = \frac{1}{\sum_{a_r \in \mathbb{I}_{rate}} N_{i,a_r}} \sum_{a_r \in \mathbb{I}_{rate}} \sum_{k=1}^{N_{i,a_r}} \hat{\mathbf{R}}_{\mathbf{y}}^{(i,k)}(a_r) \tag{2.39}$$

3) If $i \in \mathbb{L}_{rates}$, we select all the corresponding entries from $\hat{\mathbf{R}}_{\mathbf{y}}$ as well as the different versions of $\hat{\mathbf{R}}_{\mathbf{y}}(a_r)$ to jointly estimate the mean value of $\hat{r}[i]$:

$$\hat{r}[i] = \frac{1}{N_i + \sum_{a_r \in \mathbb{I}_{rate}} N_{i,a_r}} \left(\sum_{k=1}^{N_i} \hat{\mathbf{R}}_{\mathbf{y}}^{(i,k)} + \sum_{a_r \in \mathbb{I}_{rate}} \sum_{k=1}^{N_{i,a_r}} \hat{\mathbf{R}}_{\mathbf{y}}^{(i,k)}(a_r) \right) \tag{2.40}$$

It can be noticed that for the covariance matrix $\hat{\mathbf{R}}_{\mathbf{y}}(a_r)$, apart from the entries in $\hat{\mathbf{R}}_{\mathbf{y}}(a_r)$ that are used to estimate $\hat{r}[i]$ for the case $i \in \mathbb{L}_{holes}$, some entries in $\hat{\mathbf{R}}_{\mathbf{y}}(a_r)$ can also be reused to estimate the elements $\hat{r}[i]$ for $i \in \mathbb{L}_{rates}$.

After filling all the holes in the classical coprime virtual coarray, the maximum DOF can be fully used without discarding the non-contiguous part. Many mature techniques can be applied on $\hat{\mathbf{R}}_v$, including MUSIC [45] and ESPRIT [44], etc.

Suggested rules to choose the multi-rate coefficients

For any given situation, it is clear that different sets of multi-rate $\mathbb{I}_{rates}$ can be defined to fill all the holes. Here we suggest two rules to choose $\mathbb{I}_{rates}$:

• Rule 1: **Choose a_r as small as possible**. This can be seen from equation (2.30) that smaller a_r can achieve higher value of $\frac{L}{a_r}$, leading to more data for calculating $\hat{\mathbf{R}}_{\mathbf{y}}(a_r)$ and achieving better estimation performance.

• Rule 2: **Make the cardinality of $\mathbb{I}_{rates}$ as small as possible**. In the proposed scheme, we should calculate $\hat{\mathbf{R}}_{\mathbf{y}}(a_r)$ for each value of a_r. It is straightforward that more different coefficients will cause higher calculation complexity. Consequently, the cardinality of $\mathbb{I}_{rates}$

should be as small as possible to reduce the calculation complexity.

To find the appropriate value of a_r, the positions of holes are first obtained by the proposition which will be specified in the next subsection. Then the prime factorization is implemented to find the prime factors of the position value of each hole. According to the prime factors of the position values of all holes, we can choose a_r based on the above two rules. The details are given as follows:

If several values of the positions of holes have one common prime factor (CPF), we choose this CPF as one value of a_r to fill the corresponding holes.

If there exist several common prime factors for several holes, we choose the smallest CPF according to rule 1.

If the position of a hole have no CPF with other holes, we choose its minimum prime factor as one value of a_r.

For any integers greater than 1, we can always find at least one prime factor according to the principle of prime factorization. This means that we can always find at least one suitable $a_r \neq 1$ for any hole value.

For the cases of small values of M and N which have few holes in the coarray, it could be easy to perform the prime factorization and find the suitable a_r. As for the cases of large M and N with more holes, saying more than 10 hole elements (10 is an empirical value), we propose the following algorithm to simplify the process of choosing a_r:

1) We first consider $a_{r1} = 2$. This is because 2 is the smallest prime integer and it is the prime factor of all even integers. By doing so, the holes with even position values can be filled.

2) If there are still many unfilled holes (more than 10 different values), we can choose the next prime integer greater than 2, which is $a_{r2} = 3$, and the holes with position values of multiple of 3 are filled. If there are only a few holes remaining unfilled, the prime factorization is then implemented to the unfilled holes to find their prime factors and choose the suitable a_r.

The reason we choose $a_{r1} = 2$ is that a smaller integer is a common divisor of more integers, i.e., 2 is the divisor of all even integers while 3 is the divisor of one integer among

every three contiguous integers. In general, if there are many holes needed to be filled, a_r with a smaller value can fill more holes.

2.4.4 Position property of the holes

Before choosing an appropriate value of a_r, the position of missing elements in $\mathbb{L}$ should be first determined. For given system parameters M and N, the following proposition holds.

Proposition 1: The holes occur at position $\pm(b_1M + b_2N)$, where $b_1M + b_2N < (2M-1)N$, b_1, b_2 are integers, $1 \leq b_1 \leq N - 1 - \lfloor \frac{N}{M} \rfloor$ and $M \leq b_2 \leq 2M - 2$.

It should be noticed that the same expression of positions of the holes has been given in [64]. However, only the lower bounds of b_1 and b_2 are provided. The upper bounds of b_1 and b_2 have not been given. We provide the proof for the upper bounds of b_1 and b_2 so that all the holes can be analytically determined. We also provide a new way to prove the lower bounds of b_1 and b_2.

Proof of Proposition 1

1) The first hole is located at position $MN + M$ [63]. We first show that any integer number in $[0, MN+M-1]$, namely a, can be generated by the difference coarray $\pm(Nm-Mn)$. We can rewrite $a = Nm - Mn$ into

$$Nm = a + Mn$$

Under the conditions $0 \leq n \leq N-1$ and $0 \leq a \leq MN + M - 1$, for each value of a and n, we can have $a + Mn \leq 2MN - 1$. Then, it can be obtained that $N \leq Nm \leq 2MN - 1$, which is equivalent to $1 \leq m \leq 2M - \frac{1}{N}$. As $N > 1$ and m is an integer, we can obtain

$$1 \leq m \leq 2M - 1$$

It indicates that for each value of $n \in [0, N-1]$, we can always find an appropriate value of $m \in [1, 2M-1]$ to obtain $a \in [0, MN + M - 1]$.

Then we show that the value $MN + M$ can not be obtained with $\pm(Nm - Mn)$ by

using contradiction. Assuming that $MN + M = Nm - Mn$ can be obtained with some appropriate values of m, n. Then it can be derived that

$$\frac{M}{N} = \frac{m - M}{n + 1}$$

Notice that $m - M \leq M - 1$. But as M, N are coprime integers, their ratio can not be reduced to a radio of smaller integers. As a consequence, it is not possible to find proper values of m and n satisfying the above equation. Similar derivation holds if we assume $MN + M = -(Nm - Mn)$. Hence the first hole in position $MN + M$ is proved.

2) The general expression of positions of the holes $b_1M + b_2N$ $(b_1 \geq 1, b_2 \geq M)$ can be proved by contradiction, which can be found in Appendix I [64].

3) Finally, we determine the upper bounds of b_1 and b_2. Notice that the maximum number in $\mathbb{L}$ is $(2M-1)N$, the positions of the holes follow that $b_1M+b_2N < (2M-1)N$. Recalling the condition $b_1 \geq 1, b_2 \geq M$, we can have

$$\begin{aligned} b_1M &< (2M-1)N - b_2N \\ &< 2MN - N - MN \\ &< MN - N \\ b_1 &< N - \frac{N}{M} \end{aligned}$$

Since $N > M$ and b_1 is an integer, we can obtain that $b_1 \leq N - 1 - \lfloor \frac{N}{M} \rfloor$. Similarly, we can also obtain that $b_2 \leq 2M - 2$. The proposition is then proved.

2.4.5 Simulation results and discussion

In this simulation part, the MUSIC algorithm is used for estimating the frequencies. The benchmarks of comparison are to assess the maximum number of detectable frequencies and the relative RMSE of the estimated frequencies.

MUSIC spectrum and number of detectable frequencies

We first consider the case of $M = 4$ and $N = 5$ to show the MUSIC spectrum of

the proposed multi-rate coprime sampling scheme. The SNR is set to be 0dB and the number of sampling units is set to $L = 1000$. Based on the *Proposition* of positions of the holes, the set of holes can be determined as $\mathbb{L}_{holes} = \{\pm 24, \pm 28, \pm 29, \pm 32, \pm 33, \pm 34\}$. The maximum number of detectable frequencies of the coarray after filling the holes with the proposed multi-rate coprime scheme is $(2M-1)N = 35$. As explained in the previous part, parameter a_r with values in the set $\mathbb{I}_{rates} = \{2, 3, 29\}$ has been used. $\mathbb{I}_{rates} = \{3, 4, 17, 29\}$ could also be chosen but according to the suggested rules, it is preferable to use $\mathbb{I}_{rates} = \{2, 3, 29\}$ with three different a_r rather than four.

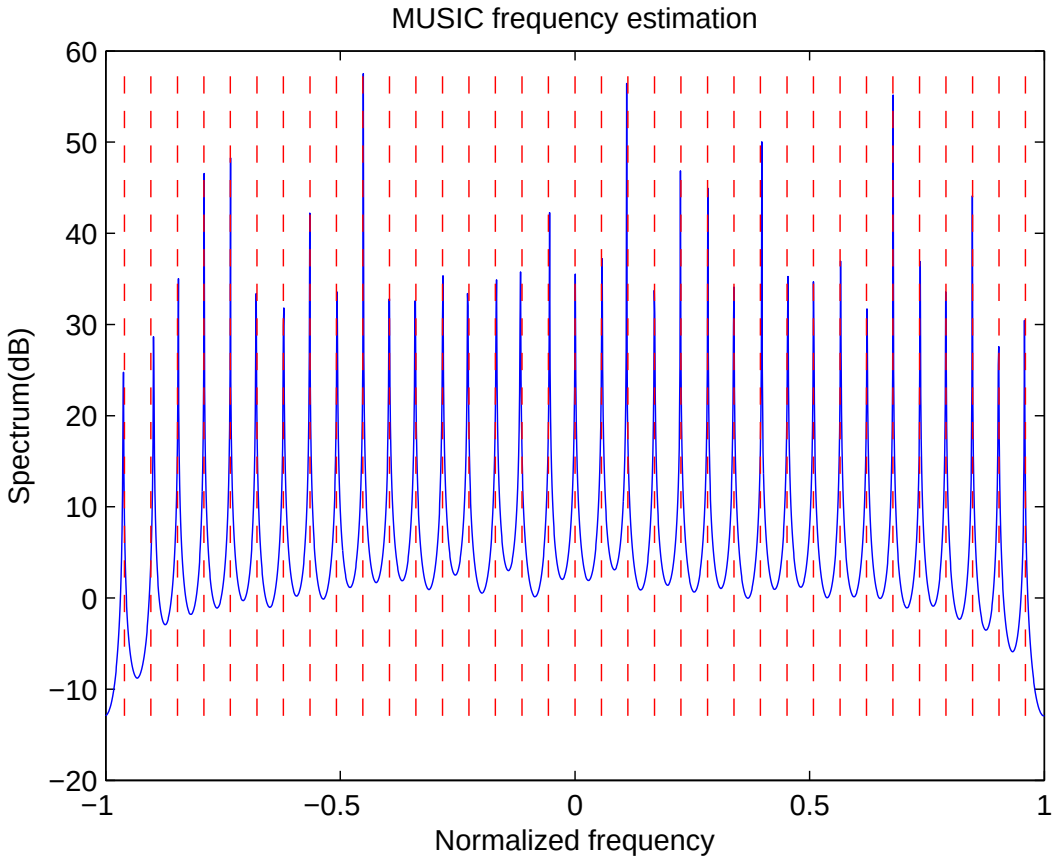

Figure 2.11 – MUSIC spectrum of estimated frequencies, $M = 4, N = 5$, 35 different sinusoidal components.

Figure 2.11 shows the MUSIC spectrum of 35 estimated frequencies which are uniformly distributed over interval $[-0.96, 0.96]$. The vertical discontinous lines correspond

to the true positions of frequencies. It can be seen that all the frequencies are correctly estimated using the proposed scheme. It should be mentioned that in the classical coprime sampling, only a maximum of 23 frequencies can be estimated due to the holes, which means that part of the DOFs has not been used. Our proposed scheme can significantly increase the maximum number of detectable frequencies.

Performance with different multi-rate coefficients

Next, we investigate the impact of the multi-rate coefficient to the proposed scheme. The data no-reusing mechanism is used in Figure 2.12 to focus on the impact of a_r. For simplicity, we consider a coprime array with $M = 2, N = 3$ which has only one pair of holes in the difference coarray (position ± 8). The number of Monte Carlo trials is set to be 500. We only need to choose one value of a_r to construct a new multi-rate coarray. The possible solutions of integer a_r are $a_r = 2, a_r = 4, a_r = 8$. The classical coprime sampling scheme with no holes filling [66] is compared with these three scenarios.

Figure 2.12 shows the performance with 4 sinusoidal components. It can be seen that the proposed scheme outperforms the classical coprime sampling scheme. This is mainly because the multiple coprime rate scheme fills the holes in the classical coprime virtual coarray. Therefore, the maximum number of detectable frequencies is 9 for the proposed method, while it is only 7 for the classical coprime scheme with $M = 2, N = 3$.

We can also observe from Figure 2.12 that a lower value of a_r leads to a better estimation performance. This benefit is due to the fact that more samples are selected from the classical coprime sample stream if a_r is set to a lower value. The estimation variance can be reduced when more samples are used for calculating the average, which is in agreement with the suggested rules. However, this benefit is very limited when a_r varies from 4 to 2. The two respective curves achieve very similar performance as shown in Figure 2.12. This is because the noise can not be thoroughly eliminated even if more samples are selected from the same sample stream. It can also be observed that there is a gap between the RMSE of the proposed method and the CRB even in high SNR region. This is consistent with the conclusion in [65] where the authors claim that the RMSE of coprime configuration converges to a positive value and CRB tends to zero when $D < M + N$. Figure

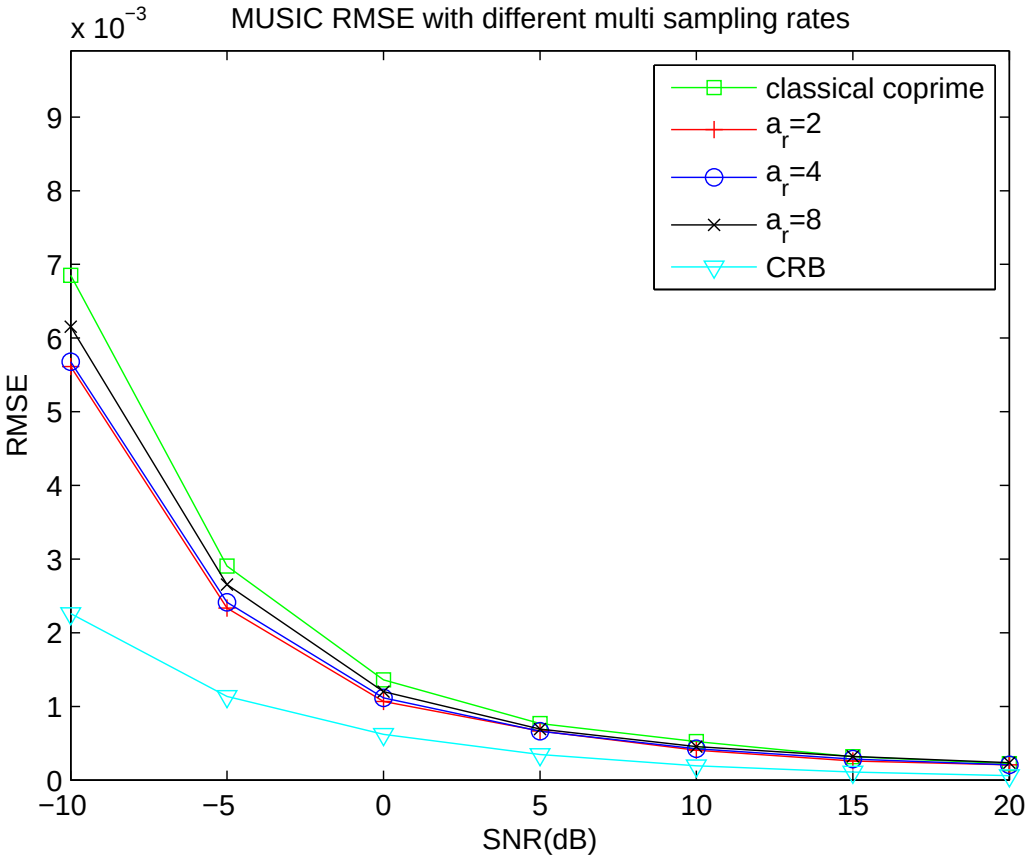

Figure 2.12 – RMSE performance with different multi-rate coefficients, $M = 2, N = 3$, 4 sinusoidal components.

2.13 compares the performance as a function of number of units. It is obvious that the estimation performance is improved when more sample units are available.

Comparison of data reusing and data no-reusing

Figure 2.14 and Figure 2.15 compare the data reusing mechanism and data no-reusing mechanism with the generalized coprime sampling scheme [63] and nuclear norm minimization interpolation scheme [75]. For the generalized coprime sampling scheme, we consider two sample units from each sampler to form a sample block hereafter. Different from the previous part with only one pair of holes, we consider $M = 4, N = 5$ such that six pairs of holes are required to be filled by choosing several different values of a_r simultaneously. The signal contains 12 sinusoidal components in Figure 2.14 and 25 components

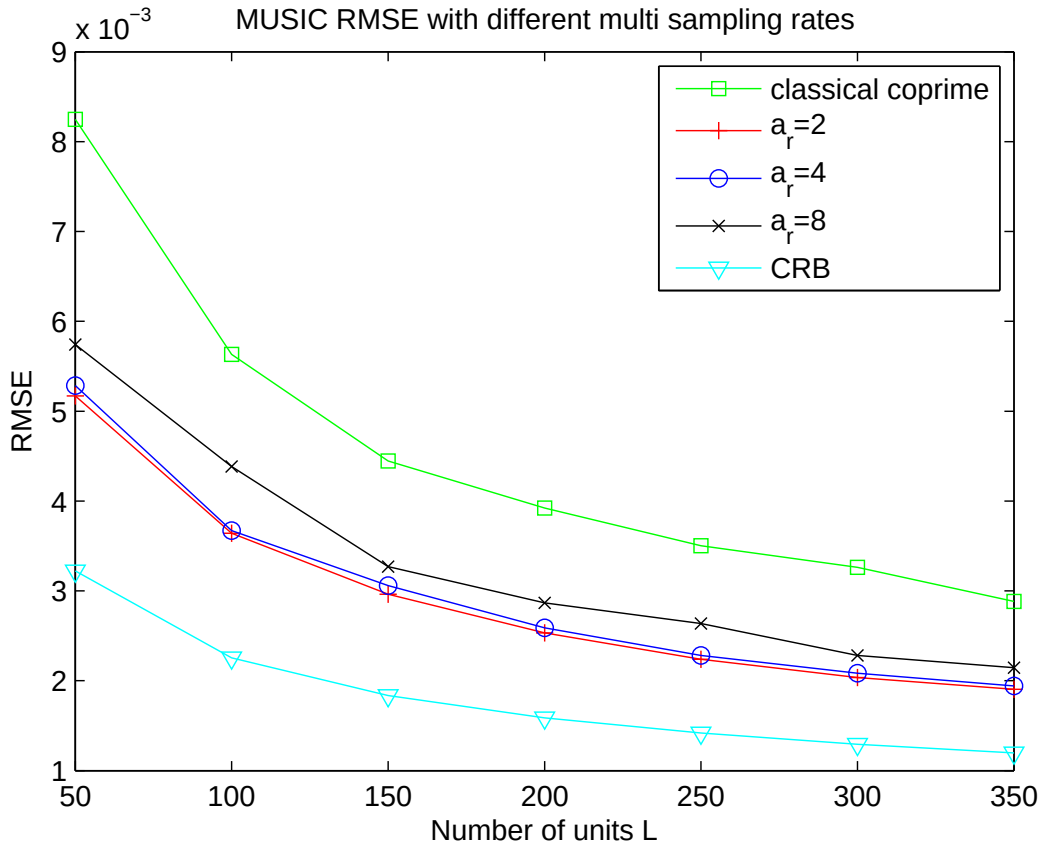

Figure 2.13 – RMSE performance with different multi-rate coefficients, $M = 2, N = 3$, 4 sinusoidal components.

in Figure 2.15. As described above, three different multi-rate coefficients $\mathbb{I}_{rates} = \{2, 3, 29\}$ are considered to fill all the holes.

As shown in Figure 2.14 and Figure 2.15, both the data reusing and data no-reusing mechanism outperform the generalized coprime and the nuclear norm scheme. This is because the generalized coprime scheme use two sample units to form a sample block in our simulation. By doing so, some holes can be filled but there still exist some unfilled holes and the maximum DOFs can not be fully utilized. In contrast, the proposed method can fill all the holes distributed in $[0, (2M-1)N]$ and achieve better performance. In addition, the proposed method also surpasses the nuclear norm scheme because the performance of nuclear norm interpolation could be strongly affected by noise level. In high SNR region, nuclear norm scheme can achieve similar performance with the proposed method.

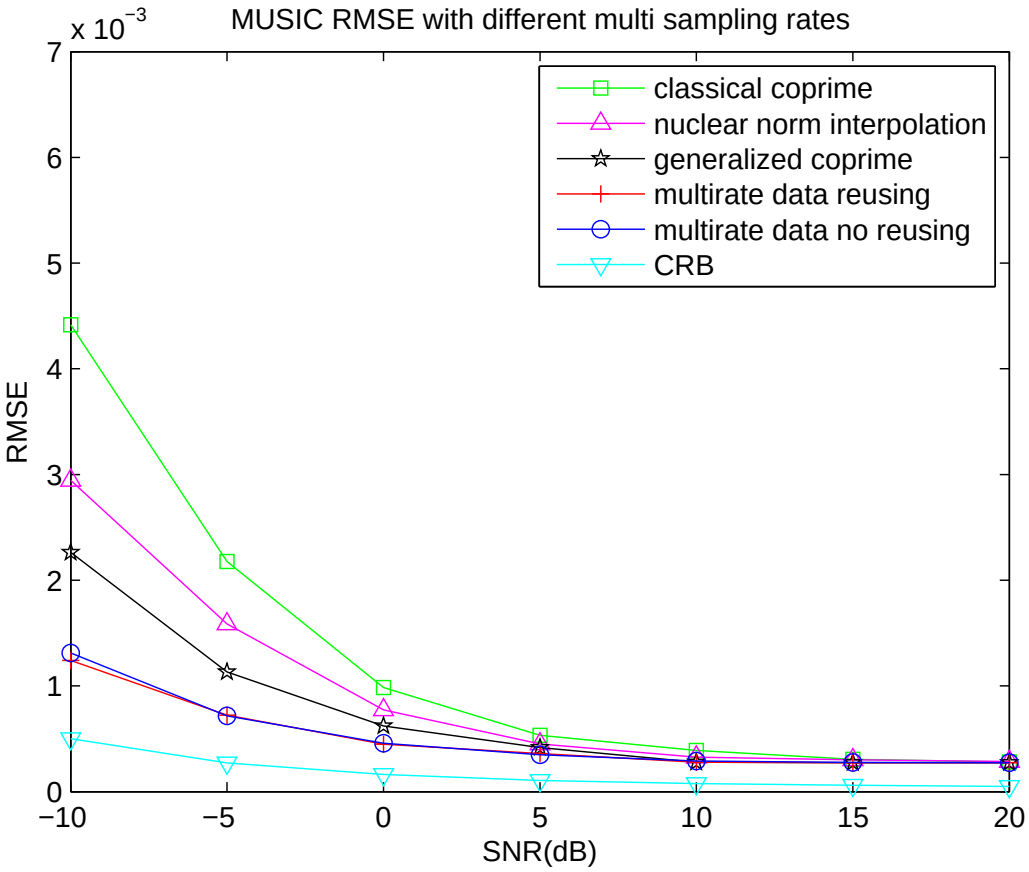

Figure 2.14 – Performance of data reusing & data no-reusing, $M = 4, N = 5$, 12 sinusoidal components.

Furthermore, the data reusing mechanism has a slightly better performance than the data no-reusing mechanism when SNR is low because more data are employed for constructing the virtual coarray. As SNR increases, two mechanisms achieve very similar performance. This is because only part of data in $\hat{\mathbf{R}}_{\mathbf{y}}(a_r)$ is selected for the data reusing mechanism. The improvement will be very limited. It is evident in Figure 2.14 that in less sources scenario (i.e. 12 sinusoidal components compared to 25 components in Figure 2.15), the performance of the generalized coprime can be close to the proposed method when SNR is high. For $M = 4, N = 5$, the maximum number of detectable frequencies of the generalized coprime is 28, while it is 23 for the classical coprime and 35 for the proposed method. It should be mentioned that the nuclear norm scheme can not always

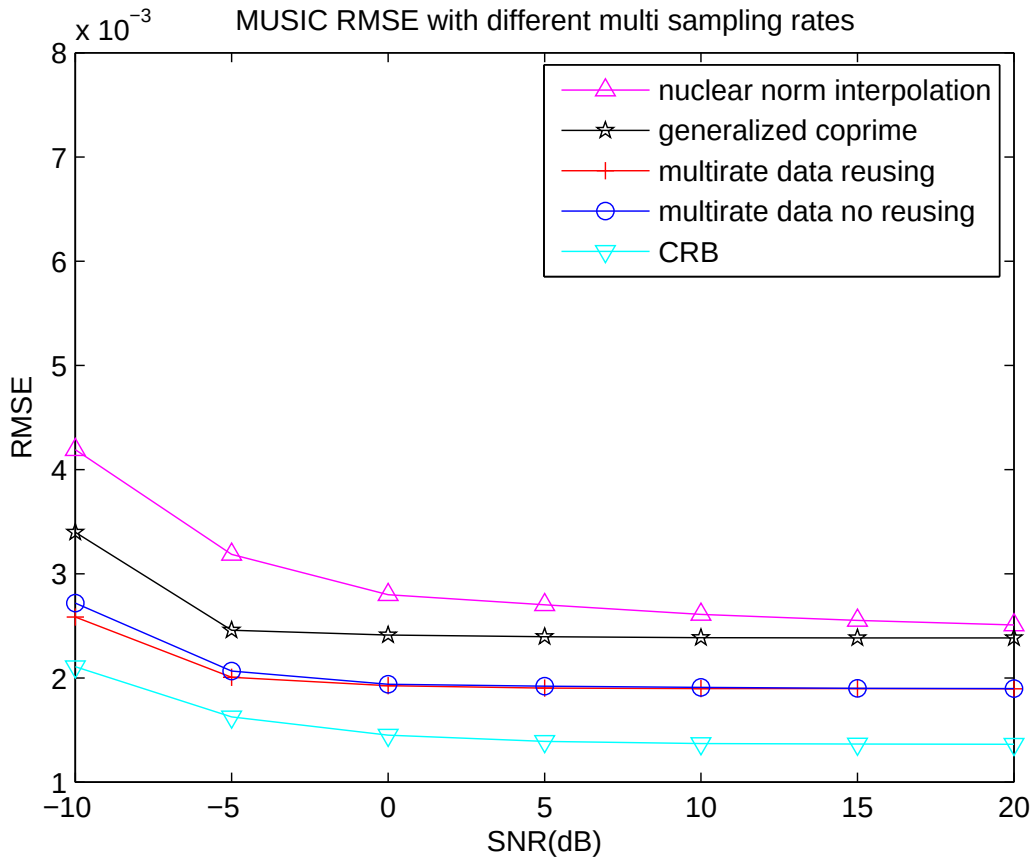

Figure 2.15 – Performance of data reusing & data no-reusing, $M = 4, N = 5$, 25 sinusoidal components.

achieve the maximum DOFs because the actual freedom is governed by non-uniform grid [75]. We consider 25 sinusoidal components in Figure 2.15 for comparison. It can be seen that there is a gap between the generalized coprime and the proposed method due to the difference of DOFs. The performance of nuclear norm scheme is the worst in Figure 2.15 and it tends to be close to the generalized coprime scheme in high SNR scheme. An interesting fact is that the virtual coarray of the generalized coprime scheme is similar to the classical coprime. The proposed method can also be easily applied to the generalized coprime scheme to fill the holes and the DOFs can be further increased.

2.5 Conclusion

In this chapter, we provide detail investigation on the coprime sampling scheme. We first analyze the coprime sampling technique within the framework of practical sampling realization, where only one realization of samples is available. The coprime sampling mechanism will suffer from diagonal property loss problem in specific conditions. We propose an embedded random delay mechanism to overcome this problem while the performance of coprime sampling is not significantly affected.

Then we focus on the holes filling problem in the 2-DC of coprime sampling. A multi-rate coprime sampling scheme is proposed to settle this problem. The principle of multi-rate coprime sampling is to construct several scaled versions of the 2-DC with different sampling rate. With properly designed sampling strategy, the holes in the original 2-DC can be found in different versions of the 2-DC and the holes can be filled by selecting these data from different scaled 2-DCs. Also, the multi-rate scheme does not cause additional sampling burden if the sampling rate parameters are set to appropriate integer values.

Chapter 3

Rearranged coprime array for passive DOA estimation using 2-DC

3.1 Introduction

In this chapter, we adopt the coprime array for DOA estimation. In the previous chapter, we have illustrated that the 2-DC of coprime configuration has some holes and the nonconsecutive part in the 2-DC can not be utilized. We focus on the holes filling problem in this chapter from the physical array geometry aspect. Notice that one main character of sparse array is its low hardware cost, which is to use few sensors to detect more sources than sensors. In this chapter, our proposition also follows this principle and avoids additional hardware cost. Also, the mutual coupling effect is considered in this chapter.

Some attempts aim to fill the holes from the physical array aspect have been proposed. The interpolation method with array moving at specific speed requires velocity control operation [80, 81]. CCA method aims to add some additional sensors to construct a complementary subarray to fill the holes in the 2-DC. However compared with the conventional coprime array, CCA requires $(M-1)$ additional sensors to fill the holes and totally $3M+N-2$ sensors are required, which is not an economical solution when M becomes large [77]. Also, the introduced sensors in CCA are closely distributed with inter-element spacing equals to half of the wavelength of incoming signals. The mutual coupling is unavoidable as the number of sensors increases.

Most recently, the thinned coprime array (TCA) [111] shows that some sensors in a

coprime array are found to be redundant. In other words, the difference coarray structure will not be modified if these redundant sensors are removed from the coprime array. The same DOFs and less mutual coupling can be achieved with fewer sensors in TCA compared with the classical coprime array [112]. Inspired by the spirit of TCA, we propose a novel coprime based geometry without requiring additional sensors to address the holes problem in the 2-DC. This is realized by rearranging the redundant sensors in the conventional coprime array to appropriate new positions, which are determined by the property of the holes in the 2-DC.

When designing the array geometry, the mutual coupling effect is also important and should be considered. The super nested array (SNA) is proposed in [85, 113] to reduce the mutual coupling effect while holding the main advantages of the nested array, such as, closed-form of sensor locations and hole free difference coarray. Another array configuration based on the nested array is the augmented nested array (ANA) [71]. ANA can increase the DOFs and reduce the mutual coupling in four different ways. However, the mutual coupling could increase when the number of sensors becomes large [112] for ANAI-1 and ANAI-2 (denoted as ANA1 and ANA2 in the following), while the other two ANA arrays have to meet complicated conditions such that no holes occur in the difference coarray. The introduced sensors in CCA are closely distributed with inter-element spacing equal to half of the wavelength of incoming signals. However, the mutual coupling of CCA is unavoidable as the number of sensors increases. It will be shown in this chapter that our proposition can limit the mutual coupling compared with the SNA, ANA, CCA.

3.2 2-DC of coprime array and holes-triangle

3.2.1 Signal model of coprime array

Assuming a coprime array with two sub-arrays consisting of $2M + N - 1$ sensors, the mutual coupling effect is considered in this chapter and the signal vector is given by

$$\mathbf{x}_\theta(t) = \mathbf{C}\mathbf{A}_\theta\mathbf{s}(t) + \mathbf{n}(t) \tag{3.1}$$

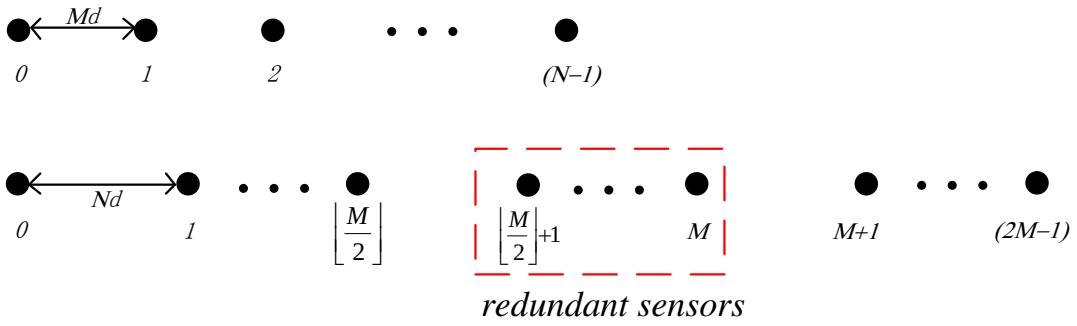

Figure 3.1 – Conventional coprime array.

Similar with the coprime sampling in time domain, we can calculate the covariance matrix and vectorize the covariance matrix to obtain a virtual signal model.

Before further elaborating our proposition, it is important to investigate the property of 2-DC. In this section, we first review the redundancy of sensors in coprime array. Then we categorize the holes into holes-triangle, which will be utilized for illustrating our proposition.

3.2.2 Redundancy of sensors and weight function

We consider the conventional coprime array, consisting of two sub-arrays, where one sub-array has N sensors with Md_0 as separation distance between two adjacent sensors and another sub-array has $2M$ sensors with Nd_0 as the distance between two adjacent sensors, with d_0 the half wavelength of impinging signals. The first sensor is shared by two sub-arrays. A graphic illustration of the conventional coprime array is given in Fig. 3.1, where M, N are two coprime integers. In this dissertation, we assume $M < N$ without loss of generality.

It is well established that there are some holes in the difference coarray of the classical coprime array. Since the difference coarray is a symmetric structure, for simplifying

illustration, we only take the non-negative part of the difference coarray into account in the following part. We rewrite the position of holes as follows [114].

$$\begin{aligned} \mathbb{H} &= \{h | h = MN + M + b_1' M + b_2' N\}, \\ s.t. \quad 0 \leq b_1' &\leq N - 2 - \lfloor \frac{N}{M} \rfloor, \quad 0 \leq b_2' \leq M - 2, \\ h &\in [MN + M, (2M-1)N) \end{aligned} \tag{3.2}$$

Apart from the holes, there could be several different sensor pairs that contribute to the same virtual sensor. For further discussion, the *weight function* [71] is defined as the number of sensor pairs leading to element m in the coarray

$$\mathbb{W}_m = \{(n_1, n_2) \in \mathbb{S}^2 | n_1 - n_2 = m\} \tag{3.3}$$

$$\omega(m) = \text{Card}(\mathbb{W}_m) \tag{3.4}$$

where $\omega(m)$ is the weight function and $\mathbb{W}_m$ represents the set of physical sensor pairs leading to the m-th virtual sensor in the coarray, $\text{Card}(\mathbb{W}_m)$ returns the cardinality of set $\mathbb{W}_m$.

If it is a hole at the m-th position in the coarray, $\omega(m) = 0$. It is well established that the values of the weight function corresponding to small sensor separation m have high mutual coupling effect. Particularly, the first three values $\omega(1), \omega(2), \omega(3)$ would be of great interest since they contribute primarily to the mutual coupling due to their small sensor separation [71, 113]. For simplification, we will exploit the first three values of weight function for analytical discussion of the mutual coupling effect in the following part.

In the conventional coprime array, it has been proved that some sensors in the $2M$-elements sub-array are redundant [111, 112]. In other words, removing these redundant sensors will not change the difference coarray geometry. As shown in Fig. 3.1, by removing the redundant sensors in the rectangle, the conventional coprime array turns out to be a TCA.

The number of contiguous redundant sensors for a conventional coprime array (except

for $M = 3$) is given by

$$S_{red} = \lceil \frac{M}{2} \rceil \tag{3.5}$$

where these redundant sensors are all in the $2M$-elements sub-array and the index of these redundant sensors starts from $\lfloor \frac{M}{2} \rfloor + 1$. The symbol $\lceil x \rceil$ returns the smallest integer greater than x and $\lfloor x \rfloor$ denotes the greatest integer less than x. The proof for the redundancy of these sensors can be found in [112].

The case of $M = 3$ is special, for which, there are still $\lceil \frac{M}{2} \rceil = 2$ redundant sensors in the $2M$-elements sub-array. However, these two redundant sensors are no longer contiguous. Their positions are MN and N. The redundancy of sensor at position MN has been proved in [112]. By applying the similar derivation, we can also prove the redundancy of the sensor positioned at N.

3.2.3 Holes-triangle

To better explain the design rules of the proposed rearranged coprime array, we first classify all the holes into a specific order with a 2D-representation. In [77], CCA method classifies the holes into several layers including $M - 1$ complete layers, and $M - 1$ extra sensors are required in the complementary sub-array to fill all the holes. Though CCA can fill all the holes, the way that these extra sensors are utilized to fill the holes is not always efficient due to the way the holes are classified. In this section, we classify the holes into several sub-triangles, where we can fill the holes in a more efficient way. Our aim is to fill the holes only with the $\lceil \frac{M}{2} \rceil$ redundant sensors such that no extra sensor is required. We classify the holes from another point of view. Based on the position of holes, we define holes-triangle to represent all the hole elements.

Definition 3: A *holes-triangle* is a triangle-like structure with its elements given by

$$h \in \mathbb{H}. \tag{3.6}$$

The holes-triangle can be divided into several sub-triangles with each consisting of a *left-side* and a *right-side*. In a *sub-triangle*, starting with a given hole element h, the *left-side*

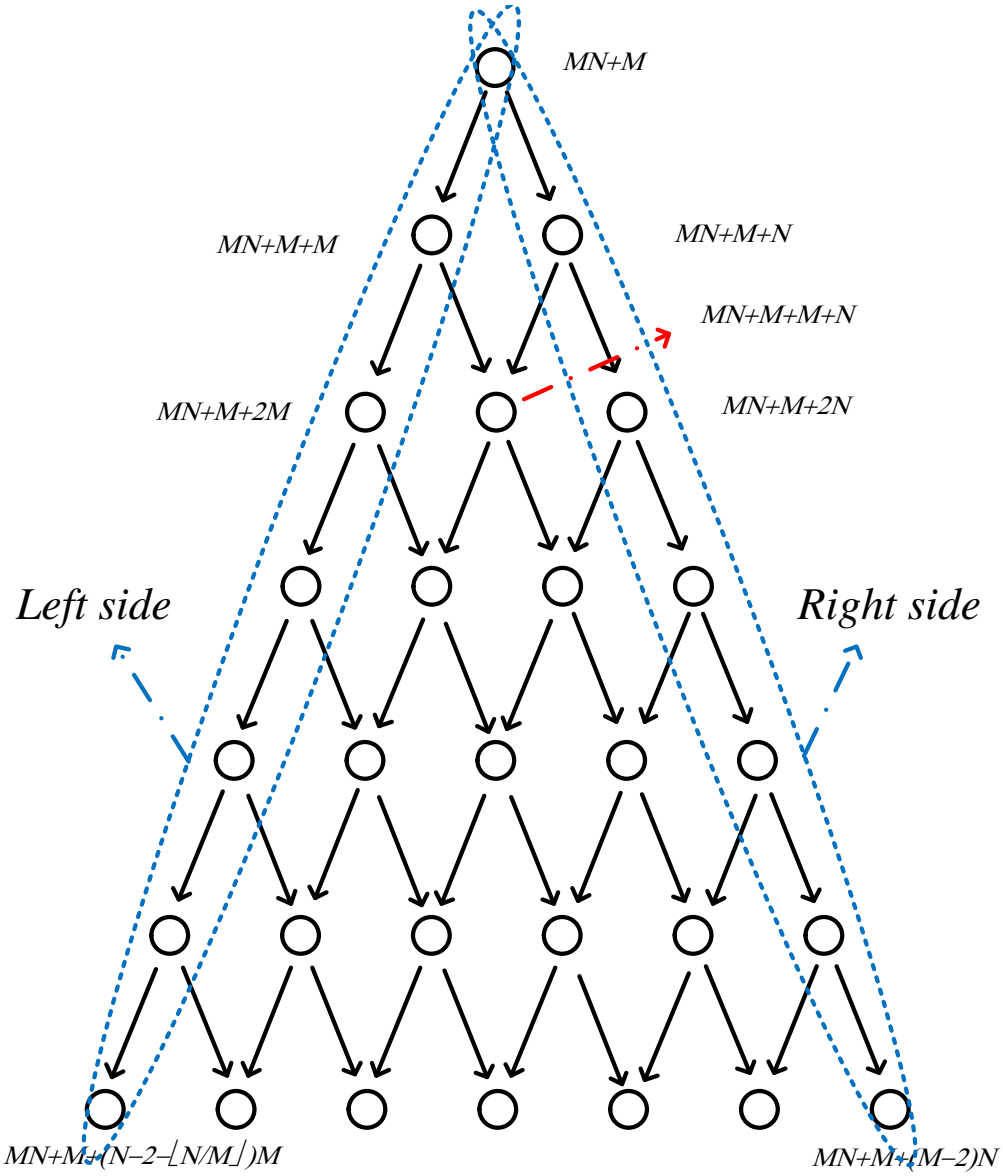

Figure 3.2 – Holes-triangle with $M = 8, N = 9$.

is defined as the set

$$\{h + b_1' M | \quad h + b_1' M < (2M - 1)N\} \tag{3.7}$$

with its elements in increasing order, and the *right-side* is defined as the set

$$\{h + b_2' N | \quad h + b_2' N < (2M - 1)N\} \tag{3.8}$$

also with its elements arranged in increasing order. The intersection element h between the *left-side* and *right-side* is called the vertex of the corresponding *sub-triangle*.

An example of holes-triangle with $M = 8, N = 9$ is given in Fig. 3.2. The hole elements are represented with circles and the arrows indicate the increasing direction between two neighbor elements. We emphasize the biggest sub-triangle with two dotted ovals for illustration, which has the most hole elements among all the sub-triangles. The value of elements on the left-side increases from $MN+M$ to $MN+M+(N-2-\lfloor\frac{N}{M}\rfloor)M$ while that of the right-side increases from $MN + M$ to $MN + M + (M - 2)N$.

3.3 Rearranged coprime array configuration

3.3.1 Rearrangement of sensors

In [77], some additional sensors are introduced at the position corresponding to the biggest value in each left-side or right-side of some sub-triangles to fill the holes. $M - 1$ additional sensors are required in the CCA method and it could be hardware expensive when M is a large value. In this dissertation, we aim to fill the holes without introducing extra sensors. This can be achieved by relocating the redundant sensors at specific sparse positions. By doing so, the length of consecutive coarray part can be significantly increased. The position of sensors after the rearrangement can be given by:

$$\mathbb{S}_1=\{n_1M|0 \leq n_1 \leq N-1\} \tag{3.9}$$

$$\mathbb{S}_2=\{n_2N|(0 \leq n_2 \leq \lfloor\frac{M}{2}\rfloor) \cup (M+1 \leq n_2 \leq 2M-1)\} \tag{3.10}$$

$$\mathbb{S}_3=\{-(MN+M+i(M+N))|0 \leq i \leq \lceil\frac{M}{2}\rceil - 2\} \tag{3.11}$$

$$\mathbb{S}_4=\{-(MN+M+(\lceil\frac{M}{2}\rceil - 1)N)\} \tag{3.12}$$

The configuration of our proposed rearranged coprime array is shown in Fig. 3.3. It can be observed that there are totally $(2M+N-1)$ physical sensors, exactly like the conventional coprime array. The sub-arrays $\mathbb{S}_1$ and $\mathbb{S}_2$ form a TCA with $(2M + N - 1) - \lceil\frac{M}{2}\rceil$ sensors.

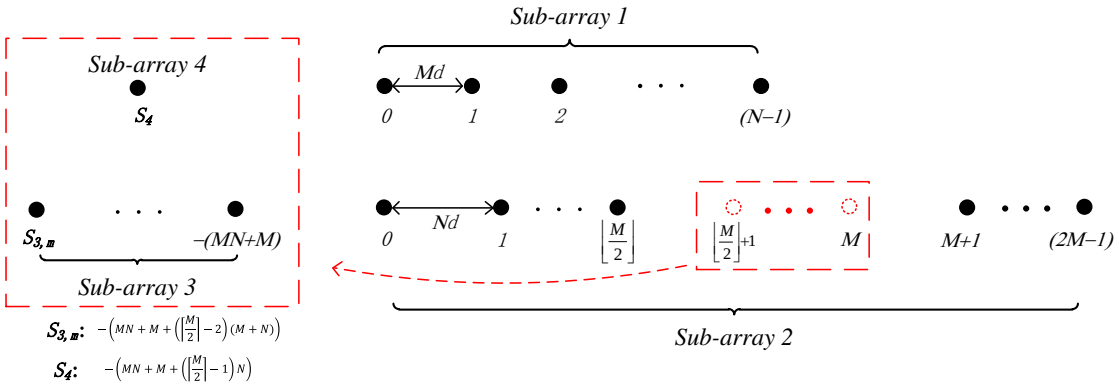

Figure 3.3 – Position of sensors in the rearranged coprime array. • : physical sensors, ○ : redundant sensors of the conventional coprime array.

The $\lceil \frac{M}{2} \rceil$ redundant sensors of the original conventional coprime array are represented by red dot circles. These redundant sensors are selected and rearranged outside the TCA to construct sub-arrays $\mathbb{S}_3$ and $\mathbb{S}_4$.

The reason of rearranging the redundant sensors at $\mathbb{S}_3$ and $\mathbb{S}_4$ is based on the following properties of the holes-triangle.

3.3.2 Holes filling after rearrangement

Property 1: For any given conventional coprime array, if one additional sensor is positioned at the symmetric negative position of a sub-triangle vertex, namely $-h$, all the holes elements on the *left-side* and *right-side* of the corresponding sub-array can be filled.

Proof. Assuming a given hole position $h \in [MN + M, (2M - 1)N)$ in the holes-triangle, its corresponding *left-side* and *right-side* elements can be given as set $\{h + iM | h + iM < (2M-1)N\}$ and $\{h+kN | h+kN < (2M-1)N\}$ respectively. Sensors of the conventional coprime array are located at two sub-arrays $\{n_1 M | 0 \leq n_1 \leq N-1\}$ and $\{m_1 N | 0 \leq m_1 \leq 2M-1\}$.

If one additional sensor is introduced at position $-h$, for any hole element $h + iM$ at the corresponding *left-side*, we can always find a sensor from the N-elements sub-array of

the conventional coprime array such that

$$h + iM = iM - (-h) \tag{3.13}$$

Then the hole element $h+iM$ can be filled. Relation (3.13) holds for all the hole elements at the *left-side* because $0 \leq i \leq N - 2 - \lfloor \frac{N}{M} \rfloor$ is a sub-set of $[0, N-1]$. Similar derivation can be applied to the corresponding *right-side*. Then *Property 1* is proved. □

Since we pick out the redundant sensors and relocate them outside the TCA, *Property 1* can be modified as

Lemma 1: For a rearranged coprime array, if one redundant sensor is relocated at the symmetric negative position of a sub-triangle vertex, all the holes elements on the *left-side* and the first $\lfloor \frac{M}{2} \rfloor + 1$ holes at the *right-side* can be filled.

Proof. Similar with the proof of *Property 1*, the elements at the *left-side* can be filled. After picking out the redundant sensors, the indexes of the first $\lfloor \frac{M}{2} \rfloor + 1$ remaining sensors in the $(2M - \lceil \frac{M}{2} \rceil)$ elements sub-array are distributed in $[0, \lfloor \frac{M}{2} \rfloor]$. For a given hole position h, the following $\lfloor \frac{M}{2} \rfloor + 1$ holes at the *right-side*, which are denoted as $h + kN$, can be filled by calculating the difference

$$h + kN = kN - (-h) \quad s.t. \quad 0 \leq k \leq \lfloor \frac{M}{2} \rfloor \tag{3.14}$$

Then *Lemma 1* is proved. □

Our goal is to fill as many holes as possible (even all holes) with the $\lceil \frac{M}{2} \rceil$ redundant sensors. For each redundant sensor, a good solution is to position it at the vertex of the sub-triangle which contains as much hole elements as possible. We have the following property for any two sub-triangles.

Property 2: For any two sub-triangles with vertex elements $h_1 < h_2$, the number of elements on the right-side corresponding to h_2 can not be greater than that corresponding to h_1.

Proof. This can be proved by contradiction. We assume that the elements on the right-side of h_2 are in the form $h_2 + i_2N$. Similarly, the elements on the right-side of h_1 are h_1+i_1N. Here, $i_1 \in [0, i_{1,max}], i_2 \in [0, i_{2,max}]$. The number of right-side elements associated to h_2 greater than the number of right-side elements associated to h_1 is equivalent to $i_{1,max} < i_{2,max}$. On the other hand, we should have $h_2 + i_{2,max}N < (2M-1)N$. Since $h_1 < h_2$, we can easily obtain $h_1 + i_{2,max}N < (2M-1)N$, which means that the right-side of h_1 has at least $i_{2,max}+1$ elements ($i_{1,max} \geq i_{2,max}$). This contradicts with $i_{1,max} < i_{2,max}$ and *Property 2* is proved. □

From *Property 1* and *Property 2*, we can know that the left-sides can be easily filled. This can be achieved by rearranging $\lceil \frac{M}{2} \rceil - 1$ redundant sensors at position set $\mathbb{S}_3$. Since we have only $\lceil \frac{M}{2} \rceil$ redundant sensors to fill the holes, we particularly focus on the right-side with the largest number of elements. This will naturally lead to the solution of position $\mathbb{S}_4$. Fig. 3.4 is an example of the holes filling process with $M = 7, N = 13$. The highlighted red triangles indicate the position of the rearranged redundant sensors at the symmetric negative position. The hollow circles represent the unfilled holes and the solid circles are the filled holes after rearranging the redundant sensors. There are totally $\lceil \frac{M}{2} \rceil = 4$ redundant sensors in this case, so we divide the holes filling process into 4 steps as shown in Fig. 3.4.

It can be observed from Fig. 3.4 that three redundant sensors are rearranged at $-[MN + M + i(M + N)]$ in the first three steps, where $0 \leq i \leq \lceil \frac{M}{2} \rceil - 2 = 2$. At the first step, according to *Lemma 1*, only the first $\lfloor \frac{M}{2} \rfloor + 1 = 4$ elements at the *right-side* can be filled with one sensor at position $-(MN+M)$. After the third step, the remaining unfilled elements, including $MN + M + (\lceil \frac{M}{2} \rceil - 1)(M + N)$, can be considered as a new sub-triangle, whose vertex is $MN + M + (\lceil \frac{M}{2} \rceil - 1)N$. Therefore, we rearrange the last redundant sensor at position $-(MN + M + (\lceil \frac{M}{2} \rceil - 1)N)$ to fill these holes.

For a given number of sensors, the cardinality of $\mathbb{U}$ will be increased if most holes are filled. Especially, we are more interested in the case where all holes in the range $[MN + M, (2M - 1)N)$ can be filled. Generally, $2M + N - 1$ sensors are used in the rearranged coprime array. It has been elaborated in the previous section that the number

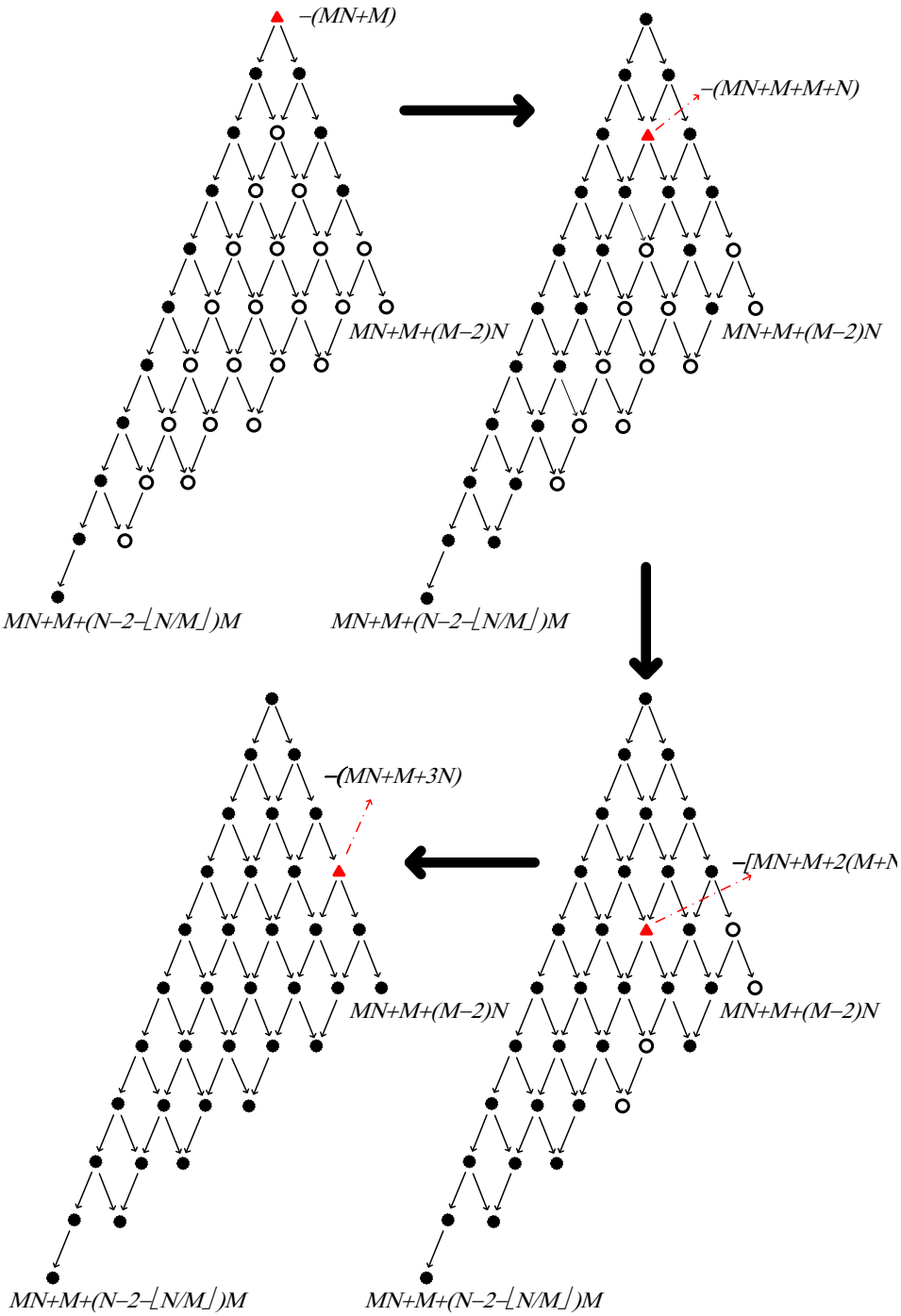

Figure 3.4 – Holes filling with the redundant sensors. $M = 7, N = 13$ ∘ : unfilled holes; • : filled holes; ▲: rearranged sensor position.

of redundant sensors is $\lceil \frac{M}{2} \rceil$. We consider the holes filling problem in two scenarios: 1) odd value of M; 2) even value of M.

Lemma 2: All the holes in $[MN + M, (2M - 1)N)$ can be filled if

$$\begin{cases} N \text{ can be any integer coprime with } M, & \text{if } M = 2, 3 \\ 3 < M \leq 7, \quad N < M + 4 + \frac{12}{M-3}, & \text{if } M \text{ is odd} \\ 2 < M \leq 8, \quad N < M + 2 + \frac{4}{M-2}, & \text{if } M \text{ is even.} \end{cases} \tag{3.15}$$

The possible values of M, N satisfying Lemma 2 are listed in Table 3.1 and the proof is provided as follows.

Table 3.1 – Possible values of M and N satisfying Lemma 2.

Possible value of M	Possible value of N
2	Odd integers greater than 2
3	Integers coprime with 3
4	5,7
5	6,7,8,9,11,12,13,14
6	7
7	8,9,10,11,12,13
8	9

Proof. From the definition of holes-triangle and *Lemma 1*, we can easily derive that the elements on the sub-triangle with vertex $MN + M$ can all be filled by arranging two sensors at positions $-(MN + M)$ and $-(MN + M + (\lceil \frac{M}{2} \rceil - 1)N)$. If there are some holes remaining unfilled, without loss of generality, we can assume that there is only one unfilled hole. Then the position of the unfilled hole can be divided into two scenarios.

1) If the unfilled hole is at the sub-triangles corresponding to $\mathbb{S}_3$, this unfilled hole will be on the right-side of sub-triangle with vertex $MN + M + M + N$. This can be derived according to *Lemma 1* and *property 2*. After removing the elements in sub-triangle with vertex $MN + M$, then $MN + M + M + N$ is the smallest value of the remaining elements. If there is another unfilled hole on another right-side corresponding to $\mathbb{S}_3$, there must be one unfilled hole at the right-side of $MN + M + M + N$. This means $MN + M + M +$

$N + (\lfloor \frac{M}{2} \rfloor + 1)N < (2M-1)N$. Equivalently, to assure that all holes are filled, we can formulate this case as

$$MN + M + M + N + (\lfloor \frac{M}{2} \rfloor + 1)N > (2M-1)N \tag{3.16}$$

2) If the unfilled hole is not at the sub-triangles corresponding to $\mathbb{S}_3$, then this unfilled hole will be on the right-side of the sub-triangle with vertex $MN + M + (\lceil \frac{M}{2} \rceil - 1)(M + N)$. This follows similar derivation as above. For the sub-triangle with vertex $MN + M + (\lceil \frac{M}{2} \rceil - 1)(M + N)$, its left-side elements are filled by the rearranged sensor at $\mathbb{S}_4$, which is $-(MN + M + (\lceil \frac{M}{2} \rceil - 1)N)$. However, if there are elements on the right-side of $MN + M + (\lceil \frac{M}{2} \rceil - 1)(M + N)$, they will remain unfilled. Then the smallest element is equal to $MN + M + (\lceil \frac{M}{2} \rceil - 1)(M + N) + N$. Equivalently, to assure that all holes are filled, we should have

$$MN + M + (\lceil \frac{M}{2} \rceil - 1)(M + N) + N > (2M-1)N \tag{3.17}$$

Relations (3.16) and (3.17) should both hold such that all the elements on the holes-triangle can be filled. Considering the case with M an even integer and odd integer, we can calculate (3.16) and (3.17) and obtain (3.15).

For the *special case* with $M = 3$, the two redundant sensors are not contiguous, which are located at MN and N. According to the definition of the holes-triangle, there are at most two elements at the right-side of each sub-triangle because $b_2 \leq M-2 = 1$. Therefore, all the holes will be filled by rearranging these two redundant sensors at $-(MN + M)$ and $-(MN + M + N)$.

Then *Lemma 2* is proved. □

It should be mentioned that even if condition (3.15) is not met with other values of M and N, the rearranged coprime array can still fill most of the holes in $[MN + M, (2M - 1)N)$. The consecutive part of the difference coarray can still be significantly enlarged. In this case, the consecutive part ranges from 0 to $h_0 - 1$, where h_0 is the first hole in the coarray of the rearranged coprime array. Then we can derive the following Lemma.

Lemma 3: For M, N values that do not satisfy Lemma 2, the first hole occurs at

$$h_0 = \begin{cases} \text{M is odd} \begin{cases} a_1, & \text{if } N < \frac{M(M-3)}{2} \\ a_2, & \text{if } N > \frac{M(M-3)}{2} \end{cases} \\ \text{M is even} \begin{cases} a_1, & \text{if } N < \frac{M(M-4)}{4} \\ a_2, & \text{if } N > \frac{M(M-4)}{4} \end{cases} \end{cases} \tag{3.18}$$

where $a_1 = MN + 2(M+N) + \lfloor \frac{M}{2} \rfloor N$ and $a_2 = MN + \lceil \frac{M}{2} \rceil (M+N)$.

Proof. If the condition in Lemma 2 is not met, there will be some unfilled holes in range $(0, (2M-1)N)$. Considering only one unfilled hole, it can be written that

$$a_1 < (2M-1)N \tag{3.19}$$

$$a_2 < (2M-1)N. \tag{3.20}$$

Either (3.19) or (3.20) holds if only one hole is unfilled. If M is an odd value, without loss of generality, it can be assumed that the unfilled hole occurs at position a_1, which means

$$a_1 < a_2. \tag{3.21}$$

Then it comes that $N < \frac{M(M-3)}{2}$ for (3.21). Similarly, if M is an even value, we can follow the same derivation and obtain the solution $N < \frac{M(M-4)}{4}$. Lemma 3 is then proved. □

It is worth mentioning that our method does not require extra sensor to fill the holes. While rearranging the redundant sensors, there is a trade-off between expanding the consecutive coarray part and having more redundant lags for averaging. On the one hand, the sensor rearrangement could reduce the redundancy of some lags, which could potentially increase the estimation error in very finite data case. On the other hand, the sensor rearrangement can fill most of the holes. This directly provides some new information instead of holes and allows the utilization of the inconsecutive coarray part. In general, as M, N increase, the inconsecutive coarray part of the conventional coprime array becomes

larger (approximate 50% of the whole coarray aperture [112] with sufficient big M, N) and much information is wasted. If we can reduce this inconsecutive part by rearranging few redundant sensors, it can bring more benefit for the estimation.

3.3.3 Weight function

Apart from a larger consecutive part in the difference coarray, another benefit of the proposed rearranged coprime array is its less mutual coupling effect. It is well known that the mutual coupling is strongly dependent on the distance separation between sensors [82, 115]. Especially, sensors with a small distance separation could contribute strong mutual coupling. Since $\omega(m)$ indicates the number of physical sensor pairs contributing to separation m, we approximately quantify the mutual coupling with the help of the weight function. For simplification, we particularly focus on the first three weight function values, i.e. $\omega(1), \omega(2), \omega(3)$.

In the rearranged coprime array, sub-arrays $\mathbb{S}_1$, $\mathbb{S}_2$ form a TCA. For a given number of M and N, the corresponding first three weight function values of TCA, denoted as $\omega^{'}(1), \omega^{'}(2), \omega^{'}(3)$, have been provided in [112]. Considering the contribution of sub-arrays $\mathbb{S}_3$, $\mathbb{S}_4$, we have the following property.

Property 3: For the proposed rearranged coprime array, the interaction between $\mathbb{S}_3$ and $\mathbb{S}_4$ contributes at most one additional value to either one of $\omega^{'}(1), \omega^{'}(2), \omega^{'}(3)$, which can be formulated as:

$$\begin{aligned} \omega(1)+\omega(2)+\omega(3) &\leq \omega^{'}(1)+\omega^{'}(2)+\omega^{'}(3)+1 \\ s.t. \quad \omega(1) &\geq \omega^{'}(1) \\ \omega(2) &\geq \omega^{'}(2) \\ \omega(3) &\geq \omega^{'}(3) \end{aligned} \tag{3.22}$$

Proof. The interaction between $\mathbb{S}_1$ and $\mathbb{S}_2$ leads to $\omega^{'}(1), \omega^{'}(2), \omega^{'}(3)$. The minimum spacing between $\mathbb{S}_3$, $\mathbb{S}_4$ and $\mathbb{S}_1$, $\mathbb{S}_2$ is $M+N \geq 5$. This means that the cross interaction between $\mathbb{S}_3$, $\mathbb{S}_4$ and $\mathbb{S}_1$, $\mathbb{S}_2$ has zero contribution to $\omega(1), \omega(2)$ and $\omega(3)$. Therefore, we

only need to consider the interaction between $\mathbb{S}_3$ and $\mathbb{S}_4$. The minimum inter-element spacing of $\mathbb{S}_3$ equals to $M+N$ such that the self-interaction of $\mathbb{S}_3$ has zero contribution to $\omega(1), \omega(2), \omega(3)$. On the other hand, $\mathbb{S}_4$ has only one sensor. The cross interaction between $\mathbb{S}_3$ and $\mathbb{S}_4$ can be divided into two scenarios:

(1) $(\lceil \frac{M}{2} \rceil - 2)(M+N) < (\lceil \frac{M}{2} \rceil - 1)N$;

(2) $(\lceil \frac{M}{2} \rceil - 2)(M+N) > (\lceil \frac{M}{2} \rceil - 1)N$.

In the first scenario, the only possible cross-interaction contribution to $\omega(1), \omega(2), \omega(3)$ is $d_1 = (\lceil \frac{M}{2} \rceil - 1)N - (\lceil \frac{M}{2} \rceil - 2)(M+N)$. This is obvious because for other cross-interactions, they hold the form $d_1 + k(M+N)$, which is greater than 5.

In the second scenario, there will be two sensors of $\mathbb{S}_3$ (with spacing $M+N$) at both sides of $\mathbb{S}_4$. Assuming the distance of $\mathbb{S}_4$ to the nearest sensor is $d_1^{'}$, then the distance of $\mathbb{S}_4$ to the second nearest sensor is $M+N-d_1^{'}$. It is obvious that $d_1^{'}$ and $M+N-d_1^{'}$ are the only two possible contributions to $\omega(1), \omega(2), \omega(3)$. Due to the coprime property of M, N, the minimum value of $M+N$ is 5 for $M=2, N=3$. With $M=2, N=3$, there is only one redundant sensor located at $\mathbb{S}_3$ and it brings no contribution to $\omega(1), \omega(2), \omega(3)$. For other values of M, N, $M+N \geq 7$ and the following conditions can not hold simultaneously.

$$d_1^{'} \leq 3 \tag{3.23}$$

$$M+N-d_1^{'} \leq 3 \tag{3.24}$$

This means that $d_1^{'}$ and $M+N-d_1^{'}$ contribute at most one value to either one of $\omega(1), \omega(2), \omega(3)$. *Property 3* is then proved. □

Since $\omega(1)$ contributes the most to the mutual coupling, we especially investigate $\omega(1)$ for different M. It has been proved that $\omega'(1) = 2$ only when $M = 2$ for TCA. From the above discussion, it is obvious that our method will not increase $\omega(1)$ when $M = 2$. This is because there is only one redundant sensor and the rearrangement of this redundant sensor will not change $\omega(1)$, which means $\omega(1) = \omega'(1) = 2$ for $M = 2$.

When $M > 2$, we assume the case that the interaction between $\mathbb{S}_3$ and $\mathbb{S}_4$ contributes

one value to $\omega(1)$, which can be formulated as

$$-(MN+M+i(M+N)) = -(MN+M+(\lceil\frac{M}{2}\rceil-1)N) \pm 1 \tag{3.25}$$

where $0 \leq i \leq \lceil\frac{M}{2}\rceil - 2$. Then we can obtain

$$N = \frac{iM \pm 1}{\lceil\frac{M}{2}\rceil - 1 - i} \tag{3.26}$$

Only when the value of N meets condition (3.26), the relation $\omega(1) = \omega'(1) + 1 = 2$ is satisfied. Notice that $N > M$ and $M > 2$ as assumed above, only a few values of N will have contribution to $\omega(1)$ for a given value of M. For example, with $M = 6$, only $N = 7$ meets condition (3.26). For other cases, our method holds a low value of $\omega(1) = 1$, which allows us to attenuate the mutual coupling.

Compared with other sparse array configurations, it has been proved that though second order super nested array has small values of $\omega(1), \omega(3)$, the value of $\omega(2)$ could increase with the array size. Similar phenomenon could also happen to ANA1, ANA2 and MRA [112]. TCA can obtain low values for $\omega(1), \omega(2), \omega(3)$. The proposed rearranged coprime array has similar $\omega(1), \omega(2), \omega(3)$ property with TCA, which achieves $\omega^{'}(1) = \omega^{'}(2) = \omega^{'}(3) = 1$ for odd $M \geq 5$ and $M \neq 6$. This makes the proposed rearranged coprime array structure a promising strategy to decrease the mutual coupling effect.

3.3.4 Holes filling ratio

Furthermore, since the number of redundant sensors is limited to $\lceil\frac{M}{2}\rceil$, it is important to fill the holes in an efficient way. We define the *holes filling ratio* to evaluate the holes filling efficiency.

Definition 4: For a given number of sensors that are rearranged to fill the holes, the holes filling ratio is defined as the number of holes that can be filled by these sensors

$$r = \frac{\text{Card}(\mathbb{H}) - \text{Card}(\mathbb{H}^{'})}{S_r} \tag{3.27}$$

Here, Card($\mathbb{H}$) and Card($\mathbb{H}'$) are the cardinality of hole elements between $[MN+M, (2M-1)N)$ before holes filling and after holes filling respectively. S_r is the number of rearranged sensors, i.e. $S_r = \lceil \frac{M}{2} \rceil$ for the proposed rearranged coprime array and $S_r = M-1$ for CCA since it requires $M-1$ additional sensors to fill the holes. A higher value of r indicates that the rearranged sensors can fill more holes.

It can be derived that for given values of M and N, if the CCA mechanism and rearranged coprime array can fill the same number of the holes, the proposed rearranged coprime array could achieve higher value of r because $\lceil \frac{M}{2} \rceil \leq M-1$. With the increase of M, the difference between $\lceil \frac{M}{2} \rceil$ and $M-1$ becomes larger and the proposed array can achieve a higher r. Even in the case that the rearranged coprime array cannot fill all the holes but fill most holes, it could still achieve a high value of r.

3.3.5 DOFs comparison with other coprime based configurations

To fairly compare our proposed method with the other coprime based methods, we consider the optimum values of M, N for different methods for a given number of sensors. In the following, we denote M, N for the conventional coprime array and our proposed method, M_c, N_c for CCA and M_t, N_t for TCA.

It is obvious that our proposed method can achieve larger consecutive coarray than the conventional coprime array because it fills the holes in the coarray constructed from the conventional coprime array. For comparison with TCA and CCA, we consider the case where our method can not fill all the holes. In this case, we denote the consecutive coarray length by $\min(a_1, a_2)$, with $a_1 = MN + 2(M+N) + \lfloor \frac{M}{2} \rfloor N$ and $a_2 = MN + \lceil \frac{M}{2} \rceil (M+N)$. By referring to the selection strategy of CCA [77], M_c, N_c rely on the maximum number of DOFs and can not be directly compared with our proposed method. We compare our method and CCA from another point of view. Given $K = 2M + N - 1$ sensors, without loss of generality, we assume that $a_1 < a_2$ for our method such that the consecutive coarray length is a_1. Then we calculate M_c, N_c for CCA by assuming that its maximum number of DOFs is a_1. Thus, from [77] it comes that CCA requires $3M_c + N_c - 2$ sensors. If $3M_c + N_c - 2 > K$, then CCA requires more than K sensors to achieve the maximum

number of DOFs of a_1.

We first consider K as an even value. In this case, the two coprime integers of our method are set to $M = \frac{K+2}{4}, N = \frac{K}{2}$ [64]. Substituting these M, N values to a_1 and simplifying, we obtain

$$a_1 > a_1' = \frac{3K^2 + 22K + 16}{16} \tag{3.28}$$

Then we assume that a_1' is the maximum number of DOFs of CCA, the values of M_c, N_c can be given as [77]

$$M_c = \sqrt{\frac{a_1'}{6}} + \frac{1}{2} \tag{3.29}$$

$$N_c = \sqrt{\frac{3a_1'}{2}} \tag{3.30}$$

Therefore

$$\begin{aligned} 3M_c + N_c - 2 - K &= \sqrt{6a_1'} - (\frac{1}{2} + K) \\ = \sqrt{\frac{9K^2 + 66K + 48}{8}} &- \sqrt{\frac{8K^2 + 8K + 2}{8}} \end{aligned} \tag{3.31}$$

Given that $K > 0$, it is obvious that the difference in (3.31) is greater than 0, meaning that more sensors are required by CCA to obtain a given number of DOFs compared with our method. Similarly, when $a_2 < a_1$ or K is an odd value, the same result can be obtained. Then we can get the conclusion that our method can achieve larger consecutive coarray part than CCA with a given number of sensors.

To compare with TCA, we notice that there are $\lceil \frac{M_t}{2} \rceil$ sensors which can be removed. If $M_t = M, N_t = N$, TCA has less sensors than the conventional coprime array. In other words, for a given total number of sensors $K = 2M + N - 1$, M_t, N_t should be selected as two values bigger than M, N to construct a TCA with K sensors. Without loss of generality, we assume that $M_t = M + y_1$, $N_t = N + y_2$ with $y_1, y_2 \geq 0$ and the total number of sensors in TCA is $K = 2M_t + N_t - 1 - \lceil \frac{M_t}{2} \rceil = 2M + N - 1$. It is obvious that $2y_1 + y_2 = \lceil \frac{M_t}{2} \rceil$ and the consecutive coarray length of TCA is $M_t N_t + M_t$.

Similar with the above discussion, the optimum values of M, N meet the condition $N = 2M - 1 = \frac{K}{2}$ when K is an even value. Furthermore, we assume that $2M_t + N_t - 1$ is also an even value such that the optimum values of M_t, N_t satisfy $N_t = 2M_t - 1$. Then it comes that

$$y_2 = 2y_1 \tag{3.32}$$

Notice that $2y_1 + y_2 = \lceil \frac{M_t}{2} \rceil$, which leads to

$$y_1 = \frac{1}{4} \lceil \frac{M_t}{2} \rceil \tag{3.33}$$

Then it can be derived that

$$\begin{aligned} M_t &= M + y_1 = M + \frac{1}{4} \lceil \frac{M_t}{2} \rceil \\ &< M + \frac{1}{4}(\frac{M_t}{2} + 1) \end{aligned} \tag{3.34}$$

Reformulating (3.34), the following inequality can be obtained

$$-(M_t N_t + M_t) = -2M_t^2 > -\frac{8}{49}(4M + 1)^2 \tag{3.35}$$

Therefore

$$\begin{aligned} a_1 - (M_t N_t + M_t) &= a_1 - 2M_t^2 \\ &> 3M^2 + \frac{5M}{2} - 1 - 2M_t^2 \end{aligned} \tag{3.36}$$

Substituting (3.35), it can be easily shown that $a_1 - (M_t N_t + M_t) > 0$. Similarly, we can also get $a_2 - (M_t N_t + M_t) > 0$, which indicates that our method can achieve a larger consecutive coarray part than TCA. Furthermore, the same conclusion can be achieved when $K = 2M + N - 1$ is an odd value. Based on the above discussion, our method can achieve larger consecutive coarray part than the existing coprime based configurations.

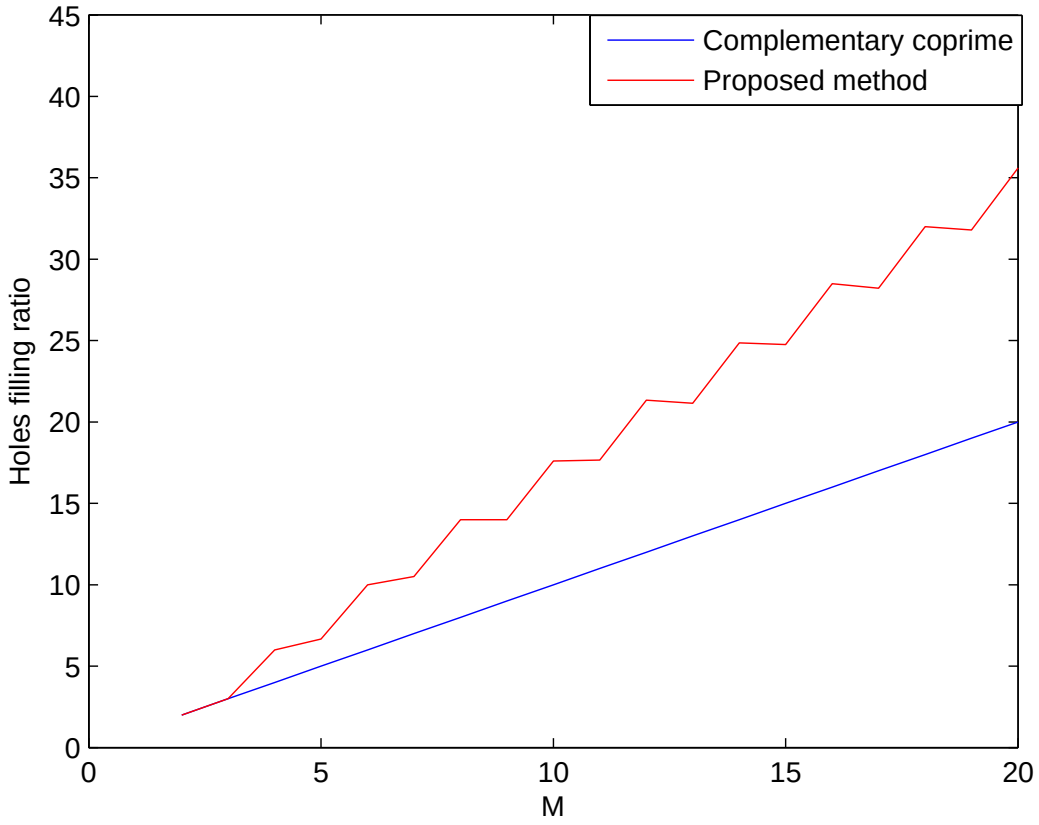

Figure 3.5 – Holes filling ratio curves for the proposed method and CCA. $N = M + 1$.

3.4 Simulation results

In this section, we evaluate the holes filling ratio and the weight function for several sparse arrays. The DOA performance is assessed by applying the spatial smoothing based (SS) MUSIC algorithm. Several sparse arrays are considered for comparison, including the nested array, second order SNA (Q=2), third order SNA (Q=3), MRA, ANA1, ANA2, CCA, TCA. Since the conventional coprime array has the same difference coarray as TCA for the same values of M and N, we only take TCA for comparison.

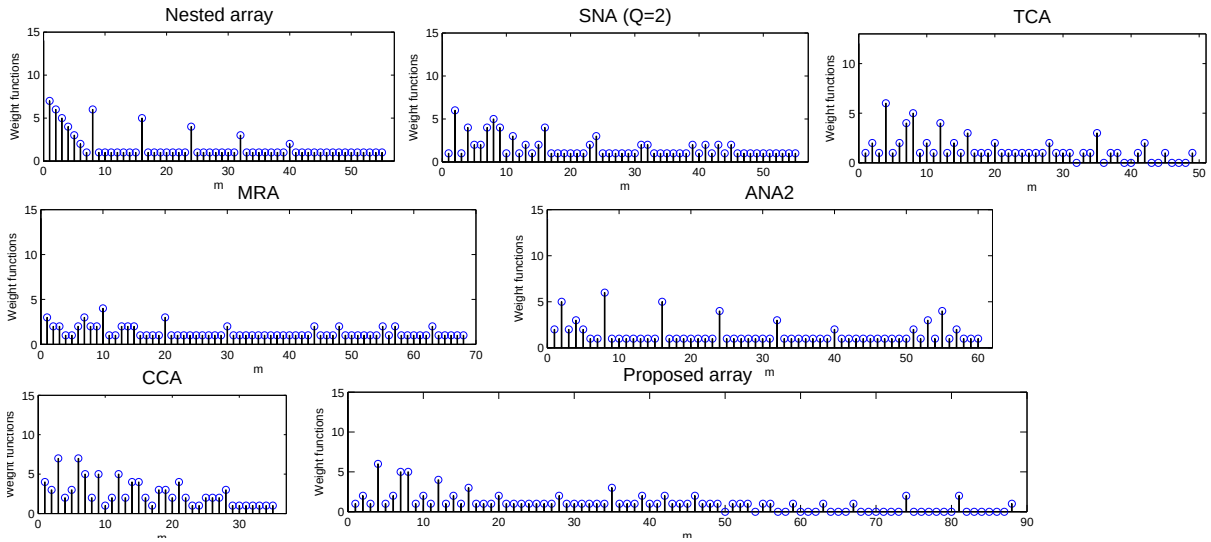

Figure 3.6 – Weight function of seven different arrays.

3.4.1 Holes filling ratio

We first examine the holes filling ratio. The method we consider for comparison is CCA. It should be mentioned that the CCA method utilizes additional sensors to fill the holes while our rearranged coprime array uses only the redundant sensors from the original conventional coprime array. From this point of view, our method is more hardware economic compared to CCA. To assure that M and N are coprime, we set $N = M + 1$. It can be seen from Fig. 3.5 that when M is small, the holes filling ratio of CCA and the proposed rearranged coprime array is very close. As M becomes larger, the proposed rearranged coprime array surpasses CCA and the difference between the two methods becomes larger, which indicates that each rearranged sensor of our proposed method can fill more holes than that of CCA.

3.4.2 Weight function

Then we compare the weight function of the nested array, ANA2, MRA, SNA (Q=2), TCA, CCA with the proposed configuration. 14 sensors are considered in this part. For the proposed array, we set $M = 4, N = 7$. The sensor positions of MRA are given in the set $\{0, 1, 2, 8, 15, 16, 26, 36, 46, 56, 59, 63, 65, 68\}$ [71]. For CCA, we set $M = 3, N = 7$.

It can be observed from Fig. 3.6 that the nested array and CCA have high values of $\omega(1), \omega(2), \omega(3)$, which are $\omega(1) = 7, \omega(2) = 6, \omega(3) = 5$ for the nested array and $\omega(1) = 4, \omega(2) = 3, \omega(3) = 7$ for CCA. The ANA2 and SNA (Q=2) have small values of $\omega(1), \omega(3)$ but still hold a high value of $\omega(2)$, which are $\omega(2) = 5$ and $\omega(2) = 6$ respectively. The MRA achieves $\omega(1) = 3$ and $\omega(2) = \omega(3) = 2$ while TCA has smaller value of $\omega(1) = 1$, $\omega(2) = 2$ and $\omega(3) = 1$. Though CCA can fill all the holes, the length of the difference coarray is limited to 35, which is only slightly larger than the consecutive part of TCA (31 as shown in Fig. 3.6). This is due to the small value of M. The proposed method achieves the same $\omega(1), \omega(2), \omega(3)$ as TCA. It can also be noticed that TCA has some holes which are denoted as set $\{32, 36, 39, 40, 43, 44, 46, 47, 48\}$, while the proposed array can fill all these elements.

An interesting fact is that the proposed strategy can also lead to some additional DOFs beyond $(2M - 1)N$, which are the elements greater than 49 in Fig. 3.6. These additional DOFs can be used if the compressive sensing based DOA estimation methods are applied [101, 116]. By doing so, the proposed method can detect even more sources. In this work, our main concern is to fill the holes and enlarge the consecutive part. We only consider the SS-MUSIC afterward.

3.4.3 RMSE

Next, we take the mutual coupling effect into account and evaluate the RMSE of these sparse arrays. As illustrated above, though CCA can fill the holes, its length of the difference coarray is dramatically limited and it also has a high value of $\omega(1), \omega(2), \omega(3)$. For a fair comparison, we will not compare CCA in this part.

The number of sensors is set to 18 and $M = 5, N = 9$ are considered for the proposed rearranged coprime array. Notice that TCA only requires 15 sensors in this case and 3 redundant sensors are not used. For a fair comparison, we set $M = 7,\ N = 9$ for TCA such that all 18 sensors can be utilized. By setting a larger M value, the consecutive part of TCA is increased and the respective inter-element spacing is also increased. The sensor positions of MRA are given by the set $\{0, 1, 8, 18, 28, 38, 48, 58, 68, 78, 88, 90, 92, 94, 97, 99, 101, 103\}$

[117].

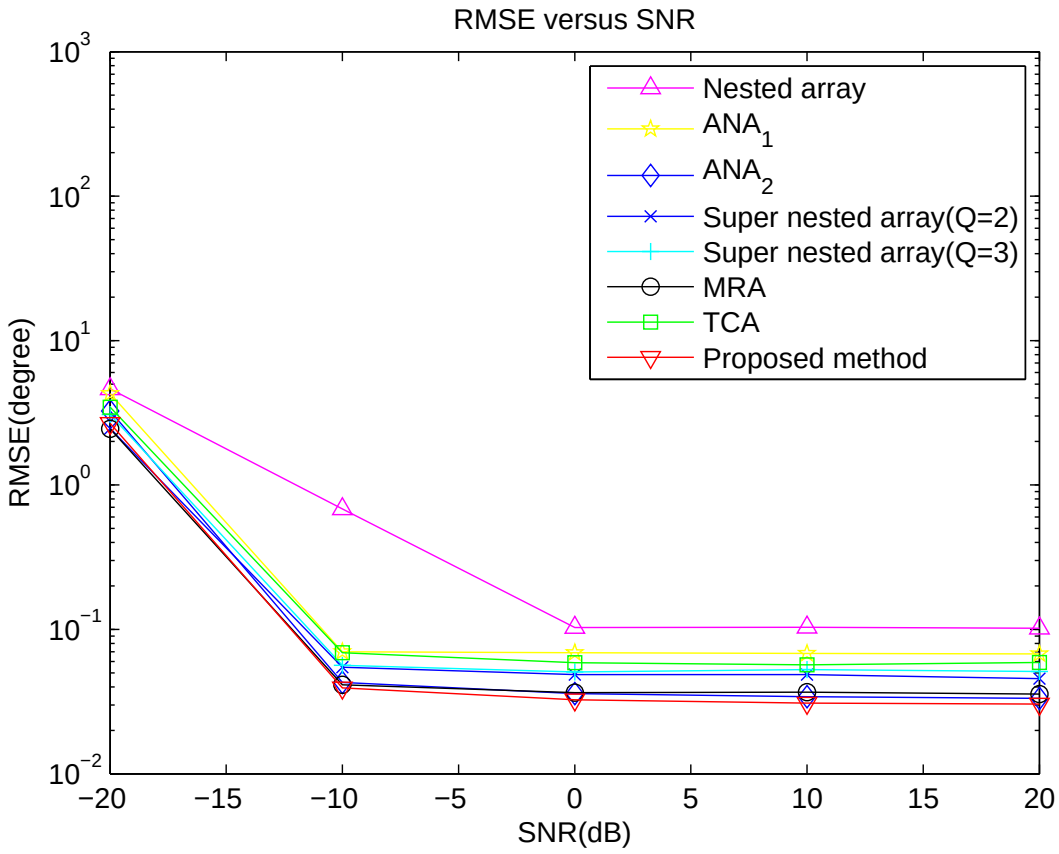

Figure 3.7 – RMSE versus input SNR with 18 sensors, 12 sources, 1000 snapshots, $|c_1| = 0.3$.

Fig. 3.7 and Fig. 3.8 examine the performance versus SNR. The number of snapshots is set to 1000 and the mutual coupling parameters are set to $c_1 = |c_1|e^{j\pi/3}$ with $|c_1| = 0.3$, $c_l = c_1 e^{-j(l-1)\pi/8}/l$ and $B = 100$. When 12 sources uniformly located between $-40°$ and $-40°$ impinge on the sparse arrays, the nested array exhibits the worst performance due to its closely distributed sensors. Our proposed method achieves the best performance compared to other methods as shown in Fig. 3.7. In the case with more sources than sensors (25 sources in Fig. 3.8), ANA1 and ANA2 have worse performance than SNA since they still have higher value of $\omega(1)$, $\omega(3)$ as shown in Table 3.2. The proposed method can show very similar performance as MRA, which is slightly better than the first few orders of SNA (Q=2, Q=3).

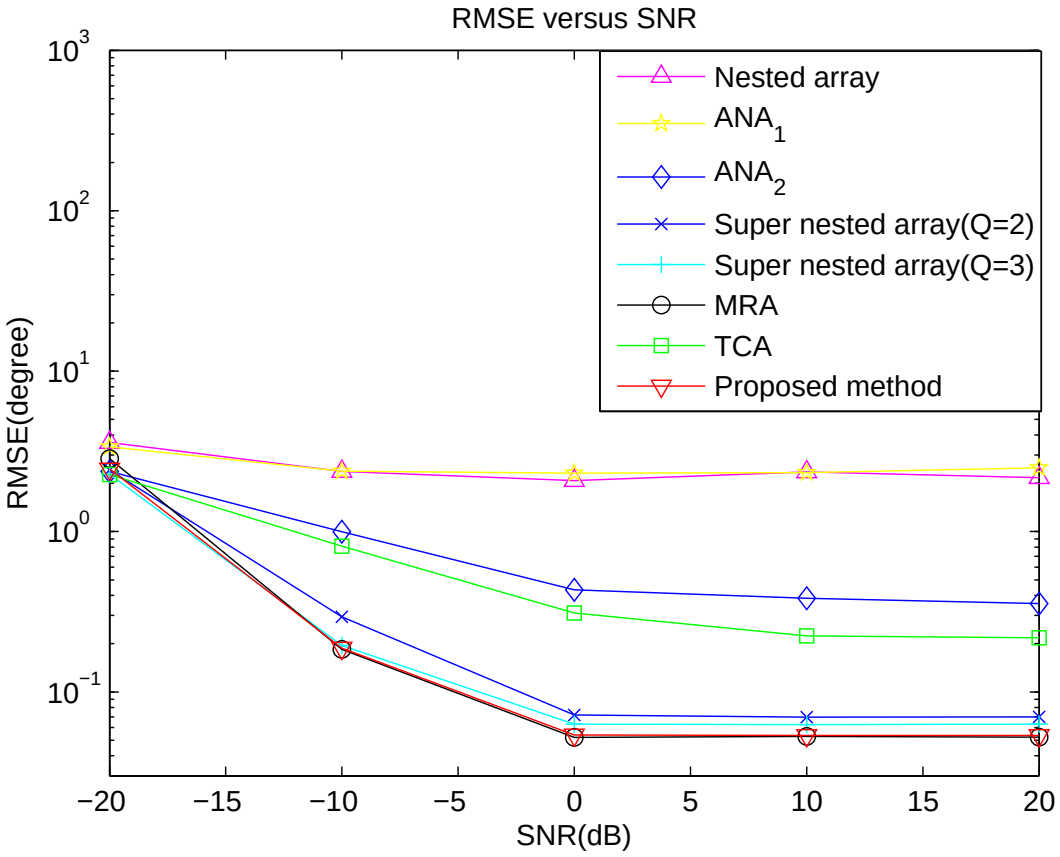

Figure 3.8 – RMSE versus input SNR with 18 sensors, 25 sources, 1000 snapshots, $|c_1| = 0.3$.

For a clear comparison, we also give the weight function and the maximum number of detectable sources (max sources) with 18 sensors for SS-MUSIC in Table 3.2. The proposed method and TCA show the lowest value of $\omega(1), \omega(2), \omega(3)$. An interesting phenomenon can also be observed that the proposed method can detect up to 86 sources in this case, which is greater than $(2M-1)N = 81$ and very close to that of SNA. This means that when the proposed strategy rearranges the redundant sensors to fill the holes within $[MN+M, (2M-1)N)$, they may also further enlarge the consecutive part to a value greater than $(2M-1)N$ simultaneously. This phenomenon happens for several different values of M, N. On the other hand, the TCA can only detect 69 sources even though higher values of $M = 7, N = 9$ are used in this case.

Fig. 3.9 and Fig. 3.10 compare the performance in terms of different number of snap-

Table 3.2 – Weight function and maximum detectable sources with 18 sensors.

	$\omega(1)$	$\omega(2)$	$\omega(3)$	max sources
Nested array	9	8	7	89
ANA2	2	7	2	96
MRA	1	6	1	103
SNA(Q=2)	1	8	1	89
TCA	1	1	1	69
Proposed array	1	1	1	86

shots. SNR is set to 0dB and $|c_1| = 0.3$ is used. As the increase of the number of snapshots, the performance tends to different stable values for all methods. The length of TCA consecutive part limits its performance, while the proposed method can expand the consecutive part and achieve similar performance as the other arrays.

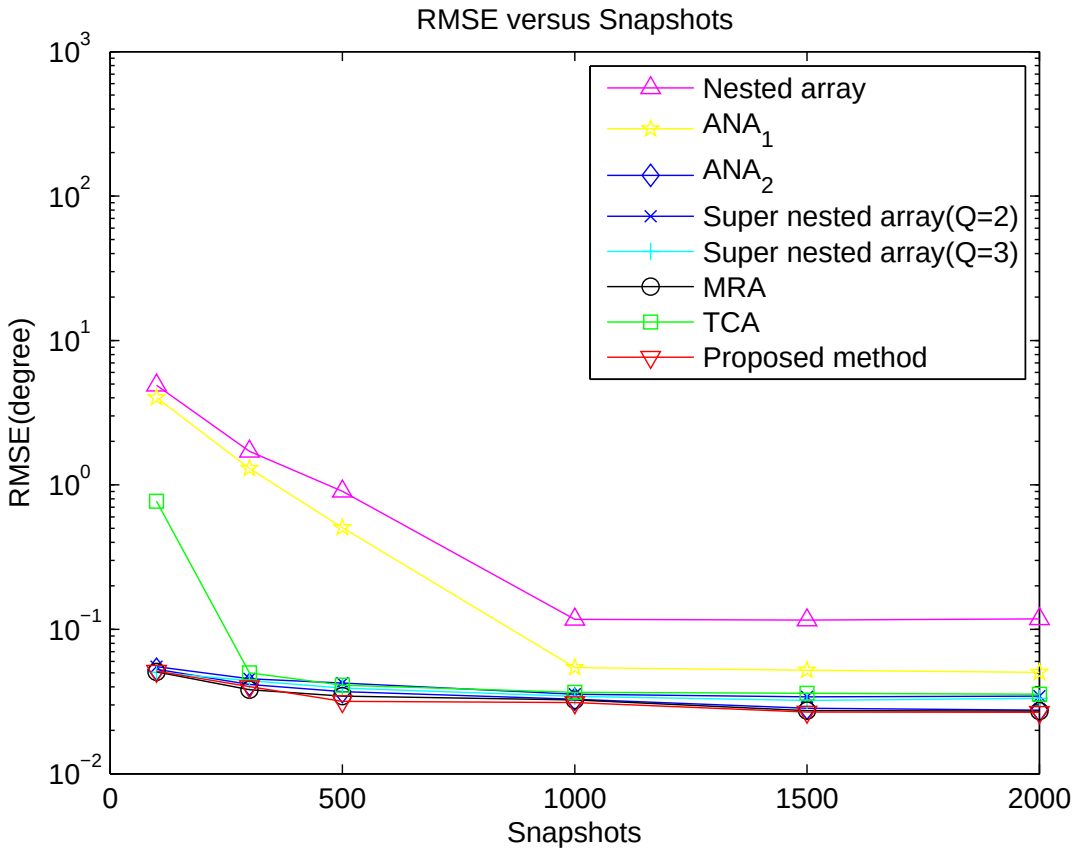

Figure 3.9 – RMSE versus snapshots with 18 sensors, 12 sources, SNR=0dB, $|c_1| = 0.3$.

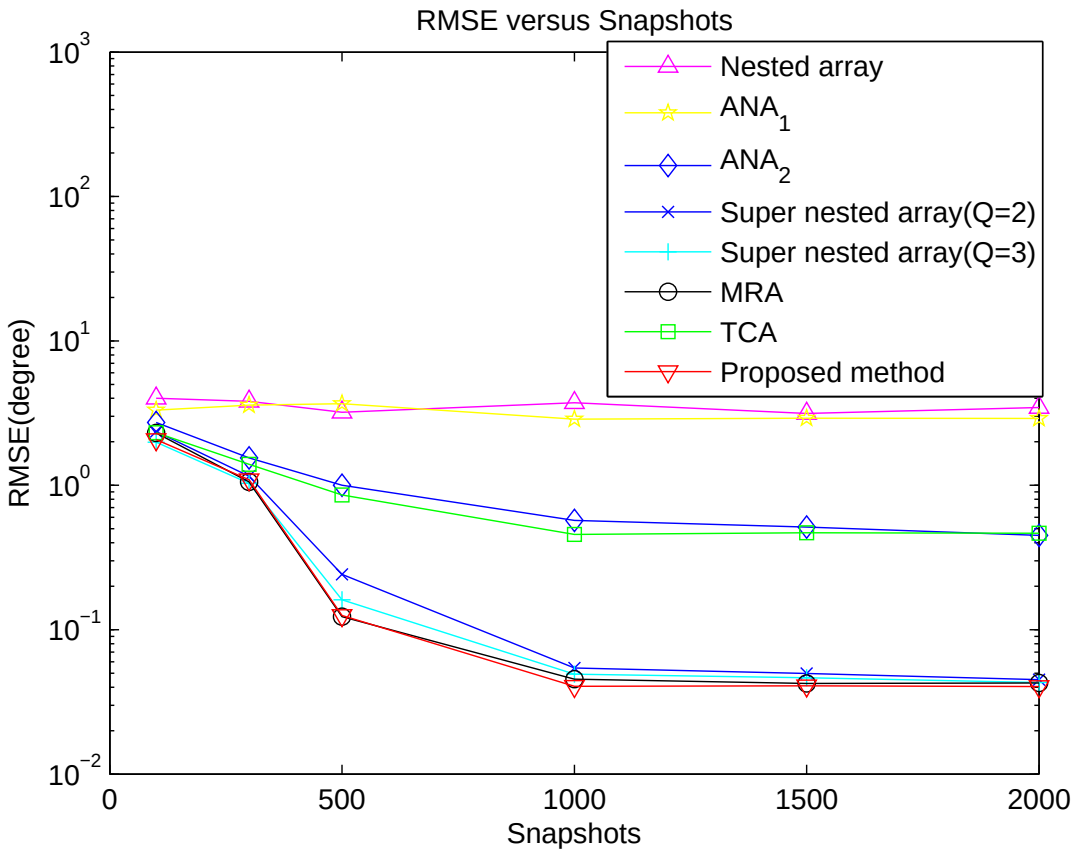

Figure 3.10 – RMSE versus snapshots with 18 sensors, 25 sources, SNR=0dB, $|c_1| = 0.3$.

Finally, we investigate the performance under different magnitudes of mutual coupling coefficient $|c_1|$. 1000 snapshots are used and SNR is equal to 0dB. We examine the cases with fewer sources to test the high mutual coupling scenarios, 10 sources in Fig. 3.11 and 20 sources in Fig. 3.12 respectively. The performance decreases for all methods when the coupling coefficient becomes stronger. It can be observed from Fig. 3.11 that the proposed array shows superiority to the other methods under high mutual coupling. Though the TCA method has small value of $\omega(1), \omega(2), \omega(3)$, its performance is affected by the short consecutive coarray. For the case of more sources than sensors, the proposed array does not exhibit significant superiority compared to other arrays in low mutual coupling region. As the coupling coefficient increases to values greater than 0.4, the proposed method starts to achieve better performance than others.

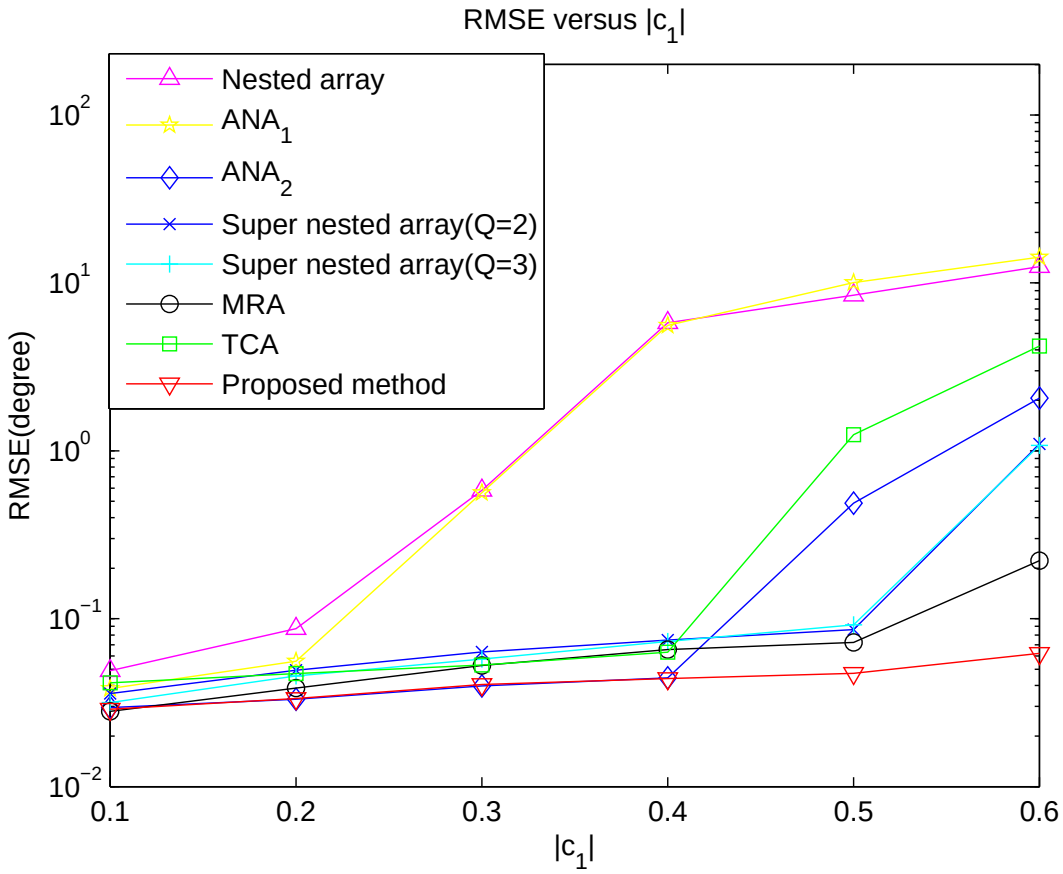

Figure 3.11 – RMSE versus $|c_1|$ with 18 sensors, 10 sources, SNR=0dB, 1000 snapshots.

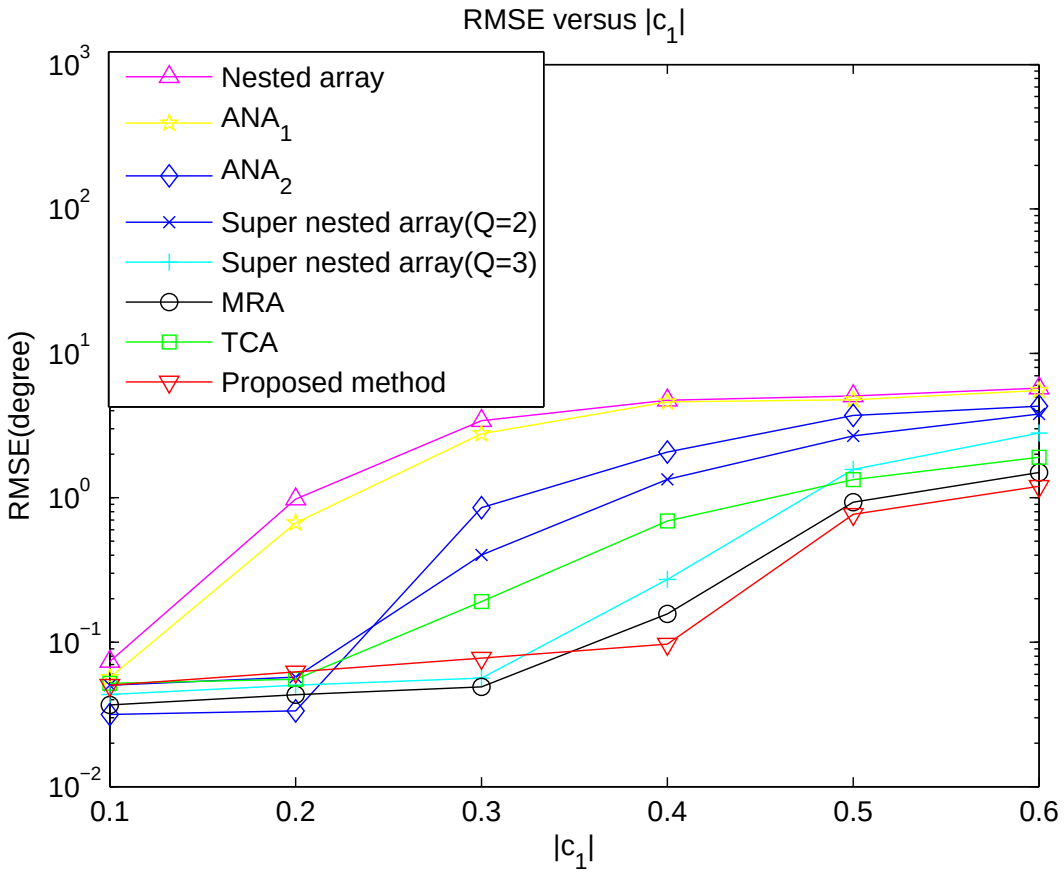

Figure 3.12 – RMSE versus $|c_1|$ with 18 sensors, 20 sources, SNR=0dB, 1000 snapshots.

3.5 Conclusion

In this chapter, we focus on DOA estimation with coprime array. Concerning the holes filling problem, we take it into account from the aspect of physical array geometry. The property of the holes in the 2-DC of coprime array is investigated before formulating the holes into a holes-triangle structure. We also review the redundant property illustrated by the TCA, which indicates that some sensors in coprime array are redundant.

Inspiring by the TCA, we rearrange this redundant sensors to proper position such that most of the holes can be filled. The holes-triangle is used to illustrate the proposed rearrangement strategy of the redundant sensors. Also, the mutual coupling effect is also considered in the proposition. The rearranged sensors are located at sparser position such that the mutual coupling can be reduced.

Chapter 4

Active DOA with sparse array using fourth order cumulants

4.1 Introduction

In this chapter, we investigate the active sensing using sparse arrays. The MIMO radar for active DOA sensing is inspired by the MIMO communication theory. A MIMO radar system consists of a transmit array including multiple transmitting antennas and a receive array with multiple receiving antennas. In the previous chapters, only the difference coarray is considered in the sparse arrays to enhance the DOFs. Apart from the difference coarray, adopting the sum coarray is also a strategy to increase the DOFs.

The sum coarray signal has been simply discussed in the introduction chapter. To the best of our knowledge, most literatures adopt second order statistics for MIMO radar. In [118], the fourth order cumulants are considered in MIMO radar for DOA estimation. However, the coarray concept is not considered in [118]. Most recently, the 4-DC related to fourth order cumulants is analyzed in the scenario of passive DOA sensing to increase the DOFs. But in MIMO system, the 4-DC corresponding to fourth order cumulants has not been investigated thoroughly.

In our work, we first adopt the fourth order cumulants in sparse array MIMO system. The considered sparse array configuration is the coprime array and our work can be easily extended to other sparse array configurations. Compared with the second order statistics case, we will show that the DOFs can be increased when exploiting the fourth order cumulants in the MIMO system due to the constructed 4-DCSC. The property of

4-DCSC is then investigated to quantify the DOFs and the holes in the coarray.

Though adopting fourth order cumulants can increase the DOFs, the enhancement of DOFs in the 4-DCSC of coprime array is still limited since the classical coprime array is designed for 2-DC. The same phenomenon happens in other sparse array configurations which are designed for 2-DC, 4-DC or 2-DCSC. Is it possible to design novel sparse array geometry such that the DOFs can be further increased for the case of 4-DCSC? Our second work provides positive answer to this problem. We reformulate the 4-DCSC geometry design problem and simplify it into two separate problems: a fourth order sum coarray (4-SC) problem and a 2-DC problem. A novel virtual nested array based MIMO geometry is then proposed and it is shown that the DOFs can be significantly increased compared to the exist sparse array configurations.

4.2 Fourth order cumulants data model

We first introduce the fourth order cumulants data model before further discussion about the fourth order difference coarray (4-DC). Assuming a K sensors linear array receives the signals from D sources, where the impinging signals are assumed to be zero-mean stationary and non-Gaussian. In our work, we also assume that the signals are statistically independent since our main goal is to properly design the array geometry. Without loss of generality, we denote the received signals in general form, which can be written by

$$\mathbf{x}(t) = [y_1(t), y_2(t), ..., y_K(t)]^T \tag{4.1}$$

Then the fourth order cumulants of variables $y_{i1}(t), y_{i2}(t), y_{i3}(t), y_{i4}(t)$ are given by

$$\begin{aligned}\text{Cum}[y_{i1}(t), y_{i2}(t), y_{i3}^*(t), y_{i4}^*(t)] = E[y_{i1}(t)y_{i2}(t)y_{i3}^*(t)y_{i4}^*(t)] - E[y_{i1}(t)y_{i2}(t)]E[y_{i3}^*(t)y_{i4}^*(t)] \\ -E[y_{i1}(t)y_{i3}^*(t)]E[y_{i2}(t)y_{i4}^*(t)] - E[y_{i1}(t)y_{i4}^*(t)]E[y_{i2}(t)y_{i3}^*(t)]\end{aligned} \tag{4.2}$$

Here, $1 \leq i1, i2, i3, i4 \leq K$. Consider a MIMO system composed of a transmitting array with N transmitters and a receiving array with $2M$ receivers with M, N two coprime

integers. The two coprime arrays share the same first element and their element positions are given by

$$\mathbb{S}_t = \{nMd_0 \,|\, 0 \leq n \leq N-1\} \tag{4.3}$$

$$\mathbb{S}_r = \{mNd_0 \,|\, 0 \leq m \leq 2M-1\} \tag{4.4}$$

The received signal model of a coprime MIMO system has been provided in Chapter 1, which is

$$\mathbf{x}_s(t) = \sum_{i=1}^{D} \mathbf{a}_t(\theta_i) \otimes \mathbf{a}_r(\theta_i) s_i(t) + \mathbf{n}(t) = \mathbf{A}_s \mathbf{s}(t) + \mathbf{n}(t) \tag{4.5}$$

Then one can write the fourth order cumulants matrix of the MIMO received signal as

$$\begin{aligned} \mathbf{C}_{4,\mathbf{x}} &= \sum_{i=1}^{D} c_{4,s_i} [\mathbf{a}_s(\theta_i) \otimes \mathbf{a}_s^*(\theta_i)] \times [\mathbf{a}_s(\theta_i) \otimes \mathbf{a}_s^*(\theta_i)]^H \\ &= \sum_{i=1}^{D} c_{4,s_i} \mathbf{a}_4(\theta_i) \mathbf{a}_4^H(\theta_i) \end{aligned} \tag{4.6}$$

where $\mathbf{a}_4(\theta_i) = \mathbf{a}_s(\theta_i) \otimes \mathbf{a}_s^*(\theta_i)$ with $\mathbf{a}_s(\theta_i) = \mathbf{a}_t(\theta_i) \otimes \mathbf{a}_r(\theta_i)$ and c_{4,s_i} is the fourth order circular cumulant of $s_i(t)$, denoted by:

$$c_{4,s_i} = \mathrm{Cum}[s_i(t), s_i(t), s_i^*(t), s_i^*(t)] \tag{4.7}$$

The vector $\mathbf{a}_s(\theta_i)$ is a $2MN \times 1$ vector such that the cumulant matrix $\mathbf{C}_{4,\mathbf{x}}$ is a $(2M)^2N^2 \times (2M)^2N^2$ matrix, which has larger dimension compared with the $(2M+N-1)^2 \times (2M+N-1)^2$ cumulant matrix in [95, 96]. Vectorizing the cumulant matrix $\mathbf{C}_{4,\mathbf{x}}$ can lead to a virtual array signal model with larger effective array aperture, which can be denoted by

$$\mathbf{c} = \mathrm{vec}(\mathbf{C}_{4,\mathbf{x}}) = \mathbf{A}_{\mathrm{vir}} \mathbf{p} \tag{4.8}$$

where $\mathbf{p} = [c_{4,s_1}, c_{4,s_2}, ..., c_{4,s_D}]^T$ is the fourth order cumulants of the D targets and $\mathbf{A}_{\mathrm{vir}}$

can be considered as the manifold matrix of the virtual array, which is given by

$$\mathbf{A}_{\text{vir}} = [\mathbf{a}_{\text{vir}}(\theta_1), \mathbf{a}_{\text{vir}}(\theta_2), ..., \mathbf{a}_{\text{vir}}(\theta_D)] \tag{4.9}$$

with

$$\mathbf{a}_{\text{vir}}(\theta_i) = \mathbf{a}_4(\theta_i)^* \otimes \mathbf{a}_4(\theta_i) \tag{4.10}$$

The elements of $\mathbf{a}_{\text{vir}}(\theta_i)$ take the following form

$$e^{j\pi(\sum_{i=1}^{2} v_i - \sum_{i=3}^{4} v_i)\sin(\theta_i)} \tag{4.11}$$

where v_i is the element of 2-SC of MIMO system, $v_i \in \mathbb{S}_s, i = 1, 2, 3, 4$. Each v_i takes values from the sum coarray set independently. Interestingly, it can be observed that

$$\sum_{i=1}^{2} v_i - \sum_{i=3}^{4} v_i = (v_1 - v_3) - (v_4 - v_2) \tag{4.12}$$

It is obvious that $v_1 - v_3$, as well as $v_4 - v_2$, are the 2-DC of the sum coarray and (4.12) is also in the form of a difference coarray. In other words, we can equivalently consider that the 4-DC of sum coarray is obtained by calculating the 2-DC one more time to the 2-DC of the sum coarray. By properly selecting the corresponding elements to construct the 4-DC, the spatial smoothing based MUSIC [66] can be used for the DOA estimations.

4.3 Property of 4-DCSC of coprime array

In the following, we want to apply the spatial smoothing MUSIC and it is important to investigate the property of the 4-DCSC. Since the 4-DCSC has close relation with the 2-DC and 4-DC, we first recall some properties of 2-DC. In the previous chapters, we have shown that the holes in the 2-DC of coprime arrays with $2M + N - 1$ sensors, occur at position

$$\pm(b_1 M + b_2 N) \tag{4.13}$$

Considering the symmetric property of the difference coarray, we classify the 2-DC of coprime arrays into two parts: the central consecutive part which ranges from $-(MN + M - 1)$ to $(MN + M - 1)$, and the inconsecutive part including holes. For simplification, we consider only the positive coarray part and obtain the following Lemma.

Lemma 4: Considering the elements and holes in the 2-DC of coprime arrays, the distance between the first hole and the i-th hole equals to the distance between the elements with farthest position and the i-th farthest position.

Proof. We first focus on the holes. Denoting the distance between the first hole and i-th hole as h_i and considering $M < N$, we can derive that

$$h_1 = 0, \tag{4.14}$$

$$h_2 = M \tag{4.15}$$

This is because that the second hole occurs at $MN + 2M$. For the third hole, h_3 takes the minimum value from $2M$ and N, which is

$$h_3 = h_1 + \min(2M, N) \tag{4.16}$$

However, the relationship between the fourth hole and the first hole is uncertain because the relationship between $2M$ and N depends on the values of M, N. Alternatively, we can establish the relationship between the fourth hole and the second hole, which is given by

$$h_4 = h_2 + \min(2M, N) \tag{4.17}$$

This can be obtained directly from (4.13). Then, it can be generalized that

$$h_{i+2} = h_i + \min(2M, N) \tag{4.18}$$

Similarly, for the elements in the 2-DC, we denote the element with the farthest position $(2M-1)N$ as the first element. The nearest element away from the first element is denoted

as the second element, and more generally the i-th farthest position element is denoted as the i-th element. Then the distance between this first element and the i-th element is referred as e_i. It is obvious that $e_1 = 0$ and $e_2 = M$ because the second element is $(2M-1)N - M$. Then for the third element, it is obtained by

$$(2M-1)N - \min(2M, N) \tag{4.19}$$

And we can have

$$e_3 = e_1 + \min(2M, N) \tag{4.20}$$

and

$$e_4 = e_2 + \min(2M, N) \tag{4.21}$$

As a result, we can derive that

$$e_{i+2} = e_i + \min(2M, N) \tag{4.22}$$

Since $h_1 = e_1, h_2 = e_2$, we can obtain that $h_i = e_i$ and Lemma 4 is proved. □

Since the 4-DC of an array is equivalent to apply the 2-DC one more time, we can consider the 2-DC with holes as a new array and the 2-DC is applied one more time to this new array. The following proposition can be obtained.

Proposition 2: For coprime arrays with $2M + N - 1$ sensors, the holes of its 4-DC occur at position

$$\pm[(2M-1)N + b_1 M + b_2 N], \tag{4.23}$$

where $1 \leq b_1 \leq N - 1 - \lfloor \frac{N}{M} \rfloor$ and $M \leq b_2 \leq 2M - 2$.

Proof. We focus only on the positive part of the 4-DC. Since the consecutive part of the 2-DC of coprime arrays ranges from $-(MN + M - 1)$ to $(MN + M - 1)$, it can be easily derived that, the elements from 0 to $2(MN + M - 1)$ in the 4-DC can be obtained by taking the difference of two elements in the consecutive part of the 2-DC. Then the elements from $2(MN + M - 1) + 1$ to $(2M-1)N + MN + M - 1$ can be obtained by

taking the difference between the element $(2M-1)N$ and one corresponding element in the consecutive part of the 2-DC.

Then we prove that the first hole of the 4-DC occurs at position $(2M-1)N+MN+M$ by contradiction. Notice that the difference between element $(2M-1)N$ and $-(MN+M)$, or $MN+M$ and $-(2M-1)N$ equals to $(2M-1)N+MN+M$. However, $\pm(MN+M)$ are two holes in the 2-DC. Assuming that there are two elements in the 2-DC that can lead to $(2M-1)N+MN+M$, denoted as a_1, a_2. It is obvious that one element should lay in the negative part $(-(2M-1)N, -MN-M)$ and another in the positive part $(MN+M, (2M-1)N)$. Without loss of generality, we assume that a_1 is positive and a_2 is negative. Then we can have

$$\begin{aligned} a_1 - a_2 &= (2M-1)N - a_0 - (-MN - M - a_0) \\ &= (2M-1)N + MN + M \end{aligned} \tag{4.24}$$

where a_0 is an integer representing the distance between a_1 and $(2M-1)N$, or the distance between a_2 and $-(MN+M)$. However, inspired by the Lemma 4, for any elements $a_1 \in (MN+M, (2M-1)N)$ with distance a_0 to $(2M-1)N$, the position $a_2 \in (-(2M-1)N, -(MN+M))$ with same distance a_0 to $-(MN+M)$ must be a hole. It is impossible to find suitable a_1, a_2 in the 2-DC that satisfy condition (4.24). Then the first hole position in the 4-DC is $(2M-1)N+MN+M$.

For the other holes, we can perform similar derivations. Proposition 2 is then proved. □

It can be noticed that the holes in the 4-DC is a shift version of the holes in the 2-DC. The consecutive part in the 4-DC is significantly enlarged. Then we extend Proposition 1 to the 4-DCSC of coprime arrays and the following proposition is achieved.

Proposition 3: For coprime array elements position set denoted by $\mathbb{S}_t \cup \mathbb{S}_r$, whose sum coarray is denoted as $\mathbb{S}_s$, with the largest position value element of transmitting array $\mathbb{S}_t$ equals to $a_{t,\max}$, and largest position value element of receiving array $\mathbb{S}_r$ equals to $a_{r,\max}$,

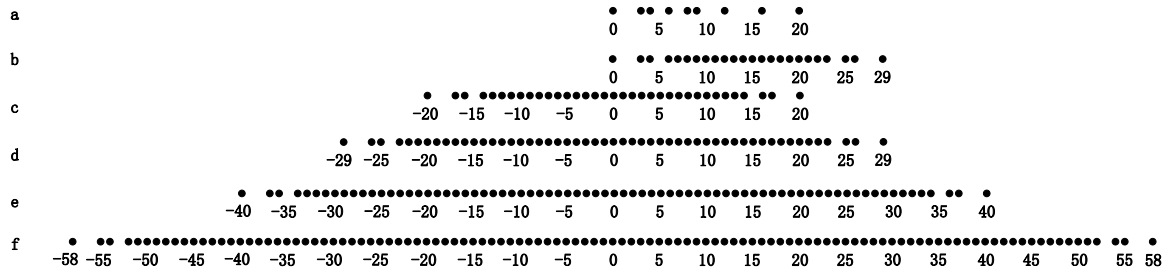

Figure 4.1 – Comparison of several coarray structures with $M = 3, N = 4$. (a) Physical array; (b) Sum coarray; (c) 2-DC of physical array; (d) 2-DCSC (e) 4-DC of physical array; (f) Proposed 4-DC of sum coarray.

the holes in the 4-DC of this sum coarray occur at position

$$\pm[2a_{t,\max} + a_{r,\max} + b_1 M + b_2 N] \tag{4.25}$$

Proof. The positions of holes in the sum coarray of a coprime array have been given in [119]. In our case with the receiver array of $2M$ sensors, the consecutive part of the sum coarray lays in the range $[(M-1)(N-1), 2MN-1]$. Some holes in the sum coarray lay at the left side of the consecutive part, given by $(2M-1)N - b_1 M - b_2 N$, while the others occur at the right side of consecutive part, given by $(N-1)M + b_1 M + b_2 N$.

We first focus on the positive 2-DC of this sum coarray and the holes of this positive 2-DC occur at $(N-1)M + b_1 M + b_2 N$. This can be proved by taking the difference of two elements in the sum coarray similar with the derivation illustrated in the Lemma 4. For the inconsecutive part on the left of the sum coarray consecutive part, the first element is 0 and the i-th element locates e_{si} away from the first element. Similarly for the inconsecutive part on the right of the consecutive part, the first hole is $(N-1)M + MN + M$ and the i-th hole locates h_{si} away from the first hole. Following the illustration in the Lemma 4, we can have $e_{si} = h_{si}$. Then it is impossible to obtain $(N-1)M + M + N$ by taking difference between two elements. This can be generalized and it leads to the holes expression of 2-DC of the sum coarray, which is $(N-1)M + b_1 M + b_2 N$.

Then we focus on the 4-DC of this sum coarray. By using similar contradiction as those illustrated in Proposition 2, we can obtain that the holes of 4-DC of the sum

coarray are also a shift version of the holes in 2-DC of sum coarray, with a shift distance of $(N-1)M+(2M-1)N$. With $a_{t,\max}=(N-1)M$ and $a_{r,\max}=(2M-1)N$, the holes are given by $2a_{t,\max}+a_{r,\max}+b_1M+b_2N$. Proposition 3 is proved. □

4.3.1 Simulation results and discussion

In this section, we will use a 9 sensors coprime array with $M=3, N=4$ in our simulation. The spatial smoothing based MUSIC is exploited for DOA estimation. The physical array geometry and the respective sum coarray, 2-DC, 4-DC and the proposed strategy are shown in Figure 4.1. We can observe that the 4-DC can significantly enlarge the coarray aperture compared to the 2-DC. However, our proposed strategy can even further increase the aperture. Up to 52 targets can be resolved with our proposition compared to 34 resolvable targets in 4-DC of physical array.

Figure 4.2 is the estimated MUSIC spectrum of 40 targets with SNR=0dB and 500 snapshots. The targets are uniformly distributed in $[-75°, 75°]$. It is clear that the 4-DC of physical array method is not able to identify 40 targets while our proposition can do it.

4.4 Virtual nested array using postage stamp problem

In this section, we assume that the transmit array and the receive array of the MIMO system are identical. Though the 4-DCSC can increase the DOFs compared with the 2-DCSC for a same MIMO geometry, the coprime MIMO is mainly designed for the 2-DC. Also, most existing sparse array geometries are designed for 2-DC, 4-DC or 2-DCSC. When they are adopted for constructing a 4-DCSC, further improvement is still possible if the array geometry is optimized. Since the 4-DCSC is equivalent to apply the 2-DC one more time to the 2-DCSC, the cross correlations between the elements in the 2-DCSC make the array geometry design problem more complicate than the 2-DCSC. To address this problem, we propose a new nested array based MIMO approach which can achieve

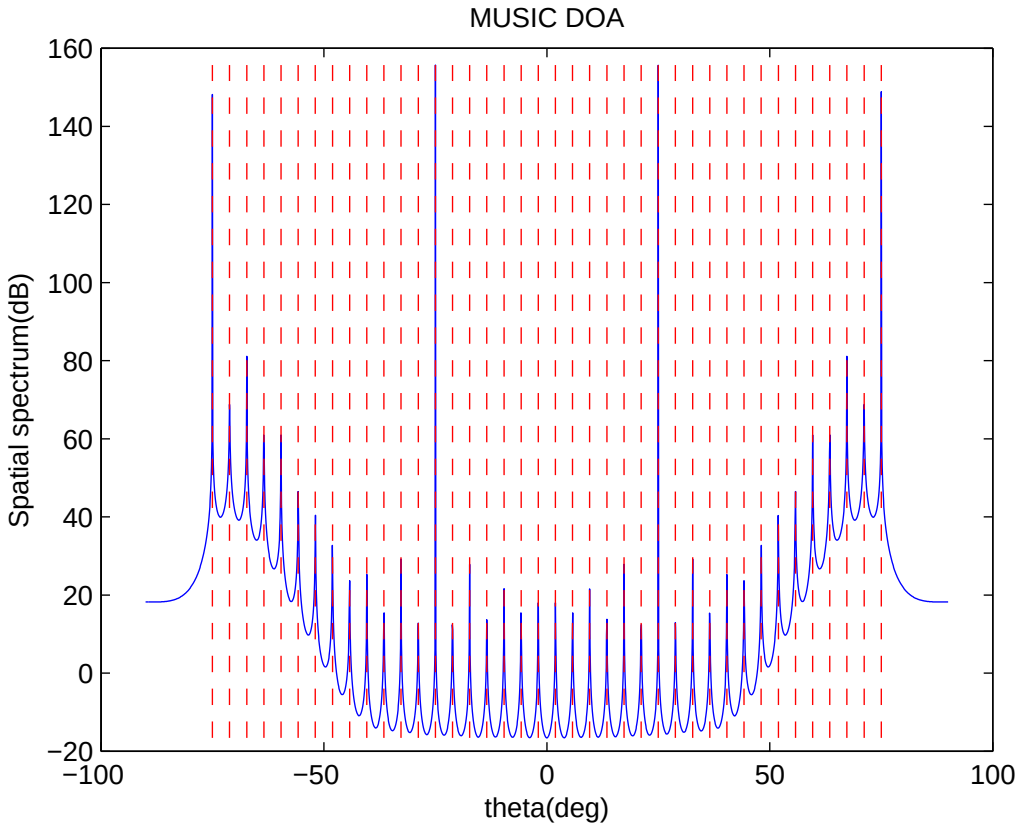

Figure 4.2 – MUSIC spectrum of DOA estimation using proposed 4-DC of sum coarray. $M = 3, N = 4$.

large number of consecutive DOFs in the 4-DCSC. Our proposition can be summarized as follows;

1) We reformulate the 4-DCSC geometry design problem and simplify it into two separate problems: a fourth order sum coarray (4-SC) problem and a 2-DC problem.

2) We separately consider the optimization of the 4-SC and the 2-DC. We formulate the 4-SC problem as a postage stamp problem and use only a few integers to achieve a 4-SC integer set which contains a wide range of consecutive integers.

3) The 4-SC integer set is utilized to represent a virtual nested array to which the 2-DC is applied. The inter-element spacing of the virtual nested array is determined according to the elements in the 4-SC. By doing so, the DOFs of the corresponding 4-DCSC are significantly increased.

4.4.1 Reformulation of 4-DCSC

To properly design the array geometry, we first reformulate the 4-DCSC. We extract the 4-DCSC term and rewrite it by substituting the definition of the 2-SC

$$\begin{aligned} & (v_1 - v_2) - (v_3 - v_4) \\ = \; & [(c_{i1} + c_{j1}) - (c_{i2} + c_{j2})] - [(c_{i3} + c_{j3}) - (c_{i4} + c_{j4})] \\ = \; & (c_{i1} + c_{j1} + c_{i4} + c_{j4}) - (c_{i2} + c_{j2} + c_{i3} + c_{j3}) \end{aligned} \tag{4.26}$$

where $c_{i1}, c_{j1}, ..., c_{i4}, c_{j4} \in \mathbb{S}$. Without loss of generality, we define the 4-SC of a given physical array as follows.

Definition 5 The 4-SC of $\mathbb{S}$ is the 4 times summation of elements in $\mathbb{S}$, denoted by

$$\mathbb{S}_{4sc} = \{u = c_{i1} + c_{i2} + c_{i3} + c_{i4} \mid c_{i1}, c_{i2}, c_{i3}, c_{i4} \in \mathbb{S}\} \tag{4.27}$$

It can be seen that (4.26) can be considered as the 2-DC of elements in $\mathbb{S}_{4sc}$. If we properly design $\mathbb{S}$ and its corresponding $\mathbb{S}_{4sc}$ is equivalent to a nested array, the 4-DCSC problem can be simplified as a 2-DC problem of nested array. To this end, we should properly design the elements of $\mathbb{S}$ to obtain a virtual nested array and the 4-DCSC can be equivalently achieved by applying the 2-DC to this virtual nested array. Before further discussion, we first introduce the postage stamp problem.

4.4.2 4-SC optimization using postage stamp problem

Given positive integers h and k, for a set of k integers $\mathbb{Y}_k = \{y_0, y_1, ..., y_{k-1}\}$ with $0 = y_0 < y_1 < y_2 < ... < y_{k-1}$, the summation of h elements in $\mathbb{Y}_k$ can generate a set of consecutive integers $\mathbb{N}_n = \{0, 1, 2, ..., n\}$, where the value of n is as large as possible [120–122]. Here, the h elements in the summation can be the repetition of a same element in $\mathbb{Y}_k$. This problem can be formulated as

$$\mathbb{N}_n \in \{\sum_{i=0}^{k-1} w_i y_i \mid w_i \geq 0, \sum_{i=0}^{k-1} w_i = h\}. \tag{4.28}$$

where coefficient w_i is a non-negative integer performing as a weight coefficient of linear combination. For given values of h and k, the possible maximum value $n = n(h, \mathbb{Y}_k)$ is denoted as h-range of set $\mathbb{Y}_k$, and the corresponding solution $\mathbb{Y}_k$ is represented as h-basis for integer k. The postage stamp problem is equivalent to the search of the optimum h-basis $\mathbb{Y}_k$ with given integers h, k such that $n(h, \mathbb{Y}_k)$ will be as big as possible. By solving the h-basis postage stamp problem, a much larger value of h-range can be obtained with a small value of k.

4.4.3 virtual nested array and 2-DC

It is obvious that the 4-SC can be considered as a 4-basis postage stamp problem. Some values of the achievable $n(4, \mathbb{Y}_k)$ are provided in Table 4.1 with $k \leq 12$ [120]. It can be observed that as k increases, $n(4, \mathbb{Y}_k)$ grows at a very fast rate. Our goal is to design an array geometry which can achieve a large number of consecutive DOFs in the 4-DCSC with as less sensors as possible.

Table 4.1 – Achievable $n = n(4, \mathbb{Y}_k)$ with given k.

k	3	4	5	6	7	8	9	10	11	12
n	10	26	44	70	108	162	228	310	422	550

Without loss of generality, we assume that the physical array geometry consists of two sub-arrays. Its integer sensor position indices set can then be expressed as $\mathbb{S} = \mathbb{S}_1 \cup \mathbb{S}_2$, where $\mathbb{S}_1$ has N_1 elements, $\mathbb{S}_2$ has N_2 elements and $\mathbb{S}_1, \mathbb{S}_2$ share the same first element equal to 0. We can separately consider the 4-SC of $\mathbb{S}_1$ and $\mathbb{S}_2$ to construct a virtual nested array. For $\mathbb{S}_1$ with N_1 sensors, we can obtain its 4-range $n(4, \mathbb{Y}_{N_1})$ by solving the postage stamp problem. Many methods for solving the postage stamp problem have been proposed in the number theory [121, 123]. One can also refer to Table 4.1 for the solution of $n(4, \mathbb{Y}_k)$ for $k \leq 12$. It will be elaborated in the numerical results part that with a small value of k, the consecutive DOFs can be a very high value, i.e. 9 sensors can achieve more than 4000 consecutive DOFs, which are sufficient for most scenarios.

Then, with N_1 elements in $\mathbb{S}_1$, we can obtain a set of integers including the following

part

$$\{0,\ 1,\ 2,\ ...,\ n(4, \mathbb{Y}_{N_1})\}. \tag{4.29}$$

Similarly, solving the postage stamp problem of $\mathbb{S}_2$ with $k = N_2$, we can obtain the following part

$$\{0,\ 1,\ 2,\ ...,\ n(4, \mathbb{Y}_{N_2})\}. \tag{4.30}$$

Interestingly, (4.29) and (4.30) can be equivalently related to two virtual sub-arrays of a nested array. Without loss of generality, we consider that the integer set in (4.29) is related to a virtual nested sub-array with inter-element spacing d_0. Then we can determine the inter-element spacing of the second virtual sub-array as $d_1 = (n(4, \mathbb{Y}_{N_1})+1)d_0$ [60] such that the positions of the virtual sensors related to (4.30) are $\{(0,\ d_1,\ 2d_1,\ ...,\ n(4, \mathbb{Y}_{N_2})d_1)\}$. By doing so, a virtual nested array is constructed and the 2-DC operation can be applied to obtain the 4-DCSC.

The number of sensors in the two sub-arrays of a nested array has been discussed in [60]. In our case, since we assume that two sub-arrays share the same first sensor, the total number of sensors is $N = N_1 + N_2 - 1$. To choose the values of N_1, N_2, we follow the same principles as in [60]. Two sub-arrays should have a similar (or the same) number of sensors, and the number of sensors in the sub-array with larger inter-element spacing should not be less than the sub-array with smaller inter-element spacing. More particularly, if N is an odd value, $N_1 = N_2 = \frac{N+1}{2}$. Otherwise, if N is an even value, $N_1 = N_2 - 1 = \frac{N}{2}$. Then the following integer range

$$[-C_{lag}, C_{lag}] \tag{4.31}$$

is a consecutive part in the 2-DC of the virtual nested array corresponding to (4.29) and (4.30), which is also the 4-DCSC of the physical array, where $C_{lag} = n(4, \mathbb{Y}_{N_2})(n(4, \mathbb{Y}_{N_1})+1)$.

It could be observed that $n(4, \mathbb{Y}_{N_1}), n(4, \mathbb{Y}_{N_2})$ are much bigger than N_1, N_2, which means that C_{lag} can be a very big value even with small values of N_1, N_2. For instance, given 7 sensors with $N_1 = 4, N_2 = 4$, the consecutive part ranges in [-702, 702] and the consecutive DOFs are $2C_{lag} + 1 = 1405$. A graphic illustration is provided in Figure 4.3.

Only the positive part of the 4-DCSC is given since the negative part is symmetrical.

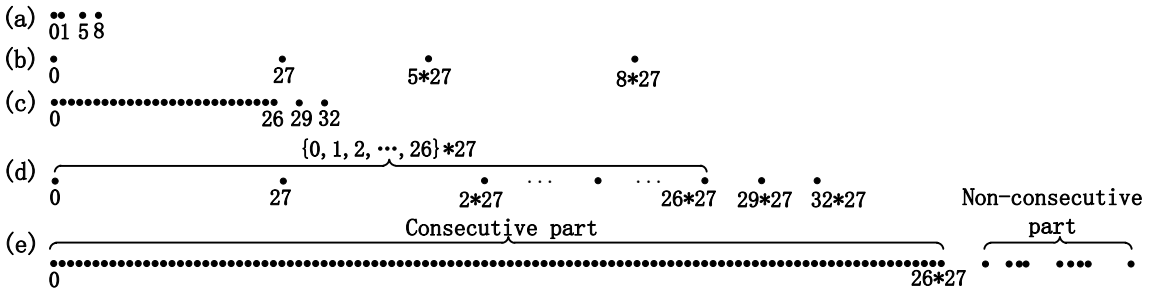

Figure 4.3 – 4-SC and 4-DCSC of $\mathbb{S}$ with $N = 7$. (a) $\mathbb{S}_1$; (b) $\mathbb{S}_2$; (c) 4-SC of $\mathbb{S}_1$; (d) 4-SC of $\mathbb{S}_2$; (e) 4-DCSC of $\mathbb{S}$.

Apart from the consecutive integer sets in (4.29) and (4.30), it is worth noting that the 4-SC of the two sub-arrays also includes some integers bigger than $n(4, \mathbb{Y}_k)$ as shown in Figure 4.3, which can be considered as non-consecutive parts. When applying the 2-DC to the 4-SC of the two sub-arrays, their non-consecutive parts can also lead to some additional elements in the 4-DCSC and the consecutive DOFs could be potentially extended. This phenomenon becomes significant when the value of k increases because more elements are included in the non-consecutive part. This phenomenon will be exemplified in the numerical results.

For the computational complexity, we consider two major parts, the cumulant matrix estimation and the eigenvalue decomposition (EVD). The 2-SC signal vector is an $K^2 \times 1$ vector and the dimension of $\mathbf{C}_{4,\mathbf{x}}$ is $K^4 \times K^4$. The EVD is implemented to a $[C_{lag} + 1] \times [C_{lag} + 1]$ dimension matrix. With L snapshots, the computation complexity is $9K^8L + \frac{4}{3}(C_{lag} + 1)^3$ [124, 125], which is higher than 2-DCSC [93]. It indicates that our proposed scheme achieves higher DOFs with the cost of higher complexity.

For a given number of physical sensors with this strategy, we can obtain a virtual nested array which contains large number of virtual sensors. The inter-element spacing of the sparse virtual sub-array is expanded to $\mathcal{O}(n(4, \mathbb{Y}_{N_1}))$, which is a significant enhancement compared with $\mathcal{O}(N_1)$ in [60]. The 2-DC can be adopted to these virtual sensors to further increase the consecutive coarray length. This property can help to enhance the consecutive DOFs efficiently with few physical sensors.

4.4.4 Simulation results and discussion

In this section, we will estimate the DOA using the well established MUSIC method and only the consecutive DOFs are utilized. The SNR is set to 0dB. The targets are uniformly distributed in the direction interval $[-60°, 60°]$.

Table 4.2 – Consecutive DOFs comparison for different array geometries.

Coarray type	Array geometry	consecutive DOFs
2-DCSC	CPA	69
	I-NA	309
4-DC	SAFE-CPA	189
	IEAS	305
	E-FL-NA	337
4-DCSC	CPA	149
	Proposed method	4357

We first compare the consecutive DOFs of different geometries with 9 physical sensors in Table 4.2. The two considered 2-DCSC geometries are CPA [93] and I-NA [94]. For a fair comparison, we consider these two geometries utilizing the entire array as both transmit and receive arrays. On the other hand, we also compare passive array geometries using 4-DC, which are referred to as SAFE-CPA [101], IEAS [126] and E-FL-NA [104]. It can be seen that the consecutive DOFs of CPA using 2-DC are limited to 69 while those of I-NA are 309 due to its increased inter-element spacing. Similar phenomenon can be observed for the 4-DC case.

When 4-DCSC is adopted to CPA, the consecutive DOFs can be increased compared with 2-DCSC. However, the number of DOFs of CPA with 4-DCSC is still smaller than some other geometries using 2-DCSC, i.e. I-NA, which indicates that proper geometry design for 4-DCSC is required if one aims to increase the DOFs. As a comparison, our proposed methods can significantly increase the DOFs to $2C_{lag} + 1 = 3961$ due to the expanded inter-element spacing in the virtual nested array. If we take into account the extended consecutive DOFs which is due to the non-consecutive part in the 4-SC, the DOFs in the 4-DCSC are increased to 4357 as shown in Table 4.2.

Since the extended consecutive part outside the range $[C_{lag}, C_{lag}]$ does not hold a

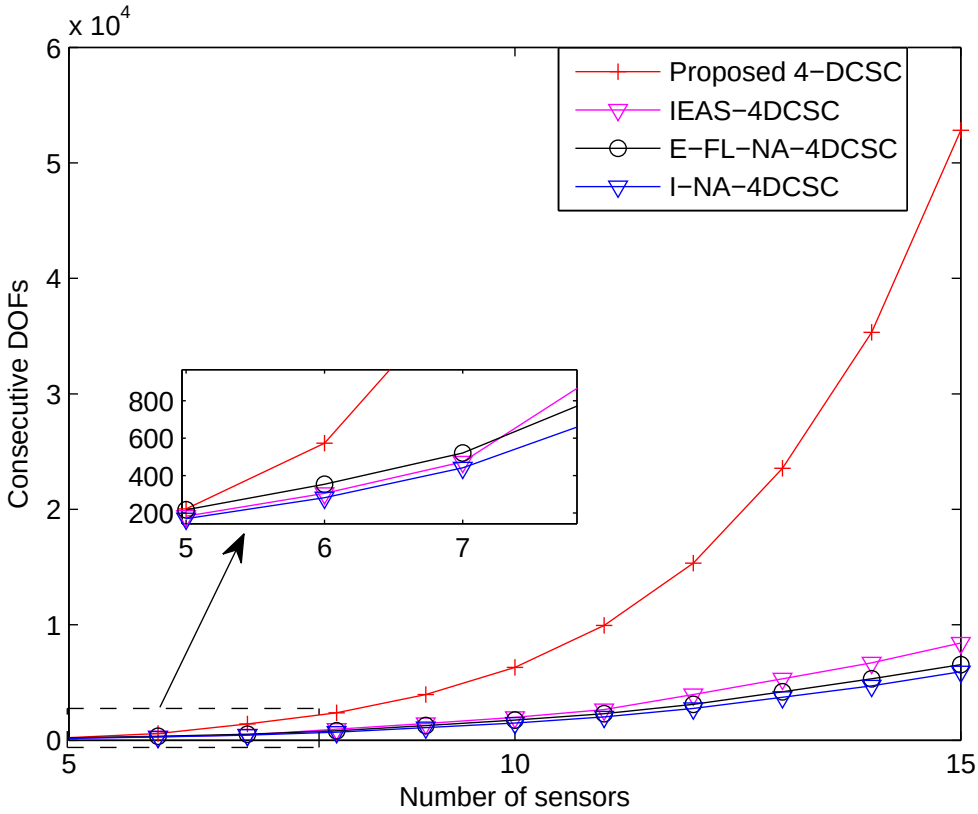

Figure 4.4 – Consecutive DOFs comparison of 4-DCSC related to different geometries versus number of sensors.

closed-form expression, we only focus on the consecutive DOFs within this range to approximately investigate the achievable consecutive DOFs with different number of sensors. For the compared geometries, we also consider 4-DCSC for fair comparison. As shown in Figure 4.4, the IEAS scheme outperforms E-FL-NA and I-NA as the number of sensors increases while our proposed geometry can significantly surpass all the three compared geometries. The consecutive DOFs can approximately achieve 10000 consecutive DOFs with a total of 11 sensors, which are sufficient for most applications. Furthermore, the consecutive DOFs increase rapidly when the number of sensors increases.

Finally, we compare the root mean square errors (RMSE) with different SNRs to evaluate the estimation accuracy in Figure 4.5. We also adopt these geometries in the MIMO case using 4-DCSC for fair comparison. For simplification, we use 6 sensors to

detect 70 targets and 500 snapshots are utilized. The number of Monte-Carlo trials is set to 200. It can be observed that the I-NA has worst performance and the E-FL-NA scheme outperforms the IEAS scheme. This is mainly because the number of consecutive DOFs strongly affects the RMSE performance and E-FL-NA has higher consecutive DOFs than IEAS with 6 physical sensors, as shown in Figure 4.3. The relation of the number of consecutive DOFs for different geometries with 6 sensors is E-FL-NA>IEAS>I-NA while the proposed method significantly outperforms the three compared methods. The enhanced DOFs significantly improve the RMSE performance of the proposed method.

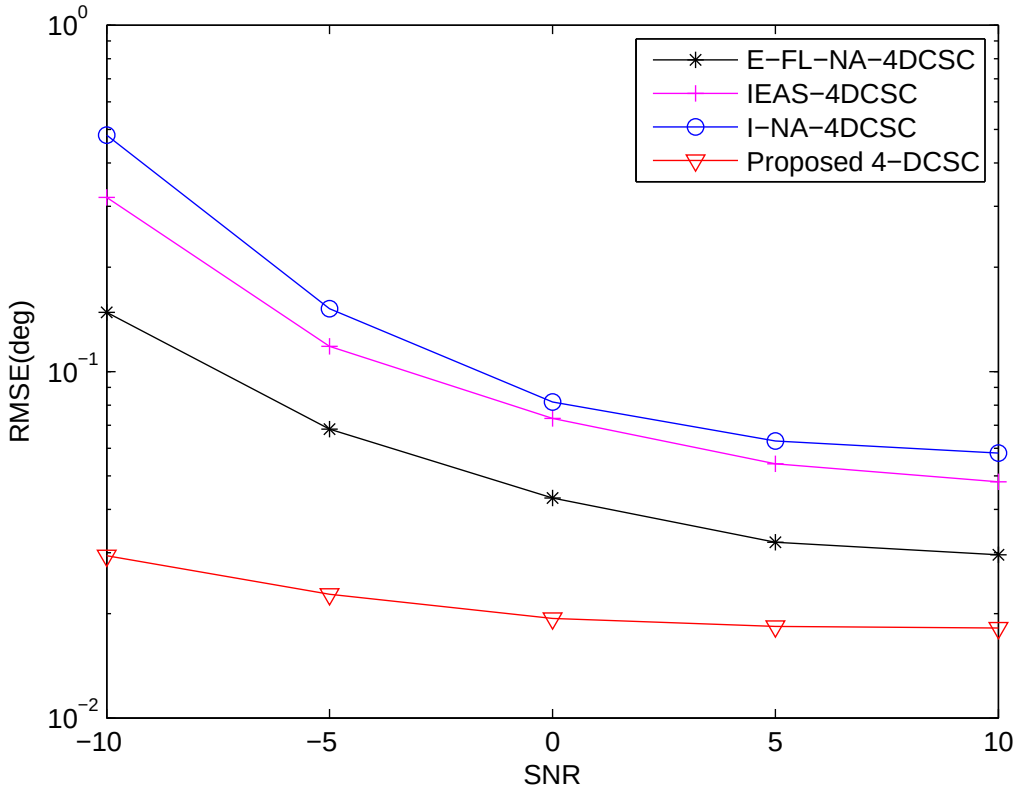

Figure 4.5 – RMSE comparison between different geometries with 6 sensors using 4-DCSC MIMO.

4.5 Conclusion

In this chapter, we work on active DOA detection with sparse MIMO radar. We first investigate the possibility for adopting fourth order cumulants to the MIMO radar. Jointly combined with the sum coarray in active sensing, the fourth order cumulants can generate a 4-DCSC, which has larger aperture than the second order covariance matrix based method. The property of the 4-DCSC of coprime MIMO is derived and we show that it holds similar holes property with the 2-DC while its DOFs are increased.

Then we reorganize the position of sensors in the MIMO array to seek for more optimal geometry for the 4-DCSC which can have higher DOFs. We simplify the 4-DCSC and reformulate it into two separate problems, which are a 4-SC problem and a 2-DC problem. Then the 4-SC problem can be solved by solving a postage stamp problem. The 2-DC problem is formulated as a virtual nested array problem and a 4-DCSC with significantly high DOFs can be obtained.

Chapter 5

Conclusion and future perspectives

5.1 Conclusion

In this dissertation, our works mainly focus on sparse array and sparse sampling reconstruction methods. Unlike the traditional ULA and Nyquist rate sampling, sparse array and sampling can greatly reduce the hardware cost by using only a few measurements. To rebuilt the sparse signals and estimate the desired parameters, the traditional MUSIC method is reformulated to coarray based MUSIC dedicating for the virtual array generated by the sparse measurements. The sparse configurations considered in our works include coprime array scheme and nested array scheme.

The coprime sampling scheme that can greatly release the sampling rate to a rate much lower than the Nyquist sampling rate is examined in Chapter 2. Only two standard samplers are required for coprime sampling. However in practice for a realization, coprime sampling method could encounter diagonal property loss problem under specific conditions. We analyze this phenomenon mathematically and give the conditions under which this problem happens. A random delay mechanism is then proposed to settle this problem. The introduced randomness ensures the robustness of coprime sampling based method under diagonal property loss conditions while the performance is slightly affected.

Apart from the diagonal property loss problem, there are also some holes in the 2-DC of coprime scheme, which limits the length of consecutive coarray and decreases the performance of the coarray based MUSIC method. We develop a multi-rate coprime

sampling mechanism to interpolate the missing information of the holes. Multiple scaled versions of the original 2-DC are generated by the multi-rate sampling before selecting the hole elements from these scaled version 2-DCs. We also derive that if the multi-rate parameters are properly designed, no extra sampling data is required and the proposed method causes no additional sampling burden to the samplers, which is an attractive feature.

In chapter 3, we focus on DOA estimation with coprime array. We investigate the holes filling problem of coprime array from another aspect, which is the rearrangement of sensors in coprime array. In conventional coprime array, some sensors are proved to be redundant and the removal of these sensors does not change the structure of the 2-DC. In our proposition, the rearrangement is considered only for these sensors and the relocated positions of these sensors are carefully designed in accordance to the hole elements such that they can fill as many holes as possible.

We also work on active DOA estimation using sparse MIMO radar in chapter 4. Contrary to most of the current sparse MIMO radar, we introduce the fourth order cumulants for MIMO radar and jointly combine the 4-DC and 2-SC to further increase the DOFs. The 4-DCSC of coprime MIMO is proved to be a promising strategy to enlarge the aperture of virtual array compared with the 2-DCSC. We then consider the MIMO radar geometry optimization problem within the framework of the 4-DCSC. A virtual nested array similar to the passive DOA estimation case is proposed and we show that the DOFs can be significantly increased.

5.2 Future perspectives

The above works are related to the frequency and DOA estimation. In the future, several potential directions may be of our interest for further development.

Joint DOA and frequency estimation problem. Our previous works consider the frequency estimation and DOA estimation separately. Since the key spirit of our works is based on the difference coarray, it seems quiet promising to jointly estimate both frequency

and DOA within a same framework.

Calibration problem. In our works, we only take the mutual coupling into account in DOA case. In practice, there are many real world calibration problems. For instance, in the time and frequency domain, the synchronization problem between samplers could bring challenge for coprime sampling since coprime sampling strongly relies on the cross correlation between the two sampled data sets. If the synchronization error becomes significant, the difference coarray structure will be collapsed and the performance of the coarray MUSIC method will be degraded.

Two dimension difference coarray problem. In this dissertation, only the one dimension linear array is considered. The difference coarray can be extended to the two dimension planar array scenario. Similarly, we can use few sensors in two dimension to generate a much larger virtual planar array. Moreover, this can be combined with a massive MIMO system, which is also a hot topic in recent years.

BIBLIOGRAPHY

[1] J. Mitola and G. Q. Maguire, « Cognitive radio: making software radios more personal », *in*: *IEEE Personal Communications* 6.*4* (1999), pp. 13–18.

[2] T. Yucek and H. Arslan, « A survey of spectrum sensing algorithms for cognitive radio applications », *in*: *IEEE Communications Surveys Tutorials* 11.*1* (2009), pp. 116–130.

[3] S Alireza Razavi, Mikko Valkama, and Danijela Cabric, « Covariance-based OFDM spectrum sensing with sub-Nyquist samples », *in*: *Signal Processing* 109 (2015), pp. 261–268.

[4] Tevfik Yucek and Huseyin Arslan, « A survey of spectrum sensing algorithms for cognitive radio applications », *in*: *IEEE communications surveys & tutorials* 11.*1* (2009), pp. 116–130.

[5] Federal Communications Commission et al., « Notice of proposed rule making and order: Facilitating opportunities for flexible, efficient, and reliable spectrum use employing cognitive radio technologies », *in*: *ET docket 03-108* (2005), p. 73.

[6] H. Sun, D. I. Laurenson, and C. Wang, « Computationally Tractable Model of Energy Detection Performance over Slow Fading Channels », *in*: *IEEE Communications Letters* 14.*10* (2010), pp. 924–926.

[7] G. Ganesan and Ye Li, « Agility improvement through cooperative diversity in cognitive radio », *in*: *GLOBECOM '05. IEEE Global Telecommunications Conference, 2005.* Vol. 5, 2005, 5 pp.–2509.

[8] D. Cabric, S. M. Mishra, and R. W. Brodersen, « Implementation issues in spectrum sensing for cognitive radios », *in*: *Conference Record of the Thirty-Eighth Asilomar Conference on Signals, Systems and Computers, 2004.* Vol. 1, 2004, 772–776 Vol.1.

[9] A. Ghasemi and E. S. Sousa, « Optimization of Spectrum Sensing for Opportunistic Spectrum Access in Cognitive Radio Networks », *in*: *2007 4th IEEE Consumer Communications and Networking Conference*, 2007, pp. 1022–1026.

[10] P. Qihang et al., « A Distributed Spectrum Sensing Scheme Based on Credibility and Evidence Theory in Cognitive Radio Context », *in*: *2006 IEEE 17th International Symposium on Personal, Indoor and Mobile Radio Communications*, 2006, pp. 1–5.

[11] S. Sankaranarayanan et al., « A bandwidth sharing approach to improve licensed spectrum utilization », *in*: *First IEEE International Symposium on New Frontiers in Dynamic Spectrum Access Networks, 2005. DySPAN 2005.* 2005, pp. 279–288.

[12] F. F. Digham, M. -. Alouini, and M. K. Simon, « On the energy detection of unknown signals over fading channels », *in*: *IEEE International Conference on Communications, 2003. ICC '03.* Vol. 5, 2003, 3575–3579 vol.5.

[13] Anant Sahai, Niels Hoven, and Rahul Tandra, « Some fundamental limits on cognitive radio », *in*: *Allerton Conference on Communication, Control, and Computing*, Monticello, Illinois, 2004, pp. 1662–1671.

[14] E. Axell et al., « Spectrum Sensing for Cognitive Radio : State-of-the-Art and Recent Advances », *in*: *IEEE Signal Processing Magazine* 29.*3* (2012), pp. 101–116.

[15] J. Lunden et al., « Spectrum Sensing in Cognitive Radios Based on Multiple Cyclic Frequencies », *in*: *2007 2nd International Conference on Cognitive Radio Oriented Wireless Networks and Communications*, 2007, pp. 37–43.

[16] K. Kim et al., « Cyclostationary Approaches to Signal Detection and Classification in Cognitive Radio », *in*: *2007 2nd IEEE International Symposium on New Frontiers in Dynamic Spectrum Access Networks*, 2007, pp. 212–215.

[17] K. Maeda et al., « Recognition Among OFDM-Based Systems Utilizing Cyclostationarity-Inducing Transmission », *in*: *2007 2nd IEEE International Symposium on New Frontiers in Dynamic Spectrum Access Networks*, 2007, pp. 516–523.

[18] P. D. Sutton, K. E. Nolan, and L. E. Doyle, « Cyclostationary Signatures for Rendezvous in OFDM-Based Dynamic Spectrum Access Networks », *in*: *2007 2nd IEEE International Symposium on New Frontiers in Dynamic Spectrum Access Networks*, 2007, pp. 220–231.

[19] P. D. Sutton et al., « Cyclostationary Signature Detection in Multipath Rayleigh Fading Environments », *in*: *2007 2nd International Conference on Cognitive Radio Oriented Wireless Networks and Communications*, 2007, pp. 408–413.

[20] M. Ghozzi et al., « Cyclostatilonarilty-Based Test for Detection of Vacant Frequency Bands », *in*: *2006 1st International Conference on Cognitive Radio Oriented Wireless Networks and Communications*, 2006, pp. 1–5.

[21] J. Lunden et al., « Collaborative Cyclostationary Spectrum Sensing for Cognitive Radio Systems », *in*: *IEEE Transactions on Signal Processing* 57.*11* (2009), pp. 4182–4195.

[22] A. V. Dandawate and G. B. Giannakis, « Statistical tests for presence of cyclostationarity », *in*: *IEEE Transactions on Signal Processing* 42.*9* (1994), pp. 2355–2369.

[23] John G Proakis and Masoud Salehi, *Digital communications*, vol. 4, McGraw-hill New York, 2001.

[24] B. Farhang-Boroujeny, « Filter Bank Spectrum Sensing for Cognitive Radios », *in*: *IEEE Transactions on Signal Processing* 56.*5* (2008), pp. 1801–1811.

[25] R. Tandra and A. Sahai, « Fundamental limits on detection in low SNR under noise uncertainty », *in*: *2005 International Conference on Wireless Networks, Communications and Mobile Computing*, vol. 1, 2005, 464–469 vol.1.

[26] S. Haykin, « Cognitive radio: brain-empowered wireless communications », *in*: *IEEE Journal on Selected Areas in Communications* 23.*2* (2005), pp. 201–220.

[27] S. Haykin, D. J. Thomson, and J. H. Reed, « Spectrum Sensing for Cognitive Radio », *in*: *Proceedings of the IEEE* 97.*5* (2009), pp. 849–877.

[28] D. J. Thomson, « Spectrum estimation and harmonic analysis », *in*: *Proceedings of the IEEE* 70.*9* (1982), pp. 1055–1096.

[29] Kiran Challapali, Stefan Mangold, and Zhun Zhong, « Spectrum agile radio: Detecting spectrum opportunities », *in*: *Proc. Int. Symposium on Advanced Radio Technologies*, 2004.

[30] M. Chiani and M. Z. Win, « Estimating the number of signals observed by multiple sensors », *in*: *2010 2nd International Workshop on Cognitive Information Processing*, 2010, pp. 156–161.

[31] Claude E Shannon, « A mathematical theory of communication », *in*: *Bell system technical journal* 27.*3* (1948), pp. 379–423.

[32] K. Hossain and B. Champagne, « Wideband Spectrum Sensing for Cognitive Radios With Correlated Subband Occupancy », *in*: *IEEE Signal Processing Letters* 18.*1* (2011), pp. 35–38.

[33] Z. Quan et al., « Optimal Multiband Joint Detection for Spectrum Sensing in Cognitive Radio Networks », *in*: *IEEE Transactions on Signal Processing* 57.*3* (2009), pp. 1128–1140.

[34] Z. Tian and G. B. Giannakis, « A Wavelet Approach to Wideband Spectrum Sensing for Cognitive Radios », *in*: *2006 1st International Conference on Cognitive Radio Oriented Wireless Networks and Communications*, 2006, pp. 1–5.

[35] M. Zatman, « Circular array STAP », *in*: *IEEE Transactions on Aerospace and Electronic Systems* 36.*2* (2000), pp. 510–517.

[36] E. Magill and H. Wheeler, « Wide-angle impedance matching of a planar array antenna by a dielectric sheet », *in*: *IEEE Transactions on Antennas and Propagation* 14.*1* (1966), pp. 49–53.

[37] B. D. Van Veen and K. M. Buckley, « Beamforming: a versatile approach to spatial filtering », *in*: *IEEE ASSP Magazine* 5.*2* (1988), pp. 4–24.

[38] J. Capon, « High-resolution frequency-wavenumber spectrum analysis », *in*: *Proceedings of the IEEE* 57.*8* (1969), pp. 1408–1418.

[39] John Parker Burg, « Maximum entropy spectral analysis », *in*: *37ˆ< th> Annual International Meeting, Soc. of Explor. Geophys., Oklahoma City, Okla., Oct. 31, 1967*, 1967.

[40] R. G. Lorenz and S. P. Boyd, « Robust minimum variance beamforming », *in*: *IEEE Transactions on Signal Processing* 53.*5* (2005), pp. 1684–1696.

[41] D. W. Tufts and R. Kumaresan, « Estimation of frequencies of multiple sinusoids: Making linear prediction perform like maximum likelihood », *in*: *Proceedings of the IEEE* 70.*9* (1982), pp. 975–989.

[42] Jingmin Xin and A. Sane, « Linear prediction approach to direction estimation of cyclostationary signals in multipath environment », *in*: *IEEE Transactions on Signal Processing* 49.*4* (2001), pp. 710–720.

[43] Simon S Haykin, *Adaptive filter theory*, Pearson Education India, 2005.

[44] R. Roy and T. Kailath, « ESPRIT-estimation of signal parameters via rotational invariance techniques », *in*: *IEEE Transactions on Acoustics, Speech, and Signal Processing* 37.*7* (1989), pp. 984–995.

[45] R. Schmidt, « Multiple emitter location and signal parameter estimation », *in*: *IEEE Transactions on Antennas and Propagation* 34.*3* (1986), pp. 276–280.

[46] A. Barabell, « Improving the resolution performance of eigenstructure-based direction-finding algorithms », *in*: *ICASSP '83. IEEE International Conference on Acoustics, Speech, and Signal Processing*, vol. 8, 1983, pp. 336–339.

[47] D. Datla et al., « Parametric Adaptive Spectrum Sensing Framework for Dynamic Spectrum Access Networks », *in*: *2007 2nd IEEE International Symposium on New Frontiers in Dynamic Spectrum Access Networks*, 2007, pp. 482–485.

[48] S. Stein Ioushua et al., « CaSCADE: Compressed Carrier and DOA Estimation », *in*: *IEEE Transactions on Signal Processing* 65.*10* (2017), pp. 2645–2658.

[49] M. Mishali and Y. C. Eldar, « From Theory to Practice: Sub-Nyquist Sampling of Sparse Wideband Analog Signals », *in*: *IEEE Journal of Selected Topics in Signal Processing* 4.*2* (2010), pp. 375–391.

[50] C. Herley and Ping Wah Wong, « Minimum rate sampling and reconstruction of signals with arbitrary frequency support », *in*: *IEEE Transactions on Information Theory* 45.*5* (1999), pp. 1555–1564.

[51] R. Venkataramani and Y. Bresler, « Perfect reconstruction formulas and bounds on aliasing error in sub-Nyquist nonuniform sampling of multiband signals », *in*: *IEEE Transactions on Information Theory* 46.*6* (2000), pp. 2173–2183.

[52] Z. Tian and G. B. Giannakis, « Compressed Sensing for Wideband Cognitive Radios », *in*: *2007 IEEE International Conference on Acoustics, Speech and Signal Processing - ICASSP '07*, vol. 4, 2007, pp. IV-1357-IV–1360.

[53] F. Zeng, C. Li, and Z. Tian, « Distributed Compressive Spectrum Sensing in Cooperative Multihop Cognitive Networks », *in*: *IEEE Journal of Selected Topics in Signal Processing* 5.*1* (2011), pp. 37–48.

[54] J. N. Laska et al., « Compressive sensing for dynamic spectrum access networks: Techniques and tradeoffs », *in*: *2011 IEEE International Symposium on Dynamic Spectrum Access Networks (DySPAN)*, 2011, pp. 156–163.

[55] M. Mishali and Y. C. Eldar, « Blind Multiband Signal Reconstruction: Compressed Sensing for Analog Signals », *in*: *IEEE Transactions on Signal Processing* 57.*3* (2009), pp. 993–1009.

[56] C. Yen, Y. Tsai, and X. Wang, « Wideband Spectrum Sensing Based on Sub-Nyquist Sampling », *in*: *IEEE Transactions on Signal Processing* 61.*12* (2013), pp. 3028–3040.

[57] E. Lagunas and M. Nájar, « Spectral Feature Detection With Sub-Nyquist Sampling for Wideband Spectrum Sensing », *in*: *IEEE Transactions on Wireless Communications* 14.*7* (2015), pp. 3978–3990.

[58] Eva Lagunas and Montse Nájar, « Sparse correlation matching-based spectrum sensing for open spectrum communications », *in*: *EURASIP Journal on Advances in Signal Processing* 2012.*1* (2012), p. 31.

[59] A. Ahmed and J. Romberg, « Compressive Multiplexing of Correlated Signals », *in*: *IEEE Transactions on Information Theory* 61.*1* (2015), pp. 479–498.

[60] P. Pal and P. P. Vaidyanathan, « Nested Arrays: A Novel Approach to Array Processing With Enhanced Degrees of Freedom », *in*: *IEEE Transactions on Signal Processing* 58.*8* (2010), pp. 4167–4181.

[61] A. Moffet, « Minimum-redundancy linear arrays », *in*: *IEEE Transactions on Antennas and Propagation* 16.*2* (1968), pp. 172–175.

[62] P. P. Vaidyanathan and P. Pal, « Sparse Sensing With Co-Prime Samplers and Arrays », *in*: *IEEE Transactions on Signal Processing* 59.*2* (2011), pp. 573–586.

[63] S. Qin et al., « Generalized Coprime Sampling of Toeplitz Matrices for Spectrum Estimation », *in*: *IEEE Transactions on Signal Processing* 65.*1* (2017), pp. 81–94.

[64] S. Qin, Y. D. Zhang, and M. G. Amin, « Generalized Coprime Array Configurations for Direction-of-Arrival Estimation », *in*: *IEEE Transactions on Signal Processing* 63.*6* (2015), pp. 1377–1390.

[65] M. Wang and A. Nehorai, « Coarrays, MUSIC, and the Cramér–Rao Bound », *in*: *IEEE Transactions on Signal Processing* 65.*4* (2017), pp. 933–946.

[66] P. Pal and P. P. Vaidyanathan, « Coprime sampling and the MUSIC algorithm », *in*: *2011 Digital Signal Processing and Signal Processing Education Meeting (DSP/SPE)*, 2011, pp. 289–294.

[67] C. Liu and P. P. Vaidyanathan, « Maximally economic sparse arrays and cantor arrays », *in*: *2017 IEEE 7th International Workshop on Computational Advances in Multi-Sensor Adaptive Processing (CAMSAP)*, 2017, pp. 1–5.

[68] C. Liu and P. P. Vaidyanathan, « Composite Singer Arrays with Hole-free Coarrays and Enhanced Robustness », *in*: *ICASSP 2019 - 2019 IEEE International Conference on Acoustics, Speech and Signal Processing (ICASSP)*, 2019, pp. 4120–4124.

[69] Z. Zheng et al., « MISC Array: A New Sparse Array Design Achieving Increased Degrees of Freedom and Reduced Mutual Coupling Effect », *in*: *IEEE Transactions on Signal Processing* 67.*7* (2019), pp. 1728–1741.

[70] Minglei Yang et al., « Improved nested array with hole-free DCA and more degrees of freedom », *in*: *Electronics Letters* 52.*25* (2016), pp. 2068–2070.

[71] J. Liu et al., « Augmented Nested Arrays With Enhanced DOF and Reduced Mutual Coupling », *in*: *IEEE Transactions on Signal Processing* 65.*21* (2017), pp. 5549–5563.

[72] E. BouDaher et al., « Multi-Frequency Co-Prime Arrays for High-Resolution Direction-of-Arrival Estimation », *in*: *IEEE Transactions on Signal Processing* 63.*14* (2015), pp. 3797–3808.

[73] Muran Guo, Tao Chen, and Ben Wang, « An improved DOA estimation approach using coarray interpolation and matrix denoising », *in*: *Sensors* 17.*5* (2017), p. 1140.

[74] Tao Chen, Muran Guo, and Limin Guo, « A direct coarray interpolation approach for direction finding », *in*: *Sensors* 17.*9* (2017), p. 2149.

[75] C. Liu, P. P. Vaidyanathan, and P. Pal, « Coprime coarray interpolation for DOA estimation via nuclear norm minimization », *in*: *2016 IEEE International Symposium on Circuits and Systems (ISCAS)*, 2016, pp. 2639–2642.

[76] C. Zhou et al., « Direction-of-Arrival Estimation for Coprime Array via Virtual Array Interpolation », *in*: *IEEE Transactions on Signal Processing* 66.*22* (2018), pp. 5956–5971.

[77] X. Wang and X. Wang, « Hole Identification and Filling in k-Times Extended Co-Prime Arrays for Highly Efficient DOA Estimation », *in*: *IEEE Transactions on Signal Processing* 67.*10* (2019), pp. 2693–2706.

[78] Weijiang Wang, Shiwei Ren, and Zhiming Chen, « Unified coprime array with multi-period subarrays for direction-of-arrival estimation », *in*: *Digital Signal Processing* 74 (2018), pp. 30–42.

[79] A. Ahmed, Y. D. Zhang, and J. Zhang, « Coprime Array Design with Minimum Lag Redundancy », *in*: *ICASSP 2019 - 2019 IEEE International Conference on Acoustics, Speech and Signal Processing (ICASSP)*, 2019, pp. 4125–4129.

[80] Juan Ramirez Jr and Jeffrey L Krolik, « Synthetic aperture processing for passive co-prime linear sensor arrays », *in*: *Digital Signal Processing* 61 (2017), pp. 62–75.

[81] G. Qin, M. G. Amin, and Y. D. Zhang, « DOA Estimation Exploiting Sparse Array Motions », *in*: *IEEE Transactions on Signal Processing* 67.*11* (2019), pp. 3013–3027.

[82] B. Friedlander and A. J. Weiss, « Direction finding in the presence of mutual coupling », *in*: *IEEE Transactions on Antennas and Propagation* 39.*3* (1991), pp. 273–284.

[83] K. M. Pasala and E. M. Friel, « Mutual coupling effects and their reduction in wideband direction of arrival estimation », *in*: *IEEE Transactions on Aerospace and Electronic Systems* 30.*4* (1994), pp. 1116–1122.

[84] T. Svantesson, « Modeling and estimation of mutual coupling in a uniform linear array of dipoles », *in*: *1999 IEEE International Conference on Acoustics, Speech, and Signal Processing. Proceedings. ICASSP99 (Cat. No.99CH36258)*, vol. 5, 1999, 2961–2964 vol.5.

[85] C. Liu and P. P. Vaidyanathan, « Super Nested Arrays: Linear Sparse Arrays With Reduced Mutual Coupling—Part I: Fundamentals », *in*: *IEEE Transactions on Signal Processing* 64.*15* (2016), pp. 3997–4012.

[86] T. Svantesson, « Mutual coupling compensation using subspace fitting », *in*: *Proceedings of the 2000 IEEE Sensor Array and Multichannel Signal Processing Workshop. SAM 2000 (Cat. No.00EX410)*, 2000, pp. 494–498.

[87] M. Lin and L. Yang, « Blind Calibration and DOA Estimation With Uniform Circular Arrays in the Presence of Mutual Coupling », *in*: *IEEE Antennas and Wireless Propagation Letters* 5 (2006), pp. 315–318.

[88] H. T. Hui, « Improved compensation for the mutual coupling effect in a dipole array for direction finding », *in*: *IEEE Transactions on Antennas and Propagation* 51.*9* (2003), pp. 2498–2503.

[89] F. Sellone and A. Serra, « A Novel Online Mutual Coupling Compensation Algorithm for Uniform and Linear Arrays », *in*: *IEEE Transactions on Signal Processing* 55.*2* (2007), pp. 560–573.

[90] Xianpeng Wang et al., « A sparse representation scheme for angle estimation in monostatic MIMO radar », *in*: *Signal Processing* 104 (2014), pp. 258–263.

[91] Chun-Yang Chen and P. P. Vaidyanathan, « Minimum redundancy MIMO radars », *in*: *2008 IEEE International Symposium on Circuits and Systems*, 2008, pp. 45–48.

[92] Si Qin, Yimin D Zhang, and Moeness G Amin, « DOA estimation of mixed coherent and uncorrelated targets exploiting coprime MIMO radar », *in*: *Digital Signal Processing* 61 (2017), pp. 26–34.

[93] E. BouDaher, F. Ahmad, and M. G. Amin, « Sparsity-Based Direction Finding of Coherent and Uncorrelated Targets Using Active Nonuniform Arrays », *in*: *IEEE Signal Processing Letters* 22.*10* (2015), pp. 1628–1632.

[94] M. Yang et al., « A New Nested MIMO Array With Increased Degrees of Freedom and Hole-Free Difference Coarray », *in*: *IEEE Signal Processing Letters* 25.*1* (2018), pp. 40–44.

[95] P. Chevalier et al., « On the virtual array concept for higher order array processing », *in*: *IEEE Transactions on Signal Processing* 53.*4* (2005), pp. 1254–1271.

[96] P. Chevalier, A. Ferreol, and L. Albera, « High-Resolution Direction Finding From Higher Order Statistics: The 2q-MUSIC Algorithm », *in*: *IEEE Transactions on Signal Processing* 54.*8* (2006), pp. 2986–2997.

[97] J. -. Cardoso and E. Moulines, « Asymptotic performance analysis of direction-finding algorithms based on fourth-order cumulants », *in*: *IEEE Transactions on Signal Processing* 43.*1* (1995), pp. 214–224.

[98] J. M. Mendel, « Tutorial on higher-order statistics (spectra) in signal processing and system theory: theoretical results and some applications », *in*: *Proceedings of the IEEE* 79.*3* (1991), pp. 278–305.

[99] A. B. Gershman and J. F. Bohme, « Improving the threshold performance of higher-order direction finding methods via pseudorandomly generated estimator banks », *in*: *Proceedings of the IEEE Signal Processing Workshop on Higher-Order Statistics*, 1997, pp. 285–289.

[100] P. Pal and P. P. Vaidyanathan, « Multiple Level Nested Array: An Efficient Geometry for 2qth Order Cumulant Based Array Processing », *in*: *IEEE Transactions on Signal Processing* 60.*3* (2012), pp. 1253–1269.

[101] Q. Shen et al., « Extension of Co-Prime Arrays Based on the Fourth-Order Difference Co-Array Concept », *in*: *IEEE Signal Processing Letters* 23.*5* (2016), pp. 615–619.

[102] Q. Shen et al., « Extension of nested arrays with the fourth-order difference co-array enhancement », *in*: *2016 IEEE International Conference on Acoustics, Speech and Signal Processing (ICASSP)*, 2016, pp. 2991–2995.

[103] J. Cai et al., « An Expanding and Shift Scheme for Constructing Fourth-Order Difference Coarrays », *in*: *IEEE Signal Processing Letters* 24.*4* (2017), pp. 480–484.

[104] Q. Shen et al., « Simplified and Enhanced Multiple Level Nested Arrays Exploiting High-Order Difference Co-Arrays », *in*: *IEEE Transactions on Signal Processing* 67.*13* (2019), pp. 3502–3515.

[105] P. Stoica and A. Nehorai, « MUSIC, maximum likelihood, and Cramer-Rao bound », *in*: *IEEE Transactions on Acoustics, Speech, and Signal Processing* 37.*5* (1989), pp. 720–741.

[106] P. Stoica and A. Nehorai, « Performance study of conditional and unconditional direction-of-arrival estimation », *in*: *IEEE Transactions on Acoustics, Speech, and Signal Processing* 38.*10* (1990), pp. 1783–1795.

[107] Chun-Lin Liu and PP Vaidyanathan, « Cramér–Rao bounds for coprime and other sparse arrays, which find more sources than sensors », *in*: *Digital Signal Processing* 61 (2017), pp. 43–61.

[108] A. Koochakzadeh and P. Pal, « Cramér–Rao Bounds for Underdetermined Source Localization », *in*: *IEEE Signal Processing Letters* 23.*7* (2016), pp. 919–923.

[109] Jorma Rissanen, « Modeling by shortest data description », *in*: *Automatica* 14.*5* (1978), pp. 465–471.

[110] Jeannie L Moulton, « Enhanced high-resolution imaging through multiple-frequency coarray augmentation », PhD thesis, University of Pennsylvania, 2010.

[111] A. Raza, W. Liu, and Q. Shen, « Thinned coprime arrays for DOA estimation », *in*: *2017 25th European Signal Processing Conference (EUSIPCO)*, 2017, pp. 395–399.

[112] A. Raza, W. Liu, and Q. Shen, « Thinned Coprime Array for Second-Order Difference Co-Array Generation With Reduced Mutual Coupling », *in*: *IEEE Transactions on Signal Processing* 67.*8* (2019), pp. 2052–2065.

[113] C. Liu and P. P. Vaidyanathan, « Super Nested Arrays: Linear Sparse Arrays With Reduced Mutual Coupling—Part II: High-Order Extensions », *in*: *IEEE Transactions on Signal Processing* 64.*16* (2016), pp. 4203–4217.

[114] Zhe Fu, Pascal Chargé, and Yide Wang, « Multi-rate coprime sampling for frequency estimation with increased degrees of freedom », *in*: *Signal Processing* 166 (2020), p. 107258.

[115] E. BouDaher et al., « DOA estimation with co-prime arrays in the presence of mutual coupling », *in*: *2015 23rd European Signal Processing Conference (EUSIPCO)*, 2015, pp. 2830–2834.

[116] Y. D. Zhang, M. G. Amin, and B. Himed, « Sparsity-based DOA estimation using co-prime arrays », *in*: *2013 IEEE International Conference on Acoustics, Speech and Signal Processing*, 2013, pp. 3967–3971.

[117] Masato Ishiguro, « Minimum redundancy linear arrays for a large number of antennas », *in*: *Radio Science* 15.*6* (1980), pp. 1163–1170.

[118] Jing Liu, Weidong Zhou, and Xianpeng Wang, « Fourth-order cumulants-based sparse representation approach for DOA estimation in MIMO radar with unknown mutual coupling », *in*: *Signal Processing* 128 (2016), pp. 123–130.

[119] Xinghua Wang et al., « DOA estimation based on the difference and sum coarray for coprime arrays », *in*: *Digital Signal Processing* 69 (2017), pp. 22–31.

[120] Michael F Challis and John P Robinson, « Some extremal postage stamp bases », *in*: *Journal of Integer Sequences* 13.*2* (2010), p. 3.

[121] Svein Mossige, « Algorithms for computing the h-range of the postage stamp problem », *in*: *Mathematics of Computation* 36.*154* (1981), pp. 575–582.

[122] Ronald L Graham and Neil James Alexander Sloane, « On additive bases and harmonious graphs », *in*: *SIAM Journal on Algebraic Discrete Methods* 1.*4* (1980), pp. 382–404.

[123] Samuel S Wagstaff, « Additive h-bases for n », *in*: *Number Theory Carbondale 1979*, Springer, 1979, pp. 302–327.

[124] J. Liang and D. Liu, « Passive Localization of Mixed Near-Field and Far-Field Sources Using Two-stage MUSIC Algorithm », *in*: *IEEE Transactions on Signal Processing* 58.*1* (2010), pp. 108–120.

[125] J. Li et al., « Simplified High-Order DOA and Range Estimation With Linear Antenna Array », *in*: *IEEE Communications Letters* 21.*1* (2017), pp. 76–79.

[126] Jingjing Cai et al., « An improved expanding and shift scheme for the construction of fourth-order difference co-arrays », *in*: *Signal Processing* 153 (2018), pp. 95–100.

UNIVERSITE BRETAGNE LOIRE / MATHSTIC

UNIVERSITÉ DE NANTES

Titre : Estimation de paramètres à l'aide d'échantillonneurs et de réseaux coprime

Mots clés : Estimation de la fréquence, estimation de la direction d'arrivée, configuration coprime

Résumé : Les réseaux et les capteurs éparse attirent de plus en plus l'attention en raison de leur capacité à augmenter les DOFs. La DOA ou la fréquence des signaux peut être estimée avec peu de capteurs d'antenne ou quelques échantillons sub-Nyquist collectés. Dans cette thèse, nous nous concentrons sur une structure bien reconnue, la configuration coprime, pour estimer la DOA ou la fréquence des signaux.

Nous étudions d'abord l'échantillonnage coprime pour l'estimation de la fréquence et nous avons mis en évidence le phénomène de perte de propriété en diagonale à cause duquel l'estimation échoue totalement. Pour remédier à ce problème, nous proposons un mécanisme i ntroduisant un délai aléatoire pour garantir l'efficacité des méthodes basées sur l'échantillonnage coprime.

Ensuite, nous développons également un schéma d'échantillonnage coprime à taux multiples afin d'utiliser pleinement les informations contenues dans les échantillons.

En plus de l'estimation de la fréquence, nous travaillons également sur l'estimation de la DOA avec un réseau coprime. Nous réorganisons la structure des réseaux coprimes pour augmenter encore les DOFs sans introduire de coût matériel supplémentaire. Puis, nous introduisons des cumulants de quatrième ordre dans l'estimation de la DOA active avec le radar MIMO coprime. Finalement, nous optimisons la géométrie du radar MIMO en utilisant des cumulants de quatrième ordre et les DOFs peuvent être augmentés de manière significative.

Title : Parameters estimation with coprime samplers and arrays

Keywords : Frequency estimation, direction of arrival estimation, coprime configuration

Abstract : Sparse array and sparse sensing attract increasing attention due to their capability to increase the DOFs. The DOA or the frequency of signals can be estimated with few antenna sensors or few collected sub-Nyquist samples. In this dissertation, we focus on one of the most recognized sparse structures, coprime configuration, to estimate the DOA or the frequency of signals.

We first investigate the coprime sampling for frequency estimation and come across with a diagonal property loss phenomenon for which the estimation totally fails. To address this problem, we propose a random delay based mechanism to ensure the effectiveness of coprime sampling based methods.

Then we also develop a multi-rate coprime sampling scheme to fully utilize the information brought by the coprime sampling.

Apart from the frequency estimation, we also work on the DOA estimation with coprime array. We rearrange the coprime array structure to further increase the DOFs without introducing additional hardware cost. Then we introduce fourth order cumulants in active DOA estimation with coprime MIMO radar. The DOFs of MIMO radar can be enhanced by adopting the fourth order cumulants. Finally, we optimize the MIMO radar geometry using fourth order cumulants and the DOFs can be significantly increased.